AD-A104 673 PRATT AND WHITNEY AIRCRAFT GROUP EAST HARTFORD CT COM--ETC F/G 21/4
AN ASSESSMENT OF THE USE OF ANTIMISTING FUEL IN TURBOFAN ENGINE--ETC(U)
JUN 81 A FIORENTINO, R DE SARO, T FRANZ NAS3-22045
UNCLASSIFIED PWA-5697-29 FAA-CT-81-58 NL

1 OF 2
AD A 104673

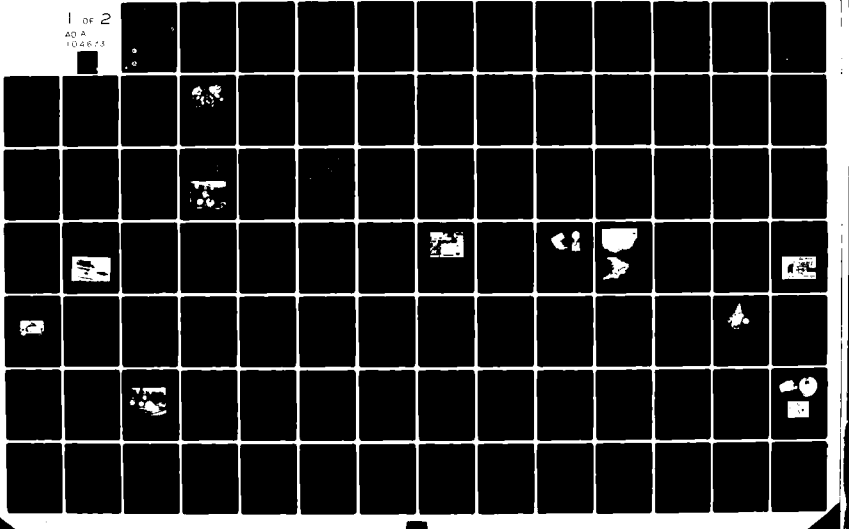

LEVEL II

NASA CR-165258
PWA 5697-29
FAA-CT-81-58

AN ASSESSMENT OF THE USE OF ANTIMISTING FUEL IN TURBOFAN ENGINES

by

A. Fiorentino
R. De Saro
T. Franz

UNITED TECHNOLOGIES CORPORATION
Pratt & Whitney Aircraft Group
Commercial Products Division

JUNE 1981

Prepared for
National Aeronautics and Space Administration
NASA Lewis Research Center
Contract NAS3-22045

and

U.S. Department of Transportation
Federal Aviation Administration
Technical Center
Atlantic City Airport, N.J. 08405

1 Report No. FAA-CT-81-58 NASA-CR-165258	2 Government Accession No.	3 Recipient's Catalog No.
4 Title and Subtitle An Assessment of the use of Antimisting Fuel in Turbofan Engines.		5 Report Date June 1981 6 Performing Organization Code
7 Author(s) A. Fiorentino T. Franz R. De Saro		8 Performing Organization Report No. PWA-5697-29 10 Work Unit No.
9 Performing Organization Name and Address United Technologies Corporation Pratt & Whitney Aircraft Group Commercial Products Division		11 Contract or Grant No. NAS3-22045
12 Sponsoring Agency Name and Address National Aeronautic and Space Administration, Washington, D.C. 20546 and Federal Aviation Administration Technical Center, Atlantic City, New Jersey 08405.		13 Type of Report and Period Covered Contractor Report 9/79 - 11/80 14 Sponsoring Agency Code

15 Supplementary Notes

Project Manager, Harold Schmidt, NASA Lewis Research Center, Cleveland, Ohio 44135 and Gary Frings, ACT-320, Atlantic City Airport, Atlantic City, N.J. 08405

16 Abstract

An evaluation was made on the effects of using antimisting kerosene (AMK) on the performance of the components from the fuel system and the combustor of a current in-service JT8D aircraft engine. The objectives were to identify problems associated with using antimisting kerosene and to determine the extent of shearing or degradation required to allow the engine components to achieve satisfactory operation. The program consisted of a literature survey and a test program which evaluated the antimisting kerosene fuel in laboratory and bench component testing, and assessed the performance of the combustor in a high pressure facility and in an altitude relight/cold ignition facility. Performance of the fuel pump and control system was evaluated in an open loop simulation. Thus far, results of the program would not preclude the use of antimisting kerosene in a jet engine application.

17 Key Words (Suggested by Author(s))	18 Distribution Statement
Antimisting kerosene Safety fuels	Document is available to the U.S. public through the National Technical Information Service, Springfield, Virginia 22161.

19 Security Classif. (of this report)	20 Security Classif. (of this page)	21 No. of Pages	22 Price*

* For sale by the National Technical Information Service, Springfield, Virginia 22161

FOREWORD

This document report describes the work conducted and completed by the Pratt & Whitney Aircraft Group, and United Technologies Research Center (UTRC) of United Technologies Corporation on Antimisting Kerosene. This final report was prepared for the National Aeronatuics and Space Administration Lewis Research Center in compliance with the requirements of Contract NAS3-32045.

The authors of this report wish to acknowledge the guidance and assistance of Harold Schmidt, NASA Manager of the Antimisting Kerosene program. The authors would also like to thank J. Marks of Pratt & Whitney Aircraft, and J. Kennedy and E. Szetela of United Technologies Research Center for their contributions to this program.

TABLE OF CONTENTS

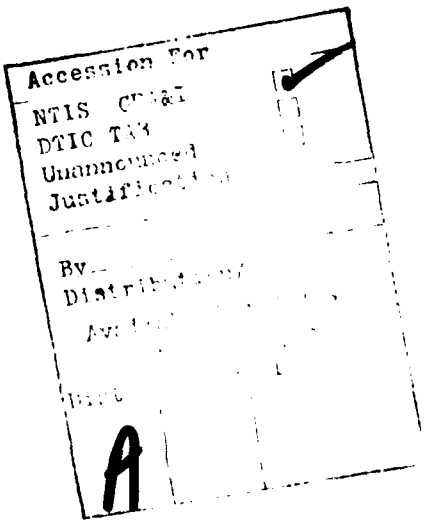

TABLE OF CONTENTS (Cont'd)

TABLE OF CONTENTS (Cont'd)

TABLE OF CONTENTS (Cont'd)

SUMMARY

This report presents the results of a thirteen month technical effort to evaluate the effects of using FM-9 antimisting additive on the performance of the components from the fuel system and the combustor of a current in-service JT8D aircraft engine.

The major objectives of this program were to identify particular problem areas associated with the use of this additive and to determine the extent of preshearing or additive degradation required to achieve satisfactory operation of the engine components. The particular antimisting kerosene fuel evaluated contained 0.3 percent by weight FM-9 additive.

The program was initiated with an extensive survey to accumulate the available laboratory test procedures and data available from previous and on-going studies and test efforts conducted with antimisting kerosene. The test program was organized into two phases with the first phase being devoted to the evaluation of the antimisting kerosene fuel in laboratory and short duration "bench" type component tests. These included the analysis of the physical and chemical properties of the fuel-additive mixture, the evaluation of fuel injector atomization characteristics, and the performance of fuel filters. Following evaluation of the results of these tests the program entered the second phase in which more comprehensive component and system tests were conducted. These tests involved the assessment of the performance of the combustor in both a high pressure facility and an altitude relight/cold ignition facility; and the performance of the fuel pump and control system in an open loop simulation.

Based on the results of this limited program nothing was uncovered which would preclude the use of antimisting kerosene in a jet engine application.

Several positive significant technical conclusions resulted from this program but further technology improvements are required for safe engine implementation:

- Antimisting kerosene can be processed (sheared) mechanically to behave similarly to Jet A in flow restricting devices found on engine fuel systems such as filters, but low temperature, water sensitivity, compatibility and long term endurance testing is required before engine applications can be considered.

- Combustor/fuel injectors have the potential of operating satisfactorily on antimisting kerosene that has been sufficiently processed, although deficiencies with respect to Jet A fuel were documented and need further investigation.

- The only major engine modification projected to be required at this time for the successful use of antimisting kerosene is the need for a practical shearing device upstream of the engine to provide the necessary level of fuel processing.

Although the literature surveys, and the laboratory and full scale component tests, and analytical projections conducted under this program revealed that antimisting fuel has the potential for engine applications there are areas requiring additional information to understand fundamental mechanisms, and the need for additional technology improvement. Recommendations for future research activities and technology development are suggested in this report.

1.0 INTRODUCTION

Post crash fires have been found to be a major cause of fatalities in commercial aircraft accidents. These fires have been in many instances attributed to the atomization of fuel from abruptly ruptured fuel tanks. This atomized fuel forms a mist in the air that becomes readily ignitable on contact with hot debris. Because the fuels used in commercial aircraft gas turbines are not extremely volatile; i.e., do not generate large quantities of vapor that could be readily ignited by hot debris, it appears that these post crash fires could be minimized by modifying the physical characteristics of the fuel so that it could not atomize when the fuel tanks are ruptured.

Antimisting kerosene is a kerosene-fraction jet fuel containing a polymer additive that reduces the flammability of the fuel in an aircraft crash circumstance. Antimisting kerosene additives, when dissolved in Jet A fuel in concentrations in the range of 0.3 percent by weight, have demonstrated the ability to inhibit ignition and flame propagation of the released fuel in simulated crash tests. The antimisting kerosene fuel resists misting and atomization from wind shear and impact forces and instead tends to agglomerate into globules.

Several antimisting kerosene additives have been developed and evaluated for their potential to reduce post-crash fires. The antimisting additive, FM-9, selected for testing in this program, was developed by the Imperial Chemical Industries and the Royal Aircraft Establishment of the United Kingdom.

The objective of this program is to conduct an evaluation of the effect of the use of the antimisting kerosene on the performance of current in-service commercial aircraft engines. This is accomplished by testing a 40 degree segment and a full annular combustor and selected components of the fuel supply and control system. All hardware tested comes from a JT8D turbofan engine. From the test results an assessment can be made of:

a. The feasibility of operating the JT8D engine with fuel containing the antimisting kerosene additive.

b. The degree of antimisting kerosene degradation necessary for compatability with existing fuel system designs.

c. The engine modification requirements (if any) for the compatible use of antimisting kerosene in the JT8D engine.

d. The applicability of the results to other engines.

The as received antimisting kerosene has been observed to clog JT8D fuel filters and to exhibit unacceptable nozzle spray characteristics. It is, therefore, necessary to degrade the antimisting characteristics of the fuel after it leaves the fuel tanks and before it reaches the first filter. In addition, the antimisting kerosene must be sufficiently degraded so that during combustion, performance, emission and operational requirements can be met. The method and evaluation of antimisting kerosene degradation and the correlation of fuel degradation level to component or combustor performance is addressed in this program.

Since Tasks 1 and 2 are management and reporting tasks and do not entail any technical effort, only the following Tasks 3 through 9 will be reported on in this report.

Task 3 - Fuel handling and quality control
Task 4 - Physical characteristics evaluation
Task 5 - Fuel filter tests
Task 6 - Fuel injector performance
Task 7 - Combustor performance tests
Task 8 - Fuel control system tests
Task 9 - Fuel pump performance characteristics

Pertinent antimisting kerosene articles are included in the bibliography.

2.0 EQUIPMENT AND PROCEDURES

To provide a better understanding of the JT8D engine components that may be influenced by the use of antimisting fuel, a description of the JT8D engine its fuel system and combustor are presented in Section 2.1. Descriptions of the hardware, test facilities, instrumentation and test procedures appear under their appropriate tasks.

2.1 GENERAL DESCRIPTION OF THE JT8D-17 ENGINE AND COMBUSTOR

2.1.1 Engine Description

The JT8D-17 engine model was selected as the baseline for this experimental program. This engine is the current production version of the JT8D engine, which is in widespread use throughout the commercial transport fleet. It is also representative of all current production gas turbines in that its clearances, filter sizes, pumps and fuel flow paths are typical. The JT8D turbofan engine is an axial flow, dual-spool, moderate bypass-ratio design. It utilizes a two-stage fan and a four-stage low pressure compressor driven by a three-stage low pressure turbine, and a seven-stage high pressure compressor driven by a single-stage high pressure turbine. Figure 1 is a cross section of the JT8D-17 showing the mechanical configuration. Key specifications for this engine are listed in Table I.

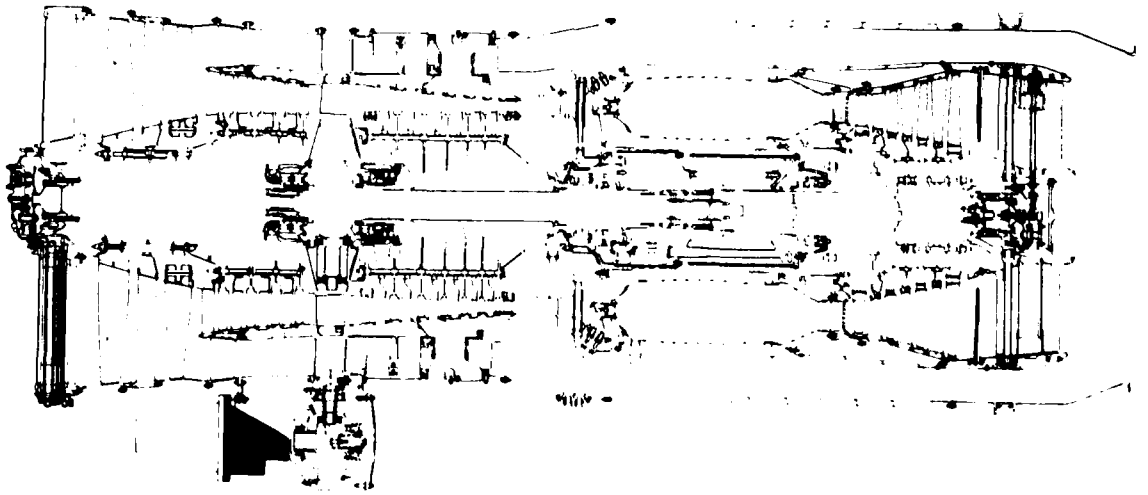

Figure 1 Cross-Section of JT8D-17 Engine

TABLE I

KEY SPECIFICATIONS OF THE JT8D-17 ENGINE

Weight (kg)	1510.5
Length (m)	3.045
Maximum Diameter, cold (m)	1.080
Pressure Ratio	16.9
Airflow Rate (kg/s)	148.3
Maximum Sea Level Static Thrust (kN)	71.2
Cruise Performance	
Mach Number	0.8
Altitude (m)	9140
Thrust (kN)	18.9
Specific Fuel Consumption (kg/Ns)	2.273×10^{-5}

2.1.2 JT8D Engine Fuel System

The function of the fuel system is to supply clean liquid fuel, free from vapor, at the required pressure and flow rate to the engine at all operating conditions. Figure 2 shows a schematic of the basic JT8D engine fuel system.

Fuel is supplied from the aircraft tanks to the engine driven fuel pump inlet. The fuel is pressurized to an intermediate pressure level by the fuel pump centrifugal stage and is passed through the air-fuel de-icing heat exchanger to the main fuel inlet filter. A pressure switch senses filter differential pressure. In the event of malfunction or blockage, valves are provided to by-pass fuel around the centrifugal stage, heat exchanger and filter. The clean filtered fuel is supplied to the high pressure gear stage and after pressurization is passed to the fuel control through a coarse mesh inlet filter. Excess pump fuel flow passes through the throttle differential pressure regulating valve and is returned to the fuel pump upstream of the high pressure gear stage. The metered fuel flow passes through the throttle valve. The throttle valve position and consequentially, flow area opening, is determined by the mechanisms within the fuel control that sense, compute and position the valve

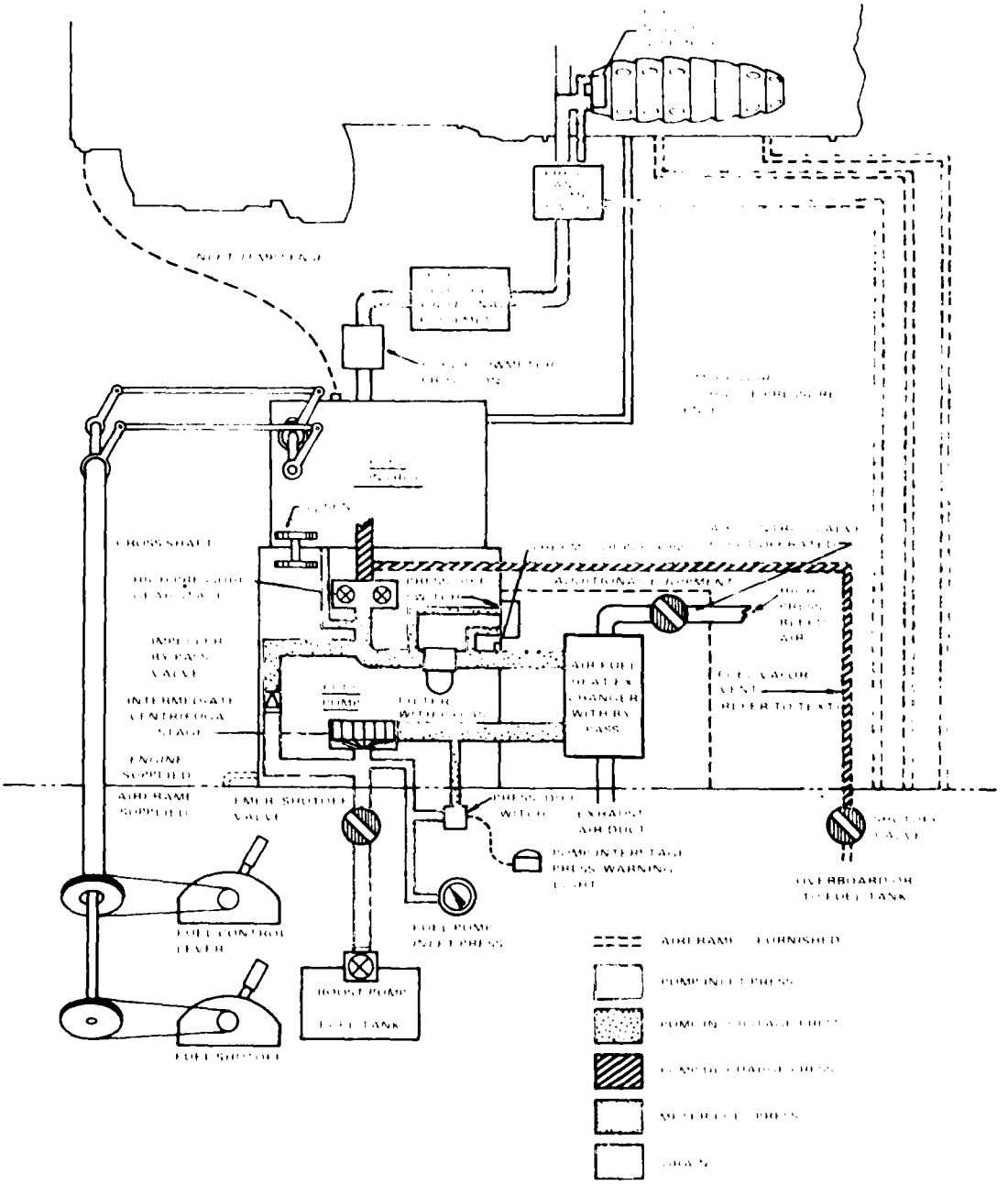

Figure 2 JT8D Turbofan Fngine Fuel System Diagram

as a function of power lever position, engine speed, engine compressor discharge pressure, and engine low compressor inlet temperature. The metered flow passes out of the fuel control via the control minimum pressure and shut off valve. The fuel flows through the airframe fuel flow meter and the fuel oil cooler to the pressurizing and dump valve. The pressurizing valve schedules flow to the fuel nozzle secondary manifold as a function of primary fuel nozzle pressure drop. The two position dump valve is hydraulically actuated by primary fuel pressure during engine operation. The dump valve has a checking feature that actuates at engine shutdown when the primary fuel pressure is reduced. The check valve closes and prevents draining of upstream fuel lines into the engine.

2.1.2.1 JT8D Engine Fuel Pump

The Model 243600 Main Fuel Pump consists of a single element gear stage with a high speed centrifugal boost stage (see Figure 3). A cartridge type relief valve is incorporated to limit the pressure rise across the gear stage. The unit provides a rigid mounting pad arrangement and a rotational splined drive for the fuel control. An integral fuel filter containing a replaceable paper barrier filter element is located between the discharge of the centrifugal stage and the inlet of the gear stage. In the event of a malfunction of the boost stage, a bypass valve opens into the inlet passage of the pump to direct flow in the gear stage. This is held normally closed by a light spring force and remains closed due to boost stage pressure. Outlet and return ports are provided between the boost stage discharge and the filter inlet for installation of an external fuel deicing heater. A drive shaft seal drain is located in the lower extremity of the mounting flange.

2.1.2.2 JT8D Engine Fuel Control

The fuel control consists of a metering and a computing system. The metering system selects the rate of fuel flow to be supplied to the engine burners in accordance with the amount of thrust demanded by the pilot, but subject to engine operating limitations as scheduled by the computing system as a result of its monitoring various engine operational parameters (power lever angle, burner pressure, engine high compressor speed and engine inlet temperature).

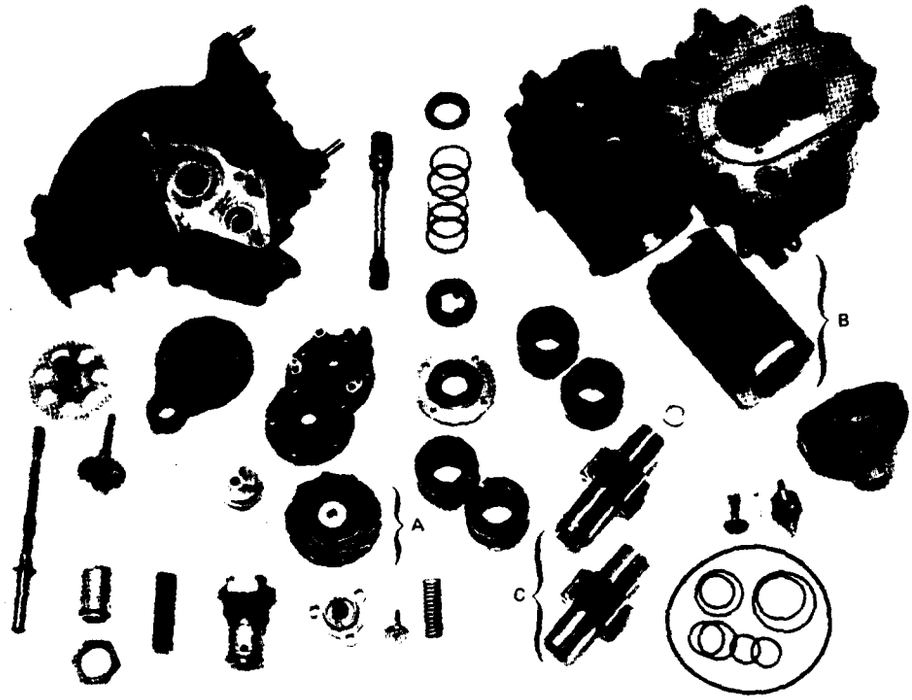

Figure 3 *JT8D Engine Fuel Pump - A. Centrifugal Stage, B. Filter, C. High Pressure Gear Stage*

The computing system senses and combines the various parameters to control the output of the metering section of the control during all regimes of engine operation.

The fuel control is composed of the following major components: the fuel filter, the filter bypass valves, the pressure regulating valve, the minimum pressure and shutoff valve, the windmill bypass and shutoff valve, the throttle valve, the compressor discharge pressure sensor, the compressor discharge pressure limiter, the compressor inlet temperature sensor, the speed sensing governor, the linkage housing, the hydraulic housing, the mounting base and the necessary linkage required to transpose the various parameters into one integrated signal resulting in the proper fuel flow.

2.1.2.3 Fuel Pressurizing and Dump Valve

The fuel pressurizing and dump valve is located downstream from the fuel control and is connected to the primary and secondary fuel manifolds to which it discharges its fuel.

Essentially the unit consists of three parts; a fuel inlet screen, a dump manifold drain valve, and a pressurizing (flow-dividing) valve.

2.1.2.4 JT8D Fuel Filter System

The JT8D engine fuel system incorporates several fuel filters differing in construction, filtration quality and filtration characteristic depending on the subsystem component protection requirements. The main inlet 40 micron paper cartridge filter, incorporated within the fuel pump, provides the primary protection for all subsystem components. This inlet filter provides protection against solid particulate matter and, in addition, at fuel temperatures below freezing, acts as a collector of fuel borne ice crystals. Periodically, the fuel deicing heater system is activated to increase fuel filter inlet temperature above the water freeze point and thereby clear the filter of collected ice.

The remaining filters have coarser filtration quality and with the exception of the control inlet filter have significantly smaller flow rate capacity. The coarser subsystem component filters varying in filtration capability from 50-325 mesh are either barrier or wash flow type and are constructed of stainless steel.

2.1.3 Fuel Control and Fuel Pump Performance Requirements

To ensure that the fuel control and fuel pump fulfills the engine metered flow requirements for accuracy and flow capacity, each component is subjected to an acceptance test initially at P&WA and periodically in airline service. Figure 4 indicates the fuel control parameters and scheduling accuracy requirements for these parameters. Table II provides the flow capacity and pressure requirements for the fuel pump at specified pump input speeds.

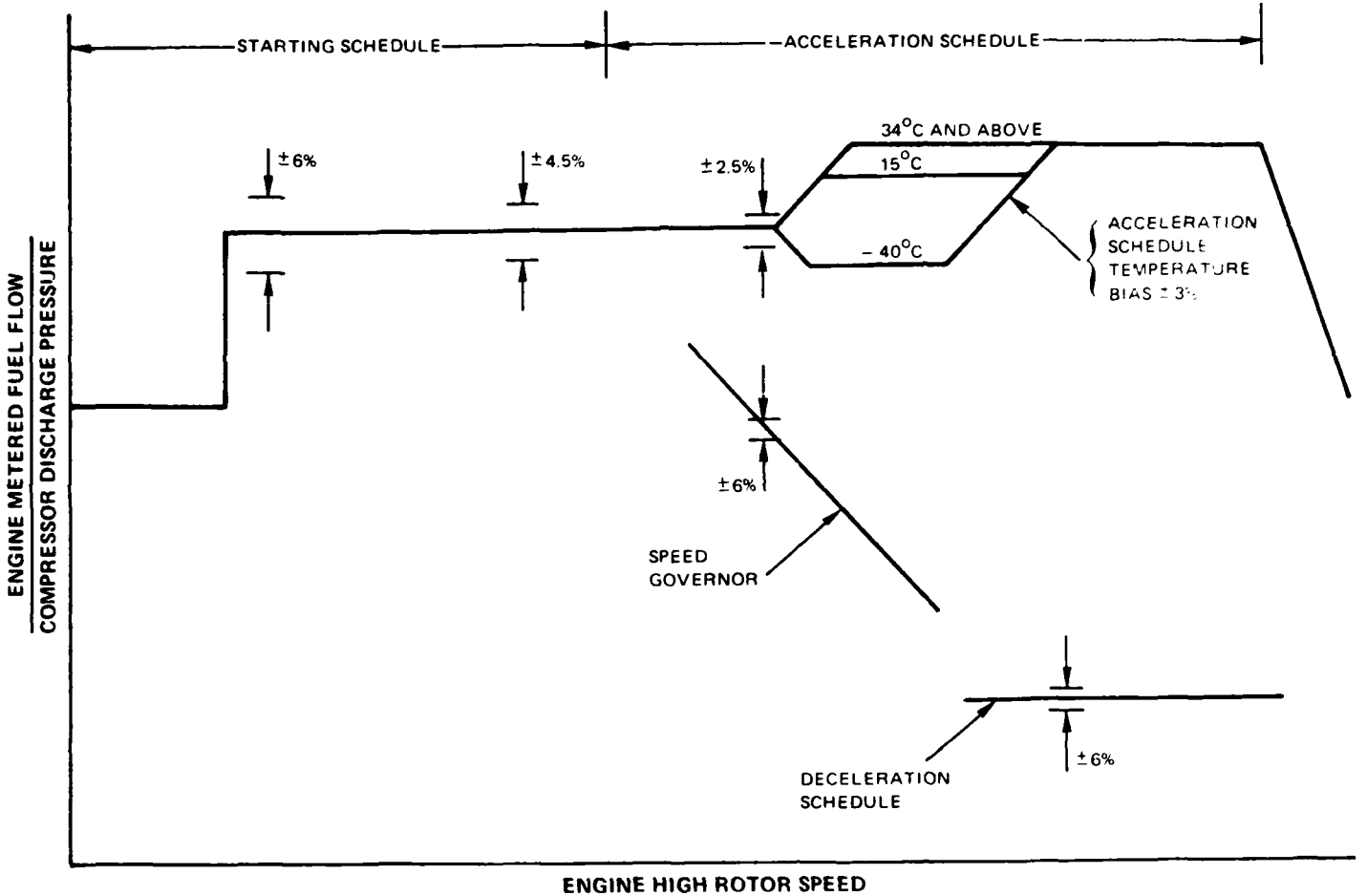

Figure 4 Fuel Control Scheduling Accuracy Requirements

TABLE II

JT8D FUEL PUMP CONDITIONS

Pump Speed (RPM)	Pump Discharge (Kpag)	Intermediate (Centrifugal) Stage Pressure Rise (Kpag)	Gear Stage Pressure Rise (kpag)	Allowable Performance Change At Pump Overhaul (%)
550	--	--	1015	10
3000	3450	--	--	5
3500	3450	--	--	5
4200	3450	--	--	3
4200	6900	Greater Than 445	--	3

2.1.4 Combustor Description

The JT8D-17 combustor section consists of nine tubular combustion chambers in a can-annular arrangement. Each chamber contains one centrally located duplex fuel nozzle. Two of the chambers are equipped with spark igniters. The nine combustion chambers are interconnected by tubes for flame propagation during starting. Each combustion chamber is of welded construction comprised of a series of formed sheet metal cylindrical liners. Each chamber is supported at the front by the fuel nozzle strut and a mount pin, and at the rear by a sliding joint at the face of the turbine inlet transition duct. A cross-sectional schematic of the JT8D-17 combustor is shown in Figure 5.

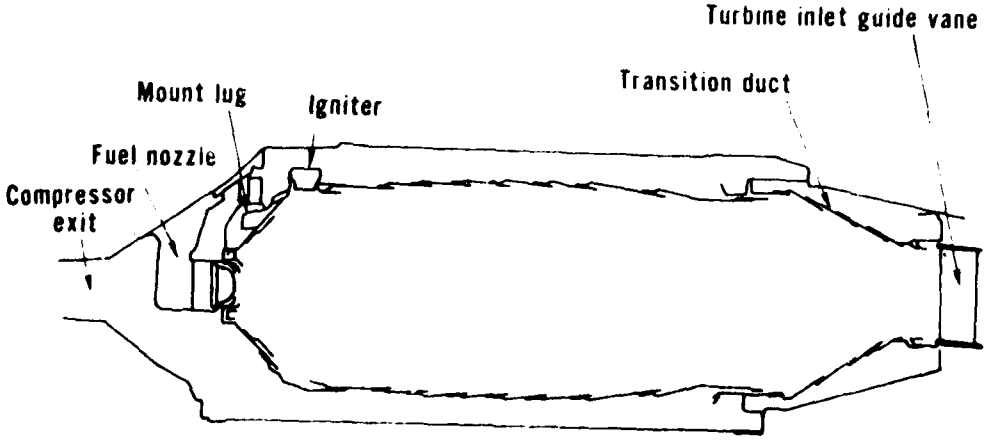

Figure 5 Cross-Sectional Schematic of the Production JT8D-17 Combustor

The JT8D-17 combustor employs a dual passage fuel injection system to obtain the required turn down ratio (ratio of maximum to minimum fuel flow) for a reasonable range of fuel pressure. The relationship between fuel flow and fuel manifold pressure for a typical engine is shown in Figure 6. The break in the curve indicates the staging point where transition is made from the primary metering system to the primary plus secondary metering system. Staging is controlled by a spring loaded pintle valve near the fuel control, which is sensitive to the difference between fuel pressure and air chamber pressure. The staging point is independent of the combustor fuel-air ratio for a particular engine operating condition.

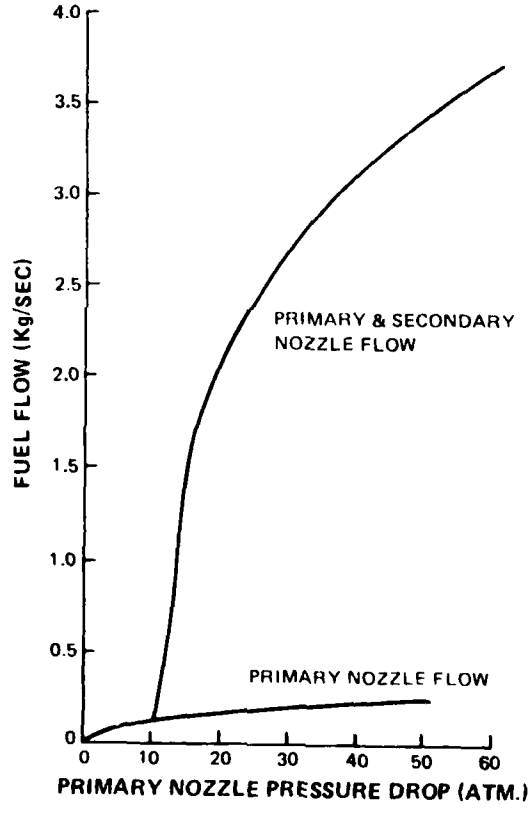

Figure 6 JT8D Dual Orifice Fuel Flow Schedule

An extensive program to reduce JT8D emissions has been in progress for some time at Pratt & Whitney Aircraft. Emissions reduction in the JT8D combustor has concentrated primarily in significantly increasing the combustion efficiency at idle operation to reduce emissions of carbon monoxide and unburned hydrocarbons. Combustor modifications include utilizing a pressure atomizing primary, aerating secondary fuel nozzle/swirler assembly coupled with a suitable alteration of the front end air entry distribution. A schematic drawing of the JT8D low emissions fuel nozzle assembly is shown in Figure 7. Achieving high idle combustion efficiency is accomplished by establishing a unique aerodynamic flow pattern in the primary zone which permits stable, stoichiometric combustion centrally located within the can while keeping fuel away from the walls. Fuel dispersion and spray angle characteristics therefore are critical to achieving low emissions.

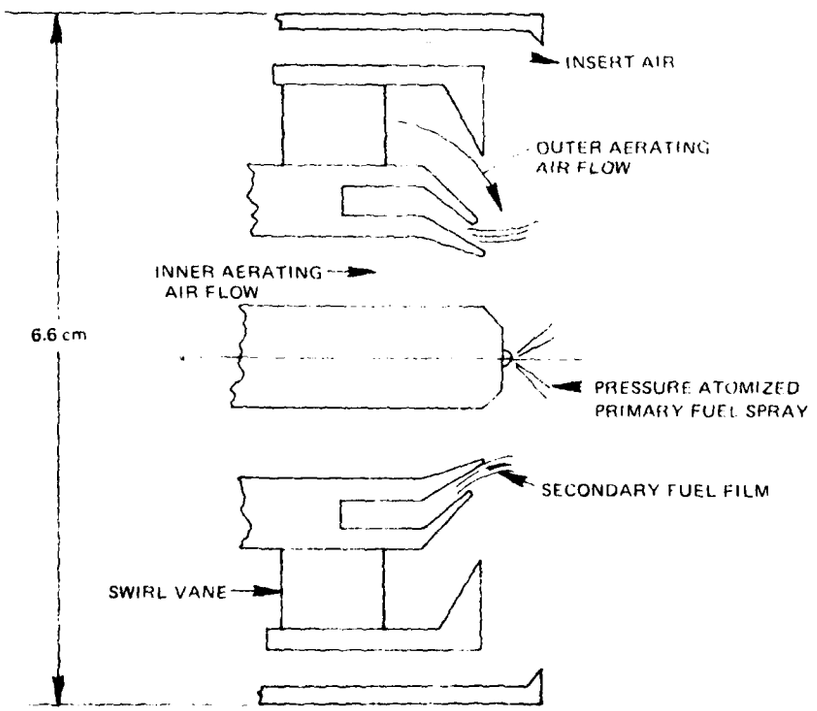

Figure 7 JT8D Low Emissions Fuel Nozzle

2.1.5 Combustor Performance Requirements

Table III lists the critical operating parameters for the JT8D-17 combustor at the four operating conditions of the Environmental Protection Agency landing and takeoff cycle and at the cruise operating condition. Other key operating parameters of the JT8D combustor at sea-level takeoff conditions are:

Compressor Exit Axial Mach Number	0.42
Combustor Section Total Pressure Loss (%)	8.2%
Combustor Exit Temperature Pattern Factor*	0.39

Figure 8 shows the design flight envelope of the JT8D-17 engine. The engine must be capable of self starting with the combustor driven only by a windmilling fan and compressor over a substantial fraction of the flight envelope as shown on the figure. Table IV lists the combustor operating conditions at the lettered points on the upper boundary of the relight envelope as defined from the windmilling performance characteristics of the JT8D-17 compressor.

TABLE III

JT8D-17 ENGINE COMBUSTOR OPERATING PARAMETERS

Operating Condition	Inlet Total Pressure (ATM)	Inlet Total Temperature (K)	Combustor Airflow (kg/sec)	Combustor Fuel Flow (kg/sec)	Combustor Fuel/Air Ratio
Idle (with bleeds)	2.4	393	12	0.14	0.0123
Takeoff	16.9	711	66	1.24	0.0188
Climb	13.2	679	53	0.90	0.0169
Approach	9.7	594	42	0.56	0.0133
Cruise	6.8	613	29	0.43	0.0148

*Pattern factor is the ratio of the difference between the maximum gas temperature and the average combustor exit temperature to the difference between the average combustor exit temperature and the combustor inlet temperature.

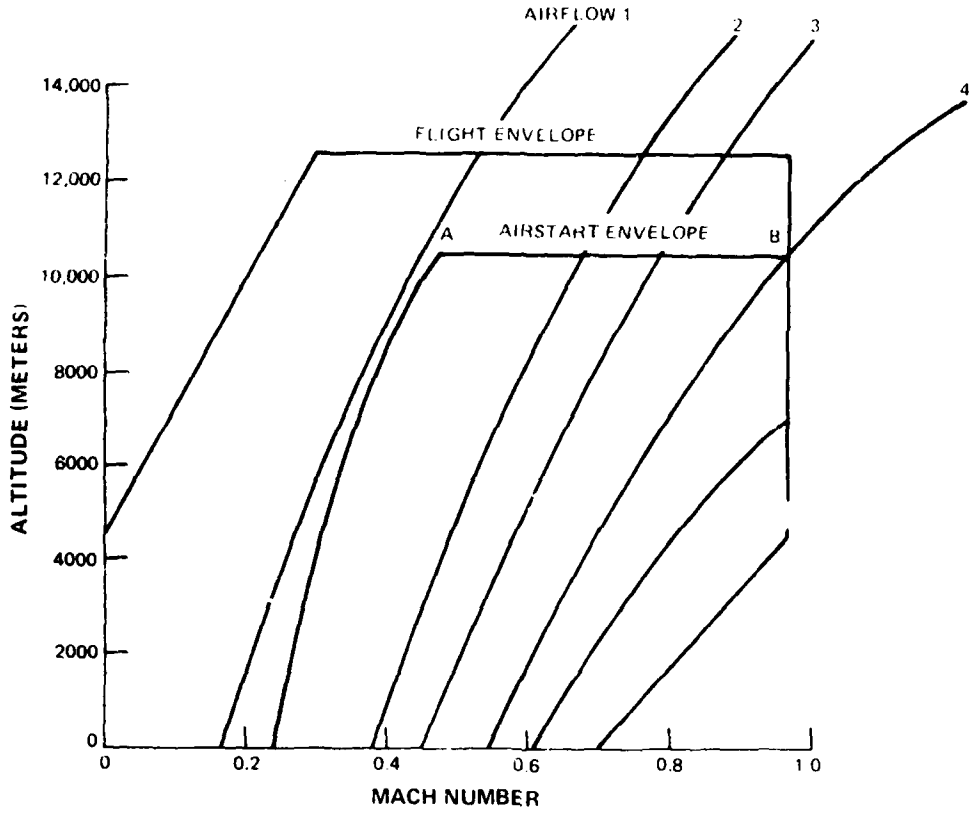

Figure 8 JT8D-17 Airstart Envelope

TABLE IV

COMBUSTOR INLET CONDITIONS AT ALTITUDE RELIGHT

Point on Figure 8	A	B
Altitude (Meters)	10,668	10,668
Flight Mach Number	0.475	0.97
Combustor Inlet Total Pressure (ATM)	0.30	0.66
Combustor Inlet Total Temperature (K)	241	294
Engine Airflow (kg/sec)	0.20	6.1
Fuel Flow* (kg/sec)	0.076	0.076

*Minimum fuel flow of JT8D engine control schedule

2.2 TASK 3 - FUEL HANDLING AND QUALITY CONTROL

2.2.1 Laboratory Degradation of Antimist Fuel

The initial degradation of small quantities of antimisting kerosene fuel for laboratory purposes was carried out in a kitchen-type blender for varying times up to 120 minutes.

2.2.2 Viscosity Measurements

2.2.2.1 Screen Mesh

A filter screen device (Standardized by U.S./United Kingdom AMK Technical Committee) was utilized as the primary method of measuring viscosity properties. The filter screen was a Dutch twill woven material designated 36L, 165 by 1400 mesh and of nominal 9 to 12 μm pore size. The absolute pore size was 16-18 μm. A sketch of the device and details of the filter holder are shown in Figure 9. A rubber stopper was placed under the filter outlet and the tube filled until it overflowed with the reference fuel. The stopper was removed and the time required for the meniscus to pass between the two reference marks was measured. All the reference fuel was allowed to flow out of the device. The stopper was then replaced and the procedure repeated with the antimisting kerosene test fuel. The remaining fuel was discarded. The ratio of the time for the antimisting kerosene to flow between the two marks and that for the reference fuel was calculated and reported as the filter ratio (FR). The filter holder was dismantled, the wire screen discarded, and the O-rings removed and wiped with a dry tissue. The filter holder was washed with acetone and dried in air. A new disc was placed in the apparatus and the device reassembled for the next measurement.

2.2.2.2 Orifice Flow Cup

The flow cup was constructed of brass with an orifice diameter of 6.6mm $\pm$0.0127mm. The cup was positioned at a sufficient height to permit the introduction of a 10 ml graduated cylinder with a glass funnel to collect fuel from the cup. The cup was filled with reference fuel while a finger was held

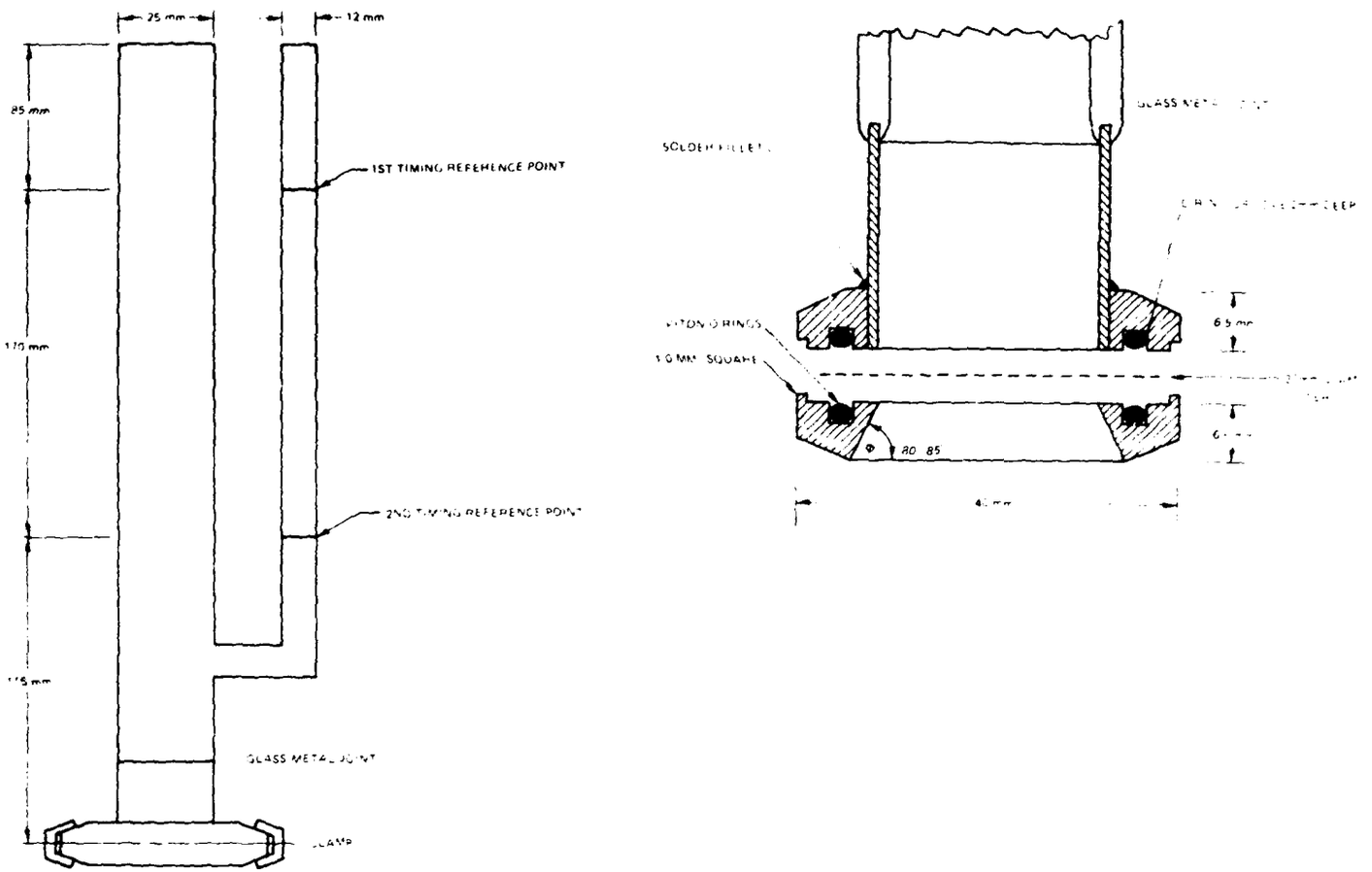

Figure 9 Filter Screer Device

over the orifice until the fuel overflowed. A beaker was placed under the cup, the finger removed and a stopwatch started. After exactly 30 seconds the graduated cylinder was placed under the cup, fuel collected for 30 seconds and the beaker again placed under the cup. The amount of fuel in the cylinder was recorded and, if within the range of 7.7 to 8.3 ml, the procedure was repeated with antimisting kerosene fuel. Replicate tests with antimisting kerosene were carried out until volumes collected agreed within 0.1 ml. Results were expressed as the ratio of flow rates of antimisting kerosene fuel to reference fuel. The reliability of the test was dependent upon maintaining cleanliness of the cup. When the cup was not being used, it was kept immersed in a beaker of jet fuel containing no antimisting kerosene additive (antimisting kerosene fuel was found to corrode the cup). The cup was rinsed with acetone and blown dry with air prior to use.

2.2.2.3 Standard ASTM Capillary Viscometer.

Viscosity of the antimisting kerosene fuel and parent fuel was measured by standard capillary viscometers according to ASTM D445 procedure. A Cannon Fenske reverse flow viscometer was used for the antimisting kerosene fuel and a Cannon Fenske routine viscometer for the parent fuel. The test is based on the time required for a given volume of fuel to flow through a capillary tube under carefully controlled conditions. A viscosity ratio was obtained by dividing the viscosity measured for the antimisting kerosene fuel by that of the parent jet fuel.

2.2.2.4 Glass Bead Bed

This apparatus consists of a bed of 210 μm glass beads packed in a 35 mm section of .64 cm inside diameter tube. The sample was forced through the bed at differential pressures up to 1 atm and the flow rate measured. In laminar flow, the flow rate is inversely proportional to the viscosity of the fluid; thus after calibration of the device with a sample of known viscosity the viscosity of unknowns can be determined.

2.2.2.5 Differential Pressure Flow Apparatus.

Filtration tests were carried out using a standard Millipore filtration apparatus (Figure 10). Tests were made with a paper filter, a polycarbonate filter and wire screen filter. The polycarbonate filters were manufactured by Nuclepore Corp. Pore diameter was 8 μm, pore density was 1 x 10^5 pores/cm^2 and nominal filter thickness was 10 μm. The filters are unique in that the pores are regular circular openings. The percent open area was calculated from the nominal pore diameter and density to be 5.0%. The characteristics of the wire screen filters are tabulated in Table V. The percent open areas of screens 316L and T304L were calculated from the difference in apparent density and the nominal density of stainless steel (7.8 g/cm^3). A fiber paper filter was tested with 40 μm nominal pore size. The test filters were cut directly from a JT8D fuel filter.

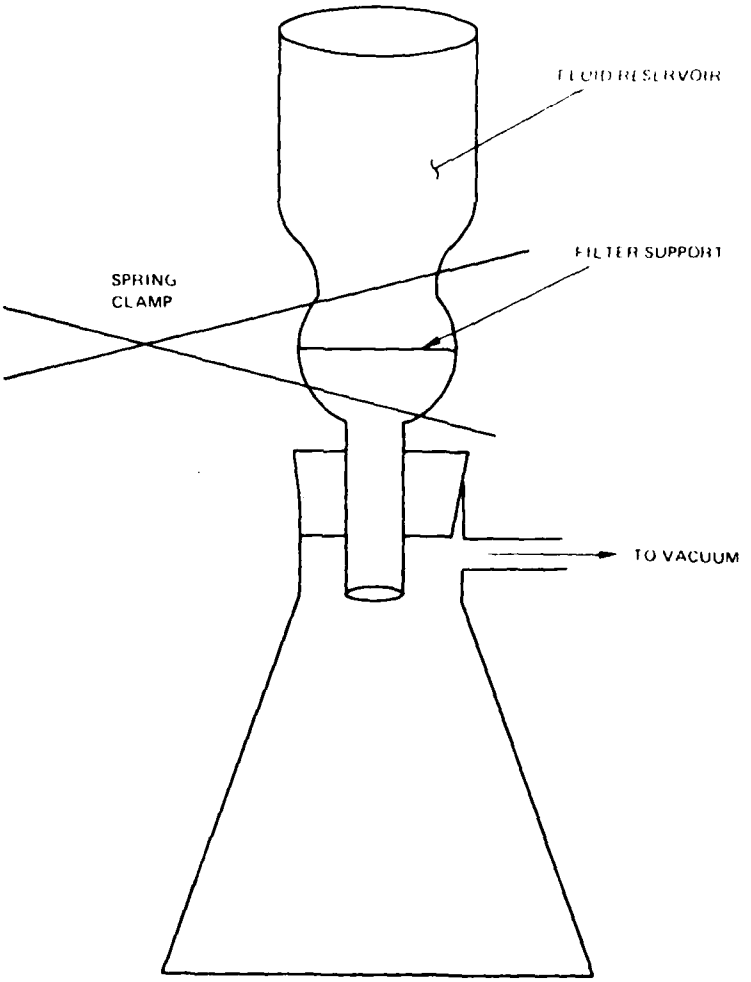

Figure 10 Millipore Apparatus

TABLE V

DUTCH TWILL WEAVE SCREEN CHARACTERISTICS

Designation	Diameter of Wires (cm)	Mesh	Pore Size Absolute	(μm) Nominal	Screen Thickness (cm)	Percent Open Area
316L	0.0071x0.0041	165x1400	16-18	9-12	0.0142	39.4
T304L	0.0038x0.0030	325x1900	9-10	2-3	0.0084	25.9

The filter tests were conducted by adding a measured quantity of antimisting kerosene to the reservoir over the filter and measuring the time with a stopwatch for the fuel to flow through the filter. The test was repeated at different vacuum settings from 8×10^4 to 87.5×10^4 Dynes/cm^2.

2.2.3 Antimisting Additive Content

The additive content of the antimisting kerosene fuel was determined by a controlled evaporation process. Duplicate 15 ml samples were transferred to clean, tared 100 ml platinum dishes. The samples were placed on a hot plate at medium heat and the volumes reduced until the samples approached a consistency of syrup (approximately 2 ml). The samples were then placed in an oven at a temperature of 150°C $\pm$2°C for two hours, after which they were transferred to a dessicator to cool. A blank prepared from the parent fuel used in blending the antimisting kerosene was subjected to an identical procedure. The weight percent of the additive was calculated from the weight of the sample residue after evaporation minus the weight of residue of the parent fuel blank. Table VI summarizes other fuel properties measured and the test methods used.

2.2.4 Fuel Shearing Comparison Between the JT8D Fuel Pump and Royal Aircraft Establishment Degrader

Comparative antimisting kerosene degrading tests were accomplished on a Pratt & Whitney Aircraft JT3D Engine Fuel Pump and a United Kingdom Royal Aircraft Establishment Degrader. The JT8D fuel pump is described in Section 2.1.2.1.

TABLE VI

FUEL PROPERTIES MEASURED AND TEST METHODS

Property	Test Method
Hydrogen and Carbon, wt. %	Perkin Elmer Model 240 Analyzer
Aromatics, vol. %	ASTM D1319
Sulfur, wt. %	Dohrmann Combustion/Titration
Specific Gravity, 288/288^{O}K	ASTM D1298
Flash Point, ^{O}K	ASTM D56
Freezing Point, ^{O}K	ASTM D2386
Carbon Residue, 10 Vol. % Bottoms, wt. %	ASTM D524
Net Heat of Combustion, cal./gm	ASTM D2382
Smoke Point, mm	ASTM D1322
Viscosity, 298K, cs	ASTM D445
Water Content, ppm	Karl Fisher Titration
Surface Tension, Dynes/ cm^{2}	ASTM D971
Thermal Stability	ASTM D3241
Distillation Curve	ASTM D86
Naphthalenes, Vol. %	ASTM D1840
Nitrogen, ppm	Kjeldahl Method
Mercaptan Sulfur, ppm	ASTM D1323
Metallic Trace Elements	Atomic Absorption

The Royal Aircraft Establishment Degrader (Model D61B), shown in Figure 11, consists of two stators, two pelton assemblies, and three rotors. The rotating assembly is supported by ball bearings. The rotors consist of flat discs perforated with holes to provide the degrading action on the antimisting kerosene. The peltons located between the rotors consist of radial rectangular cross section spokes. The stators located outboard of the rotors consist of flat discs perforated with holes. Fuel flow through the degrader is provided by external pumping means. A special fixture was designed and fabricated for mounting the degrader on the test stand gearbox. This fixture accurately aligned the degrader to ensure minimum side load on the bearings for the extremely high speed operating condition. Figure 12 shows the degrader mounted on the test stand.

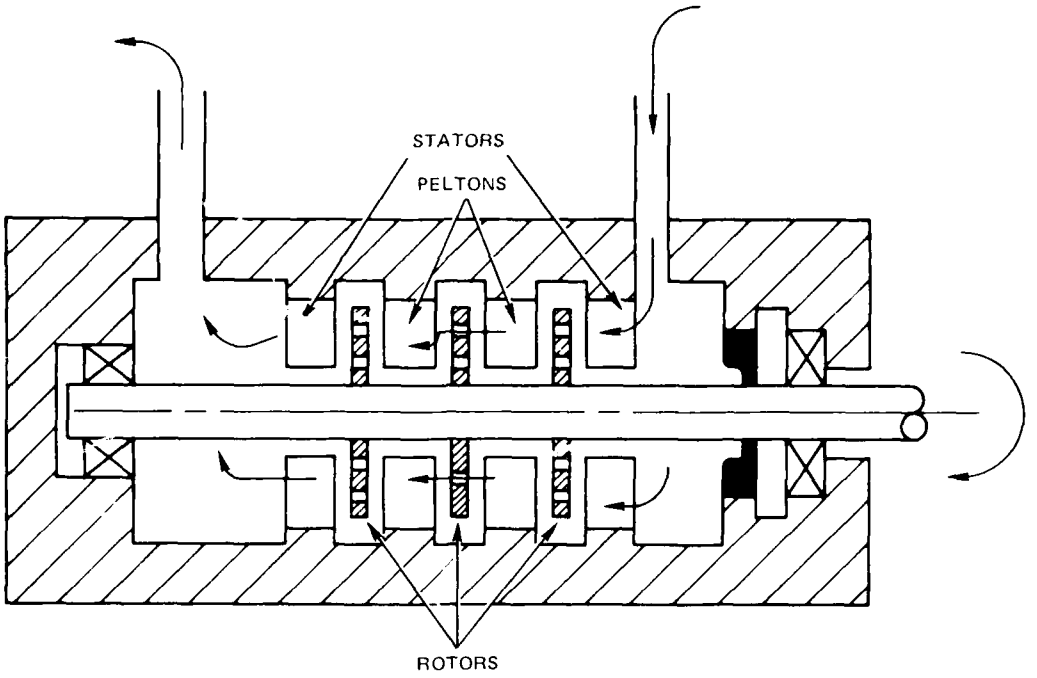

Figure 11 RAE Degrader Schematic

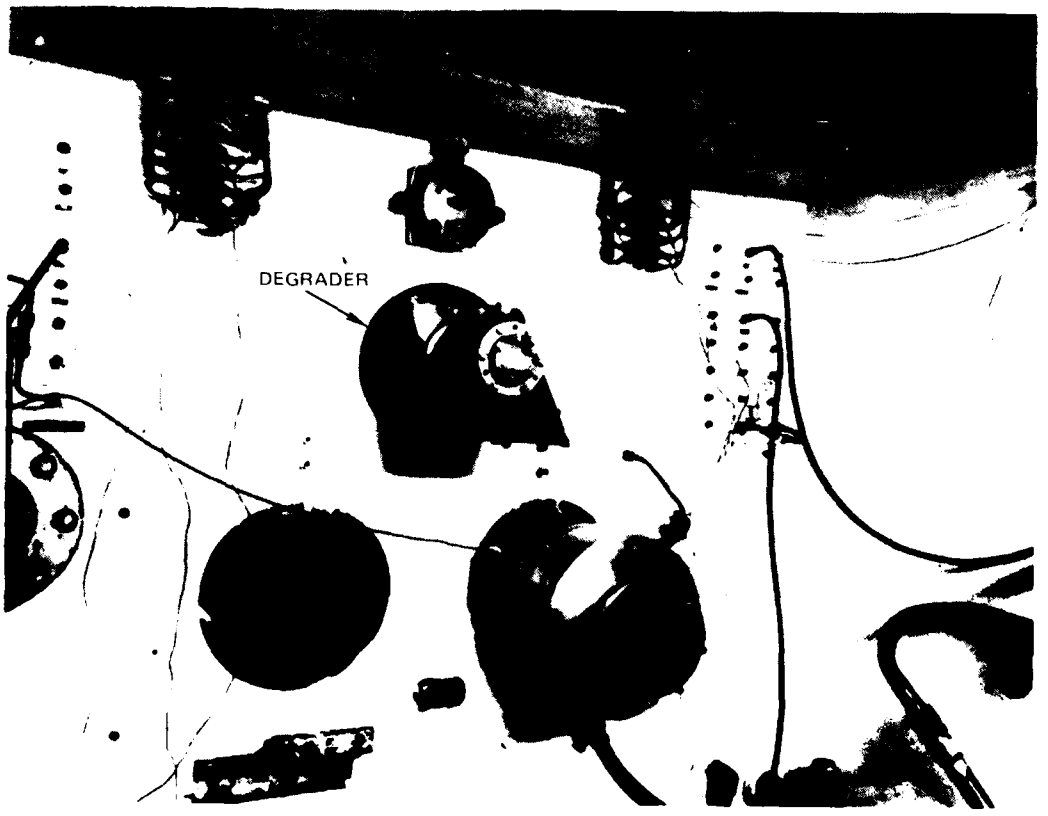

Figure 12 RAE Degrader Mounted On Test Stand

Antimisting kerosene fuel degradation, using either the fuel pump or Royal Aircraft Establishment Degrader, was processed at X-253 stand, located at the Pratt & Whitney Engine Control Systems Laboratory. It is a general purpose facility for testing fuel system components including fuel controls and fuel pumps at sea level conditions (from ambient temperature to 211K). A variable speed DC motor and gearboxes rated at 3040 kg m/s provide speeds to 14000 rpm. The stand has two flowmeter systems. The main flowmeter system has a flow range of 180 to 20,000 kg/hr. The tests are monitored on instrumentation specifically assigned or calibrated to the particular test fuels.

The test stand was modified by installing two existing Pratt & Whitney Aircraft fuel tanks and appropriate plumbing so that operation in either open or closed loop mode is available (Figure 13). In the open loop operation all the fuel flowed through the fuel pump systems to the collection tank. In the closed loop operation the flow from the discharge valve returned to the supply tank via a heat exchanger for continual operation. Figure 14 shows the specific test setup, instrumentation locations and fuel sampling locations for the JT8D fuel pump.

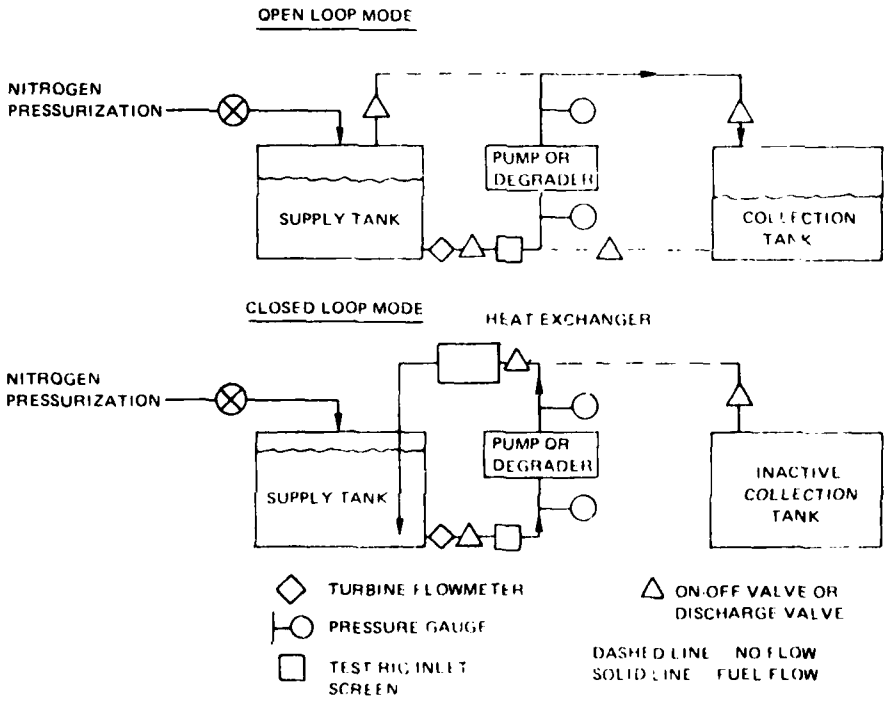

Figure 13 Schematic Arrangement of Fuel Degrading Test Rig

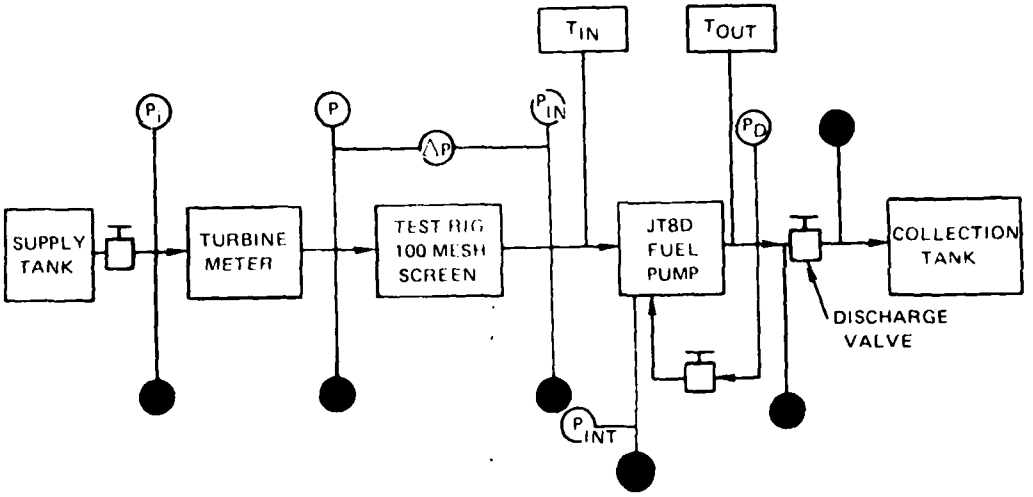

Figure 14 Instrumentation Fuel Sampling Locations

The turbine type flowmeters were calibrated initially with Jet A, undegraded and degraded antimisting kerosene by a catch and weigh technique. When subsequent levels of degraded antimisting kerosene were available, the flowmeters were again calibrated on these fuels.

Before the antimisting kerosene was processed the open and closed loop systems were operated with Jet A to familiarize personnel of stand operation and to remove contaminants that may have been present in the system.

At the completion of the degrading tests with the fuel pump using antimisting kerosene, the Royal Aircraft Establishment degrader was substituted on the test stand for a comparative evaluation with the fuel pump.

The JT8D fuel pump comparative test conditions for speed, pressure, through flow, and recirculation flow were typical of JT8D engine operating conditions. In addition to the RAE design condition, other conditions were selected to provide a direct speed and flow comparison with the JT8D fuel pump. The following parameters were recorded or monitored during the fuel degrading process.

1. Metered Fuel Flow
2. Temperature
3. System Supply Pressure-Pi
4. Degrader Differential Pressure
5. Inlet Pressure - Pin
6. Test Rig Inlet Screen Differential Pressure - ΔP
7. Fuel Pump Interstage Pressure - Pint
8. Fuel Pump Discharge Pressure - Pd
9. Drive Motor Voltage and Current
10. Filter Ratio Measurement

In the course of developing a fuel sampling test procedure, it was determined that additional degradation of the antimisting kerosene occurred while sampling from the system's high pressure locations. Figure 15 shows the sampling apparatus used to isolate the fuel and quiescently collect the sample at ambient pressure. In addition, the antimisting kerosene was loaded in the supply tank in a manner that minimized splashing or severe agitation to prevent antimisting kerosene degradation prior to a test run.

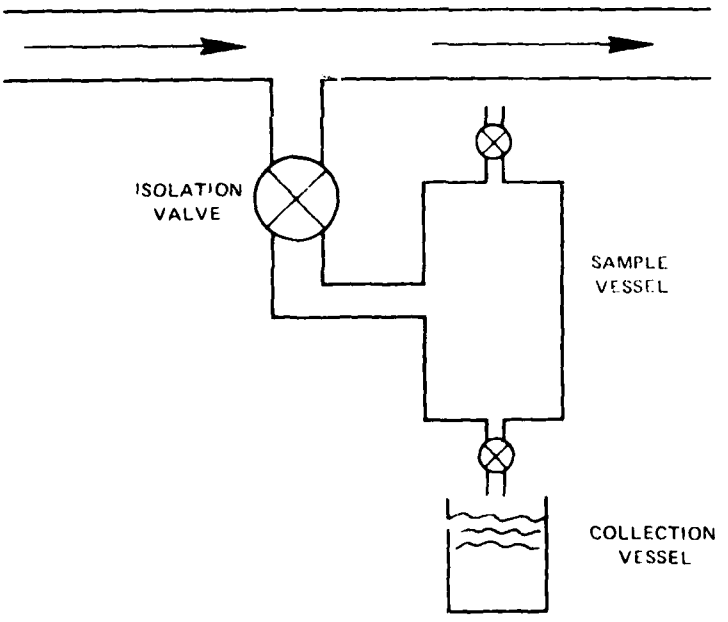

Figure 15 Sampling Apparatus

2.2.5 Procedure for Large Volume Processing of Antimisting Kerosene to Various Levels of Degradation

After completion of the JT8D engine fuel pump - Royal Aircraft Establishment Degrader comparison, the pump was considered the more effective method and was selected to process all subsequent program degraded antimisting kerosene requirements. Fuel degradation was accomplished by passing the antimisting kerosene through the JT8D fuel pump system N times. Hence, three-pass antimisting kerosene is antimisting kerosene passed through the fuel pump system three times.

To ensure that all antimisting kerosene within a batch was subjected to the degradation process for each pass, the first three passes were operated open loop. Subsequent passes were accomplished at closed loop and agitated to enhance homogeneous tank mixing. One pass for a 1514 liter (400 gallon) antimisting kerosene batch at the 24.6 liters/minute (6.5 gpm) processing rate took approximately one hour. Antimisting kerosene samples were obtained at various system locations and operating conditions and tested for filter ratio.

2.3 TASK 4 - PHYSICAL CHARACTERISTICS EVALUATION

2.3.1 Thermal Stability

The effect of antimisting kerosene additive on fuel thermal stability was determined with the Jet Fuel Thermal Oxidation Tester (JFTOT) as summarized in ASTM D3241. A schematic diagram of the fuel flow scheme is shown in Figure 16. The fuel was pumped at a fixed flow rate of 3 ml/min. through an annular passage where the fuel was heated as it flowed around an electrically heated aluminum tube. After exiting the heating chamber, the fuel entered a precision stainless steel filter (17 μm nominal porosity) where fuel degradation products were trapped. The test was run for 150 minutes and pressure drop (ΔP) across the stainless steel filter was recorded every 30 minutes. If during the 150-minute test the ΔP reached 25 mm, the filter was bypassed to finish the test. At the end of the test the deposits formed on the aluminum heater tube were compared with the ASTM Color Standard. The test failure criteria was a

\P equal or greater than 25 mm or a deposit code of 3 or greater. To determine the thermal stability breakpoint (the temperature at which a failure occurs), tests were run at successively higher temperatures until the failure occurred. Breakpoint tests were run with parent jet fuel, 3-pass (filter ratio = 1.6) and 16-pass (filter ratio = 1.2).

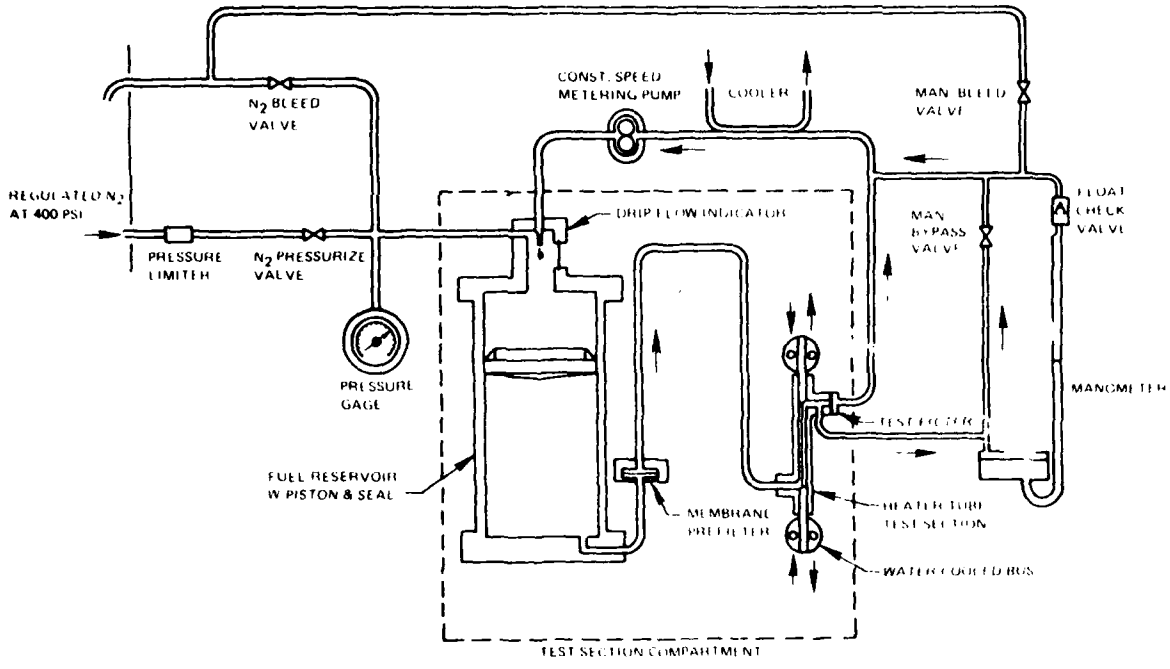

Figure 16 Thermal Stability Tester

2.3.2 Water Solubility

To determine the effect of the antimisting kerosene additive on water solubility in fuel, 100 ml of parent fuel and 100 ml of undegraded antimisting kerosene fuel were equilibrated with 10 ml water by shaking. After shaking, the samples were centrifuged to separate the water from fuel. Fuel samples were then drawn from the fuel layers and titrated by the Karl Fisher technique for water content.

2.3.3 Corrosion of Copper

It was noted that when the orifice cup viscosity device remained immersed in antimisting kerosene for several hours, the fuel took on a characteristic blue color typical of many copper compounds. It was felt that copper corrosion might potentially be harmful since traces of copper in fuel at levels of less than .02 ppm have been responsible for degraded thermal stability. To determine if antimisting kerosene gave accelerated corrosion rates with copper, approximately 400 ml of antimisting kerosene fuel and parent fuel were equilibrated with light copper turnings for 48 hours. Samples of fuel were withdrawn from both parent and antimisting kerosene samples after 2, 24 and 48 hours and analyzed for dissolved copper directly by atomic absorption spectrophotometry using Conostan standards.

2.3.4 Fuel-Oil Cooler Heat Transfer Tests

Typical fuel-oil coolers used in aircraft gas turbine engines are shell and tube heat exchangers in which the fuel flows inside the tubes and the oil flows across the tubes. Because the fuel side is usually single pass, and the fuel side velocity is somewhat low, the fuel side is usually turbulated to produce enhanced heat transfer coefficients. Pratt & Whitney Aircraft oil coolers are typically constructed from tubes which are dimpled at frequent intervals to increase heat transfer coefficients. The heat transfer tests were conducted by flowing ambient temperature fuel through an aluminum tube surrounded by a 5 cm diameter shell (See Figure 17). The inner tube is 33 cm long with an outer diameter of 0.23 cm and an inner diameter of 0.17 cm. The fuel pressure was maintained above its thermodynamic critical pressure, 22 atm, throughout the tests. Saturated steam, at 5 atm, flowed through the shell. Due to the saturated nature of the steam and the large shell to tube volume ratio, the inner tube could be considered to be surrounded by a constant temperature reservoir.

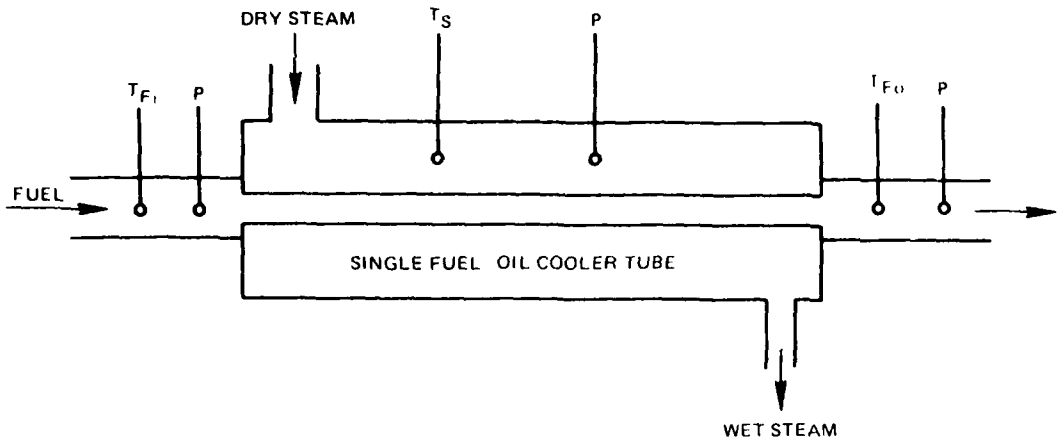

Figure 17 Heat Transfer Test Section

A heat transfer test consists of setting a fuel flow, adjusting the fuel pressure, turning on the steam, and allowing sufficient time for thermal equilibrium. Heat transfer coefficients are derived from the following energy balance (conduction terms neglected).

$$Q = W_F \, CP_F \, (T_{Fo} - T_{Fi}) = U_F \, A_F \, (\Delta T_{LMTD}) \tag{1}$$

where

$$\Delta T_{LMTD} = \frac{T_{Fo} - T_{Fi}}{\ell n \left[\dfrac{T_S - T_{Fi}}{T_S - T_{Fo}} \right]} \tag{2}$$

$$\frac{1}{U_F} = \frac{1}{\left(\dfrac{d_o}{d_i} \right) h_s} + \frac{1}{h_F} \tag{3}$$

From equation (3)

$$h_F = \frac{\left(\frac{d_o}{d_i}\right) U_F \, h_s}{\left(\frac{d_o}{d_i}\right) h_s - U_F} \qquad (4)$$

where U_F is determined from Equation 1.

The symbols used in the equations above are defined as:

A_f Cross sectional area - m^2

d_i inner diameter - m

d_o outer diameter - m

h_f film heat transfer coefficient - $\frac{cal}{hr \ m^2 \ ^oK}$

h_s steam heat transfer coefficient - $\frac{cal}{hr \ m^2 \ ^oK}$

Q heat flux - $\frac{cal}{m^2 \ hr}$

T_{ti} entering fuel temperature - K

T_{to} exiting fuel temperature - K

T_s steam temperature - K

W_f fuel flow rate - $\frac{Kgm}{hr}$

Since the geometry is known, the temperatures and flowrates can be measured and h_s can be calculated by the method of Reference 1 (h_s was found to be 25 kcal/hr m^2 ^oK), hence, h_F can be determined from Equation 4.

The fuel tested was Jet A, unsheared, 1-pass, and 3-pass antimisting kerosene. The antimisting kerosene was provided from a gas pressurized reservoir to avoid additional degradation.

Temperatures were measured with C_L-A_L thermocouples. The fuel and steam pressures were measured with pressure gauges. The tube pressure drop was measured with a calibrated differential pressure transducer. Flow rates were measured using turbine meters and a catch and weigh technique.

2.3.5 Materials Compatibility - Elastomers

Materials generally used in aircraft gas turbines were evaluated for compatibility with antimisting kerosene using procedures in accordance with ASTM D1414-72. The materials were soaked in antimisting kerosene for 6 months and periodically inspected for changes in mechanical properties. Table VII lists the test variables.

Butadiene rubber and fluorosilicone rubber are used in gas turbines for severe temperatures; up to 395K and 450K respectively.

TABLE VII

TEST VARIABLES FOR MATERIAL COMPATIBILITY TESTS

Common Name	AMS Specification	Military Specification	Part
Butadiene Rubber	7271	MS 9021	O-ring
Fluorosilicone Rubber	7273	MS 9967	O-ring
Fluorosilicone Rubber/ Fiberglass	-	-	Diaphragm (P&WA P/N 442375)

Fuels:
- Undegraded antimisting kerosene
- 3-pass degraded anti-misting kerosene

Inspection Times:
- 1 week;
- 1,2,3,4,5,6 months

Fuel Temperatures:
- 295K
- 340K

Measurements:
- Tensile strength
- Elongation
- Volume Change
- Hardness

2.3.6 Flow Meter Calibration

During this program both standard turbine meters, venturiis, and a Micro Mass Meter (Micro Motion Inc.) were used to measure antimisting kerosene flow rate. The Micro Motion Mass Flow Meter comprises two units: (1) mass flow sensor unit and (2) electronic processing and readout unit. The mass flow sensor consists of a U shaped pipe which is vibrated at its natural frequency. The oscillation of the pipe and the velocity of the flowing fluid subjects each particle of the fluid to a coriolis-type acceleration that angularly deflects the pipe an amount proportional to the mass flow rate. The angular deflection of the U shaped pipe is measured with optical detectors yielding (after a suitable calibration) the mass flow rate. Since the meter measures mass flow

rate directly, there is no need to measure velocity, temperature, viscosity or density. The accuracy and calibration of the meter is independent of the properties of the fluid being measured.

Tests were conducted with turbine meters, venturiis and the mass meter using Jet A and various levels of degraded antimisting kerosene to determine the relative performance of each instrument while measuring antimisting kerosene flow rates.

2.4 TASK 5 - FUEL FILTER TESTS

The JT8D engine fuel filter system is described in Section 2.1.2.4. The filters used in this task are described in the following paragraphs.

2.4.1 Engine Fuel Pump Paper Filter

The engine fuel pump paper filter supplied by Thompson Ramo Wooldridge and shown in Figure 3 has approximately 3600 cm^2 (570 sq. in.) of surface area. It will remove 98 percent of particles greater than 40 micron. The filter is located in the engine metered flow path downstream of the engine fuel de-icing heater and upstream of the fuel pump high pressure gear stage.

2.4.2 Engine Fuel Control Filter Assembly

The engine fuel control filter assembly supplied by Hamilton Standard Division is a two element filter as shown in Figure 18. A photograph of the filters and test fixture is shown in Figure 19. The coarse element, a 25 cm^2 area, 50 mesh filter, provides large particle contaminant protection for all fuel control components in the total fuel flow path. The wash flow element provides fine particle protection for the fuel control servo system through a 10 cm^2 surface area, 325 mesh filter.

2.4.3 Engine Fuel Control Servo System Secondary Filter

The engine fuel control servo system secondary filter also shown in Figure 19 has approximately 6.1 cm^2 surface area and 50 mesh filtration.

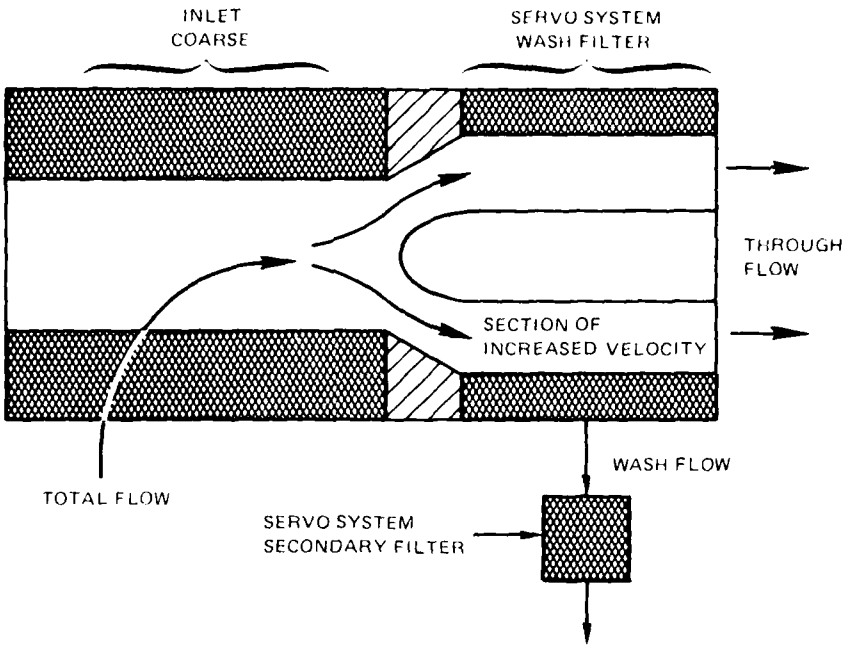

Figure 18 JT8D Fuel Control Filter Assembly

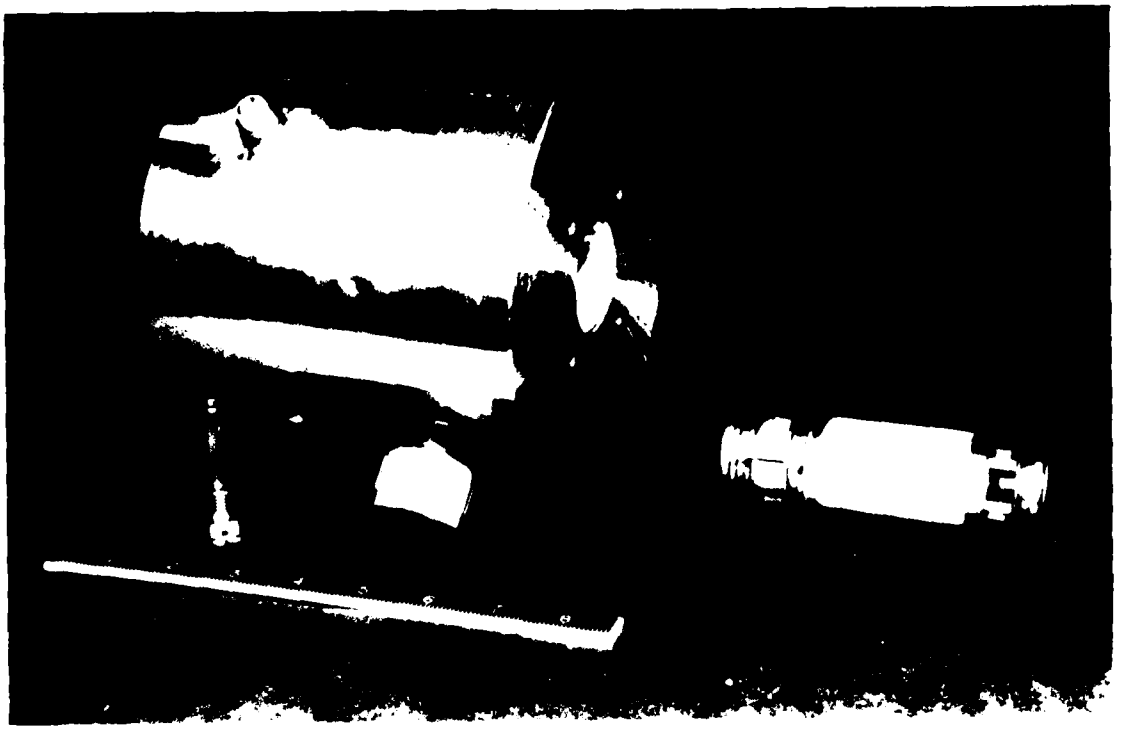

Figure 19 Engine Fuel Control Filter Assemblies and Test Fixture

2.4.4 Test Rig Inlet Screen

Although not part of the engine fuel system, the test rig inlet screen is also discussed since it was a significant item in the test system operation. This screen is similar in filtration quality to screens typically found in aircraft engine fuel systems. The screen consists of stainless steel plain weave wire, with approximately 89 cm^2 of effective open flow area and 100 mesh filtration.

2.4.5 Facilities

The low temperature test facility discussed in Section 2.2.8 was utilized for all the filter performance and extended duration tests.

The filters were flow checked in X-256 or X-257 stand, which are general purpose facilities for testing fuel controls, exhaust nozzle controls, pressurizing and dump valves, heater/filter, etc., at ambient conditions. The stands consist of an open test bench in the static test area. Fuels such as JP-4, PMC-9041, JP-5 and special test fuels can be supplied to the test component at flow rates from 159 kg/hr to 27,240 kg/hr and at pressures up to 6900 kpag over a temperature range from ambient to 339K. Nitrogen gas which is also available can be regulated up to 3450 kpag for signal pressure use. Figure 20 shows the setup used for the filter test stand. When one filter was tested, all other filters were removed from the rig. Special fixtures were designed and fabricated or modified from existing hardware for evaluation of each filter assembly. A fixture to contain the various engine fuel control filter assemblies is shown in Figure 19. In addition, the engine fuel control filter cover and centerbody details were modified to enable pressure sensing within the assembly and thereby provide measurement of the coarse filter element differential pressure and the wash filter element differential pressure. An existing JT8D engine fuel pump housing assembly along with suitable flow blockage adapters was used to individually test the fuel pump paper filter.

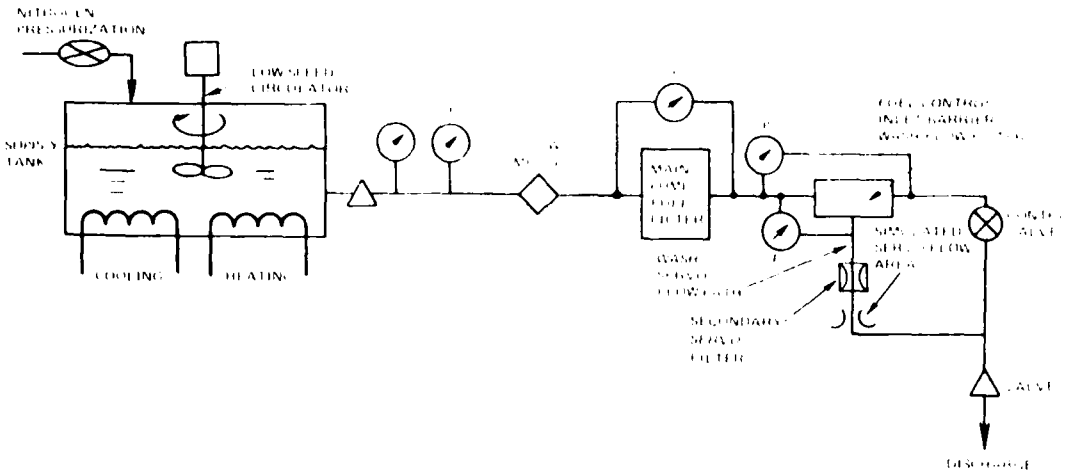

Figure 20 *Test Apparatus for Evaluating Filter Pressure Drop Characteristics*

An attempt was made to reduce antimisting kerosene consumption during the filter tests by blocking off part of the filter surface area. However, the tests exhibited nonrepeatable differential pressure charactersitics and their use was discontinued. All subsequent tests were run with the full filter area. Results were then repeatable.

2.4.6 Test Procedures

The test procedure for the performance testing of the JT8D engine fuel pump filter, fuel control filter assembly, and fuel control servo system secondary filter was the following:

1. The filter assemblies in their appropriate fixtures were initially flow checked using PMC 9041 to determine necessary instrumentation ranges for eventual operation on antimisting kerosene and Jet A. PMC 9041 conforms to MIL-F-7024A Type II test fluid.

2. Typical JT8D engine flow and resulting differential pressure data on Jet A was obtained for each filter element.

3. The system was run with the 3-pass and 16-pass degraded antimisting kerosene. Comparative flow and differential pressure was obtained for each individual filter.

The test procedure for the endurance testing of the JT8D engine fuel pump filter, fuel control filter assembly and fuel control servo system secondary filter was the following:

1. New pump and fuel control filter cartridges were incorporated in the appropriate fixtures.

2. The supply tank was filled with 16-pass antimisting kerosene.

3. The antimisting kerosene was flowed through the filter assemblies in series to simulate a typical engine operating condition. A portion of the flow was diverted through the wash flow and secondary servo filter to simulate servo flow.

The following parameters for both the performance and duration tests were monitored or recorded.

1. Supply Tank Pressure
2. Inlet Temperature
3. Total Fuel Flow, Servo Wash Flow
4. Supply Antimisting Kerosene Filter Ratio
5. Fuel Pump Filter Differential Pressure
6. Servo Wash Filter Differential Pressure
7. Servo Secondary Filter Differential Pressure
8. Inlet Screen Differential Pressure
9. Filter Discharge Filter Ratio

The inlet screen characteristics were monitored while the antimisting kerosene was processed for the various program tasks.

A summary of the filters and fuels used in Task 5 testing is given in Table VIII.

TABLE VIII

TASK 5 FILTERS AND FUELS

Filter	Fuel for Duration Test	Fuel for Performance Test
Fuel Pump Paper Filter	16-pass	PMC 9041, Jet A, 3 and 16-pass antimisting kerosene
Fuel Control Filter Assembly 1. Inlet Coarse Filter 2. Servo System Wash Filter	16-Pass	PMC 9041, Jet A, 3 and 16-pass antimisting kerosene
Fuel Control Servo System Secondary Filter	16-Pass	PMC 9041, Jet A, 16-pass antimisting kerosene
Test Rig Inlet Screen	0-16-Pass	

2.5 TASK 6 - FUEL INJECTOR PERFORMANCE TESTS

An existing ambient fuel spray test facility was used to establish the fuel spray spatial distribution and the droplet size distribution produced by the JT8D Bill-of-Material (B/M) injector, low emission (LE) airblast injector, and an air-boost injector. Spray characterization tests were conducted using four fuels; Jet A, one-pass degraded, three-pass degraded, and undegraded FM-9 antimist fuels. A Malvern Model ST1800 particle size analyzer was used to determine te droplet size distribution. Patternator probes and photographs were used to obtain spatial distribution information.

2.5.1 Description of Facility

The spray facility used in the test program is depicted in Figure 21. The facility was equipped with a 20-probe patternator rake used to evaluate the liquid distribution downstream of the injector. In this program, patternator measurements were obtained at a distance of 7.6 cm from the nozzle discharge plane. Still pictures recorded the spray pattern and served as a basis for measuring spray cone angles and to document fuel streaking. The photographs were obtained using a high power General Radio Strobolume to illuminate the spray; the ten microsecond light pulse produced by a strobe substantially stopped the droplet motion.

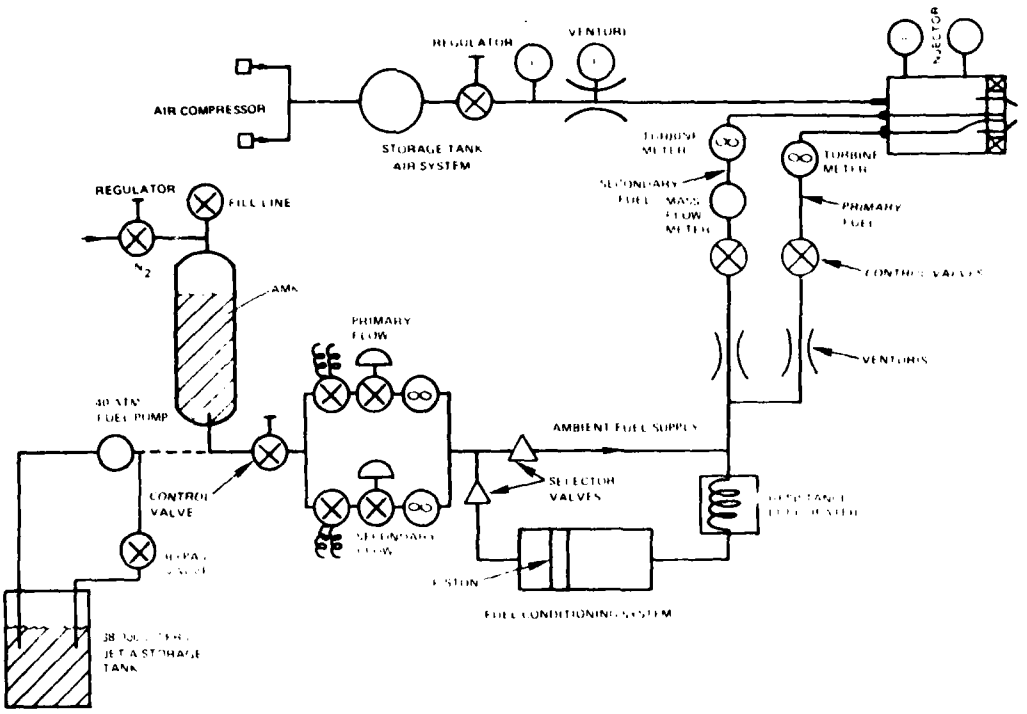

Figure 21 Ambient Pressure Spray Facility

The particle size analyzer (Figure 22) operated on the basis of the measurement and analysis of the distribution of the diffracted portion of a beam of monochromatic (laser) light which passed through the spray. An analytical program executed within a dedicated mini-computer provided a comparison of the measured light energy distribution with a calculated energy distribution based on a Rosin-Rammler droplet size number distribution. The program operated by continuously modifying the distribution function parameters (the characteristic diameter, PE, and the exponent parameter, W) until a best fit between experiment and prediction was obtained. The Rosin-Rammler distribution function is:

$$1 - v = e^{-\left(\frac{d}{PE}\right)W}$$

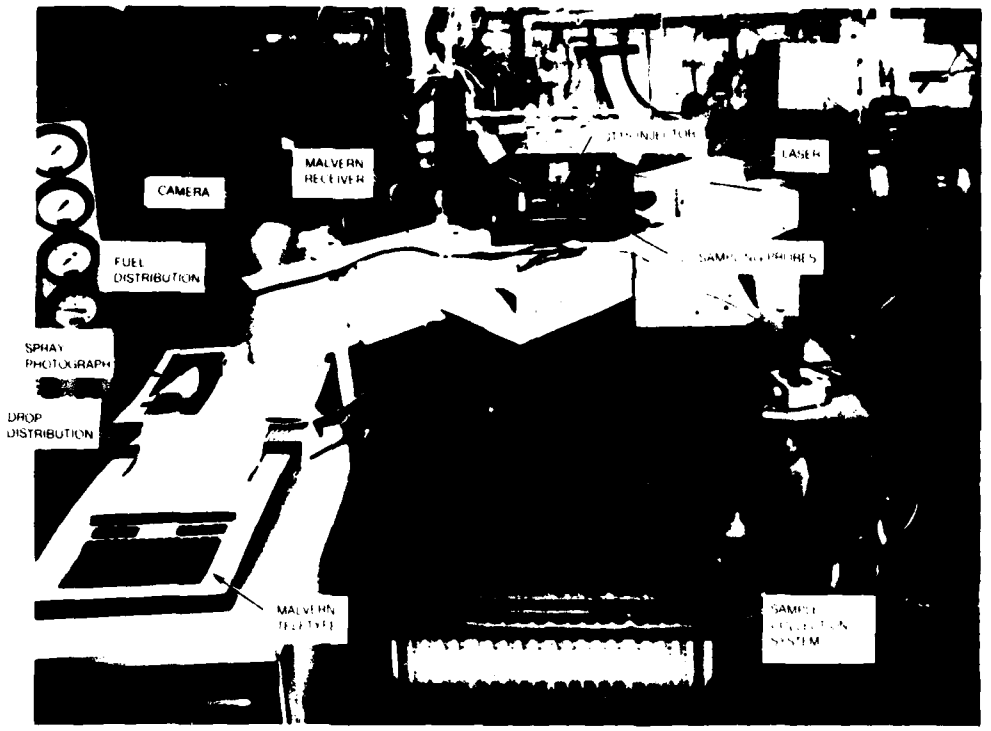

Figure 22 Malvern Droplet Distribution Analyzer

where: v is the volume fraction of droplets with a diameter less than d. The SMD is defined as the diameter of a droplet having the same volume to surface area of the entire spray. It can be calculated from the characteristic diameter and the exponent parameter as:

$$\frac{SMD}{PE} = \frac{1}{\Gamma(1 - \frac{1}{W})} = \frac{1 - (\frac{1}{W})}{\Gamma(2 - \frac{1}{W})}$$

where: $\Gamma(X)$ = Gamma Function.

In this program, all measurements were obtained at a l ation 5 cm. downstream of the nozzle tip. The range of droplet sizes that cou ı be detected by the instrument as configured for use in this program va ie from 562 microns to 5.7 microns.

Fuel was delivered to the test apparatus using the delivery system shown schematically in Figure 21. The Jet A fuel was supplied from an underground facility storage tank. The anti-misting fuels, which had previously been processed to the desired level of degradation, were stored in a 87 liter accumulator which formed a portion of the fuel temperature conditioning system. Jet A fuel was supplied either directly to the injector being tested (when Jet A was the test fuel) or was delivered to the fuel conditioning system where the Jet A was used to displace the test fuel from the accumulator. The total rate of fuel flow was obtained for all tests by measuring the Jet A flow rate using conventional turbine meters. The fuel conditioning system used a cold acetone bath to chill the test fuel to the desired temperature levels. An electrical resistance fuel heater was used to obtain the elevated fuel temperatures. After temperature conditioning, the fuel was split into the primary and secondary flows. For these tests the secondary flow rate was measured by use of a mass flow meter which was insensitive to the viscosity characteristics of the fuel.

2.5.2 Fuel Injectors

The pressure atomizing injector currently used in the JT8D engine is a duplex nozzle in which the primary flow is discharged through a central orifice and the secondary flow issues from a surrounding annular passage (Figure 23). The nozzle was fitted with an air shroud (nut) to prevent carbon from collecting on the nozzle tip. In these tests the nozzles were mounted in a cannister which supplied air to the nozzle nut. In the engine, the nozzle is surrounded by an air swirler which discharges swirler air into the head end of the combustor. The swirl air which may affect the fuel distribution, but not the atomization, was not supplied in these tests.

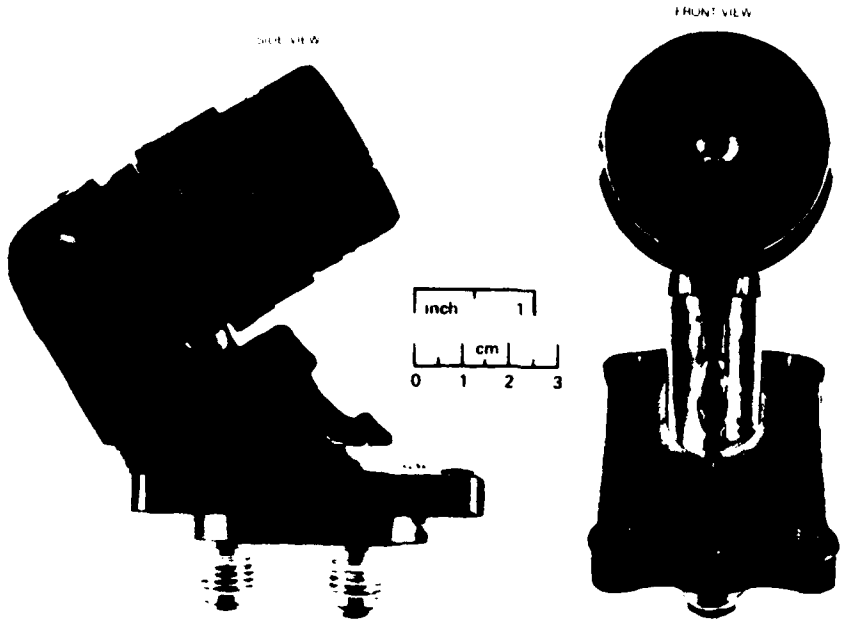

Figure 23 JT8D Bill-of-Material Injector

The low emission JT8D nozzle (Figure 24) is a hybrid nozzle composed of a pressure atomizing primary nozzle and an airblast (or aerating) secondary nozzle. Fuel is atomized in the secondary passage by shearing the fuel off an annular surface to which a film of fuel is supplied. The high velocity air used to atomize the air is supplied from the engine diffuser; the air velocity is developed by the pressure drop existing across the combustor liner. In the nozzle test program, the injector was mounted in a cannister to which air was supplied at the appropriate condition. Airblast nozzles generally produced a wider range of droplet sizes than pressure atomizers and yielded a large number of small droplets.

Because of the poor atomizing characteristics of the antimisting fuel, a nozzle having a high capability for atomizing heavy or viscous fluids was used. An air boost nozzle (Figure 25) which employed an external supply of high pressure air was tested for this purpose. This nozzle, which is not tailored for aircraft engine use, had a somewhat lower flow capacity than the JT8D nozzle. Boost air was supplied to the nozzle at 4 atm for all tests.

Figure 24 Low Emissions JT8D Injector

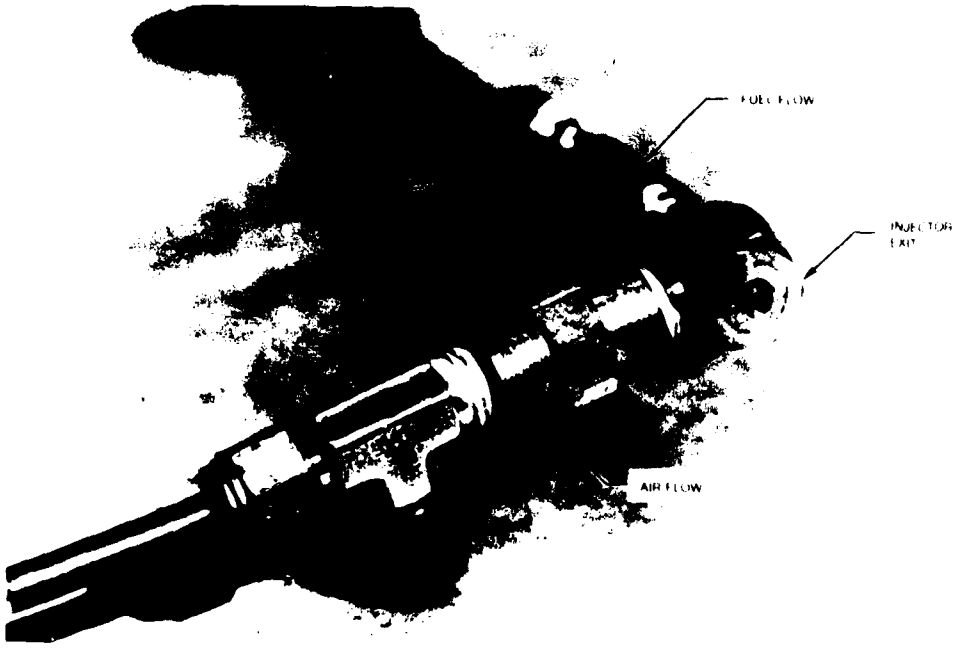

Figure 25 Delavan Air Boost Injector

2.5.3 Test Conditions

The fuel flow rates and the fuel temperatures at which the spray characterization tests were conducted are shown in Table IX. The fuel flow rates correspond to the engine ignition, idle, cruise, and sea-level-takeoff conditions. At each engine condition, tests were conducted at two fuel temperatures: room temperature and either a low temperature or a high temperature condition. Table IX also shows the air side pressure drops used in the tests. For the pressure atomizing and airblast atomizing nozzles, the air side pressure drop was set to yield the same air velocity that would exist in the engine burner at the given flight condition due to burner pressure drop. In the case of the air boost nozzle, the pressure drop indicated was the difference between the boost air supply pressure and the ambient pressure and corresponded to the maximum pressure drop recommended by the manufacturer.

TABLE IX

FUEL NOZZLE SPRAY EVALUATION -- TEST CONDITIONS

Injector: Bill-of-Material (B/M)

Engine Condition	wpri (kg/hr)	wsec (kg/hr)	Tfuel (°C)	Pair (kpa)
Ignition	30	--	15, -29	3.1
Idle	58	--	15, 46	3.4
Cruise	66	108	15, 46	6.6
SLTO	73	422	15, -29	6.9

Injector: Low Emission (LE)

Engine Condition	wpri (kg/hr)	wsec (kg/hr)	Tfuel (°C)	Pair (kpa)
Ignition	30	--	15, -29	3.4
Ignition	--	30	15, -29	3.4
Idle	58	--	15,	3.4
Idle	--	58	15, 46	3.4
Cruise	66	108	15, 46	6.6
Cruise	--	174	15, 46	6.6
SLTO	73	422	15, -29	6.9
SLTO	--	496	15, -29	6.9

Injector: Air-Boost

Engine Condition	w (kg/hr)	Tfuel (°C)	Pair (kpa)
Ignition	30	15, -29	414
Idle	45	15, 46	414
Cruise	159	15, 46	414
SLTO	227	15, -29	414

2.6 TASK 7 AND OPTIONAL TASK A - COMBUSTOR PERFORMANCE TESTS

2.6.1 Emissions and Performance Tests

Emissions and performance evaluations, exclusive of the altitude relight tests, were conducted in a high pressure test facility (X-904 stand) located at Pratt & Whitney Aircraft's Middletown test facility. Airflow capability is presented in Table X. A comprehensive description of the facility is contained in Reference 2.

TABLE X

X-904 STAND HIGH PRESSURE FACILITY

Air supply (kg/sec)	11.34
Burner Inlet Pressure (atm)	47.6 Max.
Burner Inlet Temperature (K)	922 Max.

A schematic and photograph of the JT8D combustor rig installation are presented in Figures 26 and 27. This rig simulated a 40 degree sector of the JT8D engine including compressor discharge, diffuser struts, and aircooled turbine entrance transition duct. In addition, provisions were made for extracting inner diameter and outer diameter bleeds in amounts representative of the turbine cooling air requirements of the JT8D-17 engine. This allowed a more precise simulation of the JT8D-17 engine operating conditions.

Instrumentation on this rig included combustor inlet total pressure and total temperature rakes, and airflow measurement in both the inlet and turbine cooling air extraction systems. The combustor inlet temperature and pressure instrumentation consisted of an array of 4 Chromel-Alumel total temperature thermocouples, 5 total pressure rakes each having five measurement ports, and 7 wall static pressure taps. This instrumentation was arranged in a fixed array at the plane simulating the axial position of the last compressor stage. Combustor inlet humidity was monitored using a Model 2740 Foxboro Dewcell Humidity meter. Air at a low mass flow rate was extracted from the test stand inlet duct and directed through the humidity meter.

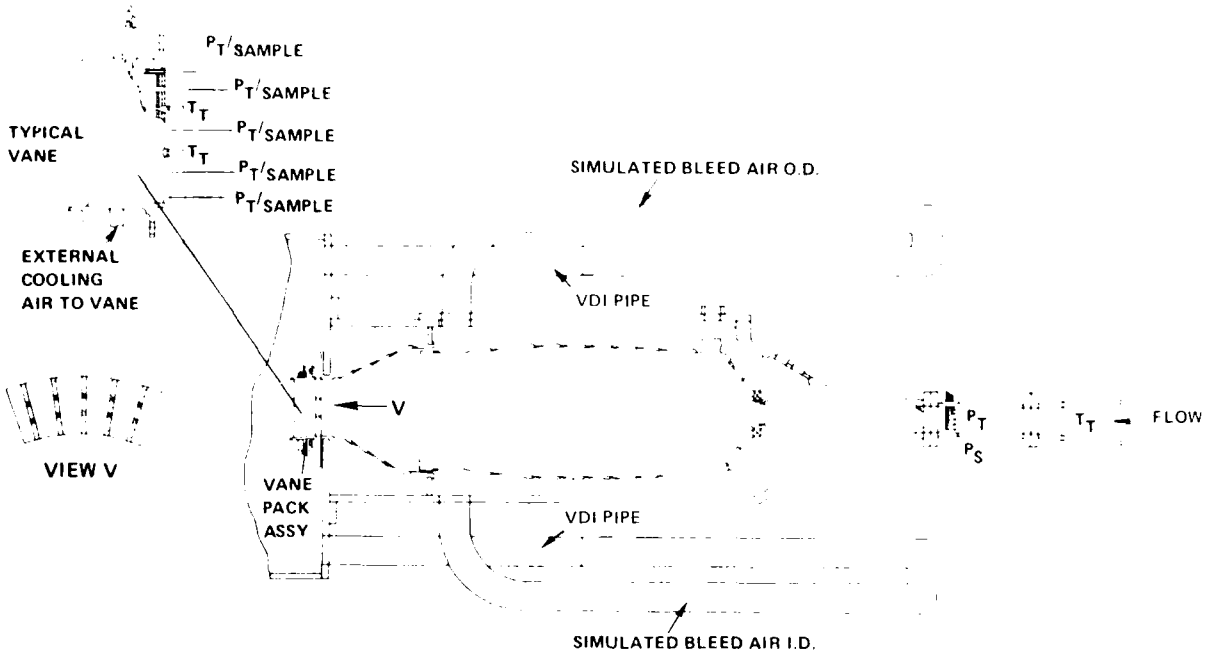

Figure 26 Schematic of JT8D Combustor Rig

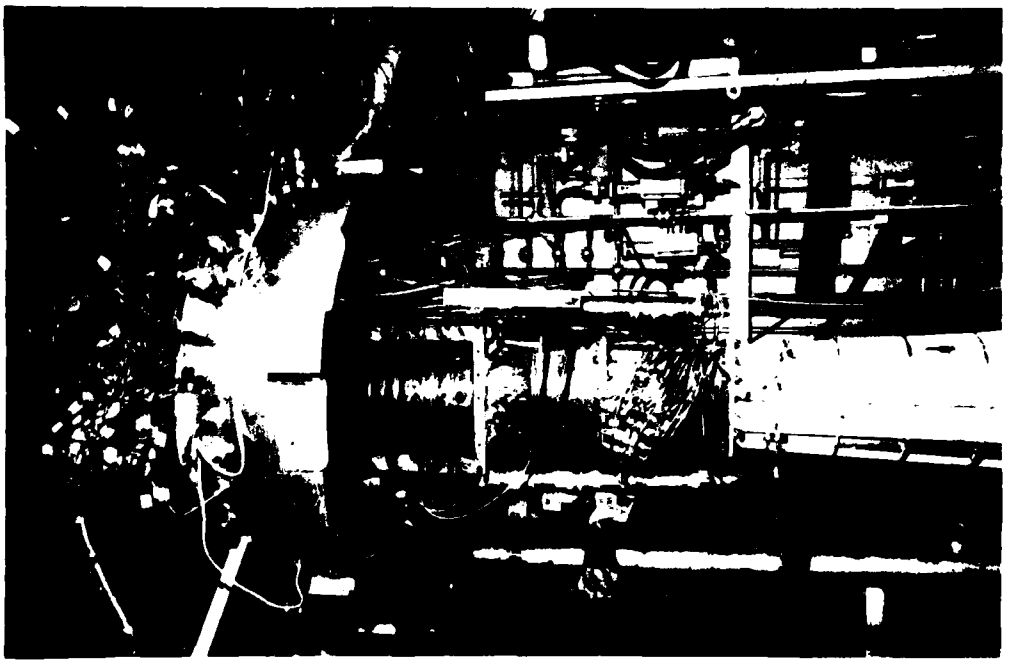

Figure 27 X-904, M.T.F., Open Rig, (Jan., 1977) R70293

Sixteen Chromel-Alumel thermocouples were installed on the louvers of each combustion can to observe any differences in liner heat load produced by combustion of antimisting kerosene.

Combustion exit temperatures and pressures were measured by a fixed instrumentation array mounted in an aircooled vane pack. Figure 28 is a photograph of the vane pack which consisted of 7 production JT8D turbine vanes. The five center vanes were each instrumented with five sampling/pressure ports and two thermocouples. The thermocouples were located near the center of each vane to concentrate temperature measurements in the expected hot areas.

Figure 28 JT8D Combustor Exit Instrumentation Vane Pack

The gas temperature thermocouples in the vane pack employed a grounded immersion type of junction with ISA Type B thermocouple wire. The calibration of this wire is accurate to 1980K. The gas sampling heads and lines were made from stainless steel tubing. When emissions or smoke were to be measured the samples from all 25 sensors were mixed in a manifold and fed to the analysis equipment. When these sensors were used to measure total pressure the sample lines were deadended by closing the selector valves and the pressure recorded

on a transducer in the [illegible]. Temperature measurements on this type of [illegible] were used to verify that the gas samples were quenched to 420 to [illegible] and the sample lines between the valves and the [illegible] were electrically or steam heated to maintain the sample temperature at about 420F to avoid condensation of hydrocarbons from the sample.

The emissions and smoke [illegible] in the Middletown Test Facility conformed to the specifications of [illegible], and AIR 1179 and those of the Federal Register, Vol. 38, No. 136, July 17, 1973 and to Vol. 43, No. 58, March 24, 1978. The burner test stand complex in the Middletown Test Facility is equipped with a computer controlled automatic data acquisition system. All data from the instrumentation [illegible] with the exception of the smoke measurements, were processed through an on-line Sigma 5 computer that provided essentially real time data analysis. The data reduction program computed combustor operating parameters such as diffuser inlet Mach Number, fuel air ratio, ideal temperature rise and emission indices. Preselected critical parameters including those derived from emissions analysis were presented on a scope in the control room for screening to establish data validity before proceeding to the next point in the test program. Hard copy printout of the entire data reduction program output was made available at a printer terminal in the Engineering Building in East Hartford within minutes after the data was acquired. Data from the smoke measurements, which were processed independently, were related to the computer processed data on a point number basis after the test is completed.

The existing fuel supply systems in this facility employed constant flow gear type pumps sized for the maximum anticipated fuel flow and recirculated unused fuel through a bypass to the pump inlet line. This type of system degraded the antimisting kerosene to unacceptable levels. Consequently, the stand fuel system was modified to that shown schematically in Figure 29. The existing Jet A fuel system was unaltered but a valve system was employed to permit switching the fuel source from Jet A to antimisting kerosene without disturbing the rig operating conditions. This feature permitted operating the rig on Jet A fuel

while inlet conditions were being set and stabilized, and permitted switching to the antimisting kerosene and operating on this fuel while acquiring data. The antimisting kerosene was consumed only during stabilization time after switching and during the data acquisition process itself. The antimisting kerosene supply system consisted of a 950 liter supply tank pressurized with nitrogen. Fuel flow rates were determined with turbine and mass meters in the supply lines. The fuel supply system instrumentation also included fuel temperature thermocouples and measured the fuel pressure in the primary and secondary systems at the entrance to the fuel injector support.

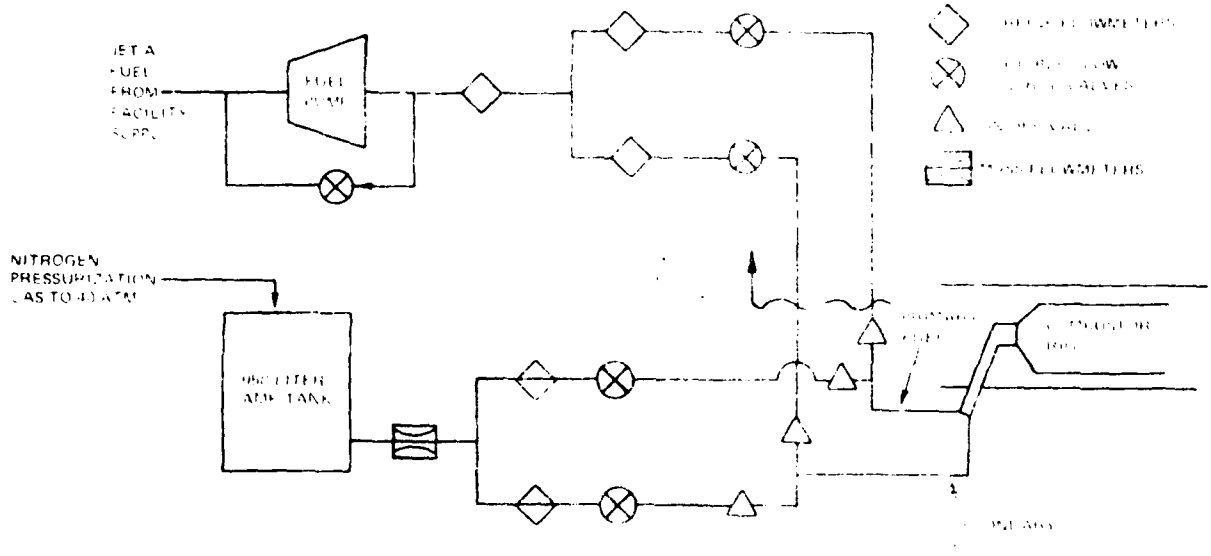

Figure 29 *Modifications to Fuel System In X-904 Test Stand for Evaluation of Anti-Mist Fuel*

The configuations and test conditions used in this test are summarized in Table XI. All test conditions were run with both the bill-of-material and low emissions combustor cans described in Section 2.1.4. In addition, two points, nominal idle and sea level takeoff, were run with the low emissions combustor can in the fully aerating mode, i.e., all fuel flowing through the secondary metering system. Three fuels were used for each of the configurations: Jet A 1-pass and 3-pass degraded antimisting kerosene. In all cases ambient fuel temperatures were maintained and samples periodically analyzed for filter ratio value.

TABLE XI

HIGH PRESSURE COMBUSTOR TEST CONDITIONS

Test Condition	Burner Can Configuration
Nominal Idle	Bill-of-Material, Low Emissions, L/E - Aer.
Rich Idle	Bill-of-Material, Low Emissions
Lean Idle	Bill-of-Material, Low Emissions
Sea Level Takeoff	Bill-of-Material, Low Emissions, L/E - Aer.
Climb	Bill-of-Material, Low Emissions
Cruise	Bill-of-Material, Low Emissions
Approach	Bill-of-Material, Low Emissions

Notes:
1) L/E - Aer. = Low Emissions, All Fuel Through Nozzle Secondary Metering System (Fully Aerating)
2) Fuel Used for each Configuration: Jet A, 1-Pass and 3-Pass Degraded Antimisting Kerosene
3) Fuel Temperature = Ambient

The testing procedure was as follows:

1. Set a test point (e.g., nominal idle) with Jet A on the bill-of-material combustor.

2. Set the same point with 3-pass degraded antimisting kerosene.

3. Set the rest of the points alternately switching from Jet A to 3-pass antimisting kerosene.

4. At the completion of conducting all the test points, disassemble, photograph, clean and reassemble the bill-of-material combustor can and fuel nozzle.

5. Repeat Steps 1 through 4 with 1-pass antimisting kerosene in place of 3-pass.

6. Repeat Steps 1 through 5 with the low emissions combustor in place of the bill-of-material.

Table XII lists the more important measured parameter and the emission measuring equipment.

TABLE XII

HIGH PRESSURE COMBUSTOR MEASUREMENTS

1. Emissions

CO	-	Nondispersive infrared - Beckman Model 315A
CO_2	-	Nondispersive infrared - Beckman Model 315A
NO_x	-	Chemilumenence Analyzer - Thermo Electron Crop. Model 10A
THC	-	Flame Ionization Detector - Beckman Model 402)
Smoke	-	Smoke meter conforming to SAE ARP 1179 (Ref. 3)

2. Lean Blow Out Limits

3. Combustor Can Cold Side Skin Temperatures

4. Combustor Can Inlet and Exit Pressures and Temperatures

5. Airflow Rate

6. Fuel Flow Rate

7. Inlet Humidity

2.6.2 Ignition and Stability Tests

The altitude relight and sea level ignition tests were conducted in X-306 stand located at the Rentschler Airport Laboratory in East Hartford. Airflow capability is presented in Table XIII. A comprehensive description of the facility is contained in Reference 7.

TABLE XIII

X-306 ALTITUDE RELIGHT FACILITY

Air supply (kg/sec)	4.54
Pressure (atm)	0.066
Temperature (K)	226 Min.

The rig contains nine JT8D-17 can-annular combustors. In addition, provisions were made for extracting OD and ID bleeds in amounts representative of the turbine cooling air requirements of the JT8D-17 engine. This allowed a more precise simulation of the JT8D-17 engine operating conditions. Operating airflow conditions in this facility were established with an orifice in the inlet duct and the rig inlet total pressure and total temperature rakes. Fuel flow rate, fuel manifold pressure, igniter current pulses and the output from thermocouple probes at the combustor exit were input to transient recorders to document ignition. The filter ratio of antimisting kerosene fuel samples was periodically checked throughout the test.

The antimisting kerosene fuel feed systems and measuring devices are the same as described in the last section.

An outline of the test conditions and configurations are given in Table XIV. All test conditions were conducted with both the bill-of-material and low emissions configuration described in Section 2.1.4.

TABLE XIV

IGNITION AND STABILITY TEST CONDITIONS

	Altitude Relight	Sea Level Ignition
Wa (kg/sec)	2.27 3.18 4.08 5.22	5.27
Wf (kg/sec)	0.068	--
P_{t4} (cm HgA)	Windmilling conditions	64
T_{T4} (K)	Windmilling conditions	290 244
T_{fuel} (K)	294	290 244
Fuel Type	Jet A 3-pass degraded antimisting kerosene	Jet A 3-pass degraded antimisting kerosene
Combustor Cans (Full Can Annular)	Bill of Materials Low Emissions	Bill of Materials Low Emissions

The relight tests were conducted by operating the rig along four different constant airflow lines covering the extent of the JT8D engine altitude relight envelope as shown in Figure 8. As the effective altitude is increased along these lines, the air inlet total pressure and total temperature progressively decrease. The tests were conducted by operating the rig at a fixed airflow and by progressively increasing the effective altitude until an altitude condition was defined at which ignition was no longer possible after a 30 sec. attempt. The altitude ignition boundary was defined by these points on the airflow lines. The ignition total fuel flow was fixed at 0.065 kg/sec which was consistent with the altitude starting fuel schedule of the JT8D engine and at ambient fuel temperature.

The combustor was also evaluated for cold fuel sea level starting capability. For these tests the rig was operated at slightly subatmospheric pressure and at an inlet Mach number and temperature representative of JT8D engine cranking at 244K and 290K ambient temperature. The test fuel was at the same temperature as the inlet air. Ignition was attempted over a range of fuel flow rates with the time to ignition being recorded.

2.6.3 Emission Data Calculation Procedure

2.6.3.1 Emission Data Processing Procedure

The raw emissions data generated at each test condition were transmitted directly to an online computer for processing. The voltage response of the gaseous constituent analyzers was first converted to an emission concentration based on the calibration curves of each instrument, and then used to calculate emission indices, carbon balance fuel-air ratio, and combustion efficiency. The equations used for these calculations were equivalent to those specified in SAE ARP 1256 (Ref. 4). Since the instrumented vane pack allowed extraction of a single representative gas sample, acquisition time was minimized and the processed emissions data were usually available within a few minutes of setting a test condition.

2.6.3.2 Adjustment Procedure

While every effort was made to set exact design conditions for the test runs, it was rarely possible to set test conditions to precisely match the design point fuel-air ratio. Therefore, the data have been corrected to design condition by interpolation, using plots of emissions as functions of the metered fuel-air ratio. The data for oxides of nitrogen have been corrected for humidity effects at all operating conditions. Where correction of oxides of nitrogen emissions data to design point conditions was not possible by interpolation, extrapolation was accomplished using the following equation (Ref. 5). These corrections were small, generally not exceeding 5 percent.

$$NO_x \text{ EI corr.} = (NO_x \text{ EI meas.}) \left(\frac{P_{t4 \text{ corr.}}}{P_{t4 \text{ meas.}}}\right)^{0.5} \left(\frac{V_{ref. \text{ meas.}}}{V_{ref. \text{ corr.}}}\right) \left(\frac{T_{t5 \text{ corr.}}}{T_{t5 \text{ meas.}}}\right)$$

$$\left(e^{18.8\,(H_{meas.} - H_{corr.})}\right) \left(e^{\left[\frac{T_{t4 \text{ corr.}} - T_{t4 \text{ meas.}}}{288}\right]}\right)$$

where:

NO_x EI = Emission index of oxides of nitrogen

P_{t4} = Inlet total pressure (atm)

T_{t4} = Inlet total temperature (K)

$V_{ref.}$ = Reference velocity (m/s)

H = Inlet specific humidity (g H_2O/g air)

T_{t5} = Combustor exit temperature (K)

and subscripts:

corr. = Relates to value at corrected condition

meas. = Relates to value at measured condition

2.6.4 Combustor Performance Data Calculation Procedure

The combustor performance parameters presented in this report were either measured directly or calculated from measured data. Table XV contains a summary of these performance parameters and indicates whether they were measured or calculated.

TABLE XV

SUMMARY OF REPORTED COMBUSTOR PERFORMANCE PARAMETERS

Parameter	Symbol	Units	Measured	Calculated
Total Airflow	W_{a4}	kg/s	X	
Total Combustor Airflow	W_{ab}	kg/s		X
Primary Fuel Flow	W_{f_p}	kg/s	X	
Secondary Fuel Flow	W_{f_s}	kg/s	X	
Inlet Total Temperature	T_{t4}	K	X	
Inlet Total Pressure	P_{t4}	atm	X	
Reference Velocity	V_{ref}	m/s		X
Inlet Air Humidity	H	g H_2O/kg air	X	
Fuel-Air Ratio	f/a	---		X
Pressure Loss	$\Delta P_t/P_t$	---		X
Combustion Efficiency	η_c	%		X

2.6.4.1 Calculated Parameters

The calculated parameters include the combustor airflow, reference velocity, metered and carbon balance ratio, pressure loss, and combustion efficiency.

The total combustor airflow was determined by subtracting the measured bleed flows from total airflow.

The reference velocity (V ref.) was defined as that flow velocity that would result if the total combustor airflow, at the com- pressor discharge temperature and static pressure, were passed through the combustor liner at the maximum cross-sectional area. This area is 0.0247 m^2 for the JT8D combustor, tested in this program.

Both metered and carbon balance derived fuel-air ratios (f/a) were calculated and recorded for all configurations tested in this program. The metered, or performance fuel-air ratio, is simply the ratio of fuel flow to total combustor airflow and can be measured quite accurately. Fuel-air ratio can also be determined by using gas sample data to determine the carbon balance of the exhaust gases. The carbon balance fuel-air ratio is appropriate for estimation of fuel mass flow rate in the calculation of emission index. It is used throughout this report for the purpose of data presentation.

The pressure loss ($\Delta P_t/P_t$) was calculated from the following equation:

$$\Delta P_t/P_t = \frac{P_{t4} - P_{t5}}{P_{t4}}$$

where:

P_{t5} = Average combustor exit total pressure

P_{t4} = Average combustor inlet total pressure

The combustion efficiency (η_c) was calculated using the measured concentrations of carbon monoxide and total unburned hydrocarbons from the gas sample data. The calculation was based on the assumption that the total concentration of unburned hydrocarbons could be assigned the heating value of methane (CH_4). The equation is:

$$\eta_c = 100 - 100 \left(\frac{4343X + 21500Y}{18.4\ (10)^6} \right)$$

where:

X = measured carbon monoxide concentration in g/kg fuel

Y = measured total unburned hydrocarbon concentration in g CH_4/kg fuel

2.7 TASK 8 - FUEL CONTROL SYSTEM TEST

Fuel control tests were conducted to evaluate the performance of a JT8D engine fuel control on antimisting kerosene in X-253 stand. The fuel control, fuel pressurizing and dump valve and fuel pump, all used in this task are described in Section 2.1.2.

2.7.1 Facility Description

The fuel control tests were conducted with a fuel pump, fuel control and fuel pressurizing and dump valve as shown on Figure 30. During performance calibration, fuel was supplied from the supply tank under moderate gas pressure and discharged into a collection tank in an open loop mode. During extended duration tests, the system was converted to closed loop operation utilizing a single tank. A nozzle and burner pressure simulator were located just downstream of the pressurization and dump valve. Figure 31 shows the fuel control and fuel pump mounted in X-253 stand which is described in Section 2.2.4.

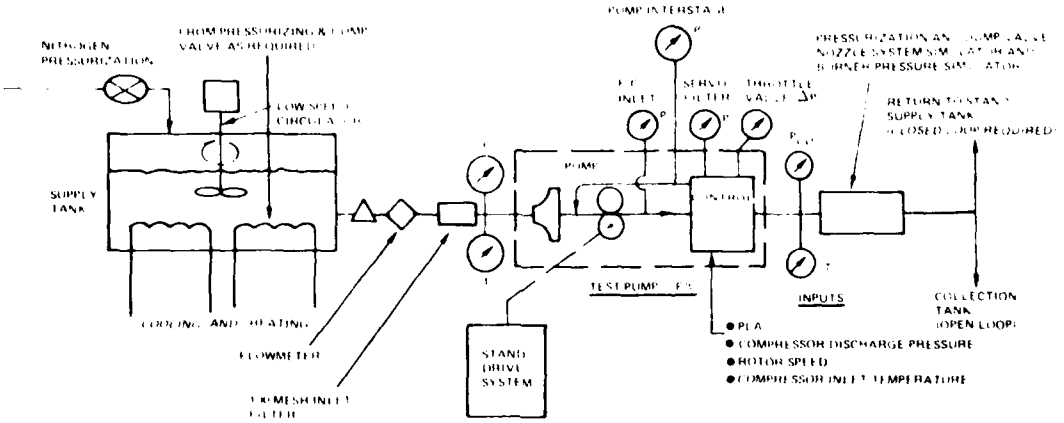

Figure 30 Schematic View of Apparatus for Fuel Control and Fuel Pump Tests

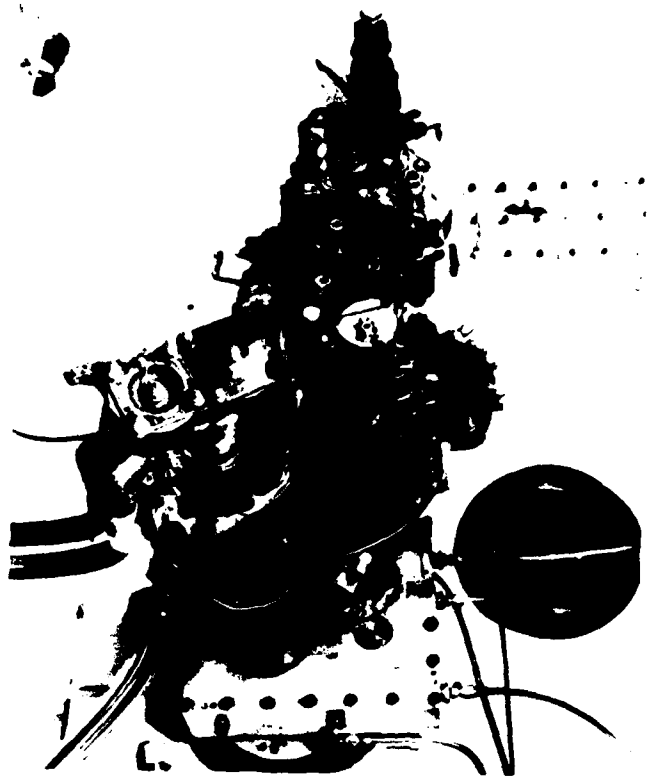

Figure 31 JT8D Engine Fuel Control and Fuel Pump

X-271 stand was used to setup the fuel control and calibrate it on PMC 9041 (conforming to MIL-F-702AA type II test fluid). X-271 stand is located at the Pratt and Whitney Engine Control Systems Laboratory. It is a general purpose, open loop fuel systems test facility designed to evaluate complete fuel control systems and individual subcomponents requiring a fuel supply and a variable speed rotational drive power system. The stand consists of an enclosed reinforced concrete room and an adjacent control room within the laboratory. One outside wall is designed as an explosion relief panel. Test component drive power is provided by a 1520 kgm/s variable speed direct current motor through a step-up gearbox and is capable of maintaining speeds to ± 5 rpm over a range of 200 to 7000 rpm. Fuel is provided at flow rates of up to 18,160 kg/hr at controlled pressures of 35 to 411 kpag and temperatures from 311K to 394K. Other systems provide fuel at up to 6900 kpag as regulated hydraulic signal pressure for activating system components, and air/nitrogen is provided at pressures from 7 to 4140 kpag for simulation of engine inlet and burner pressures and for actuation of an engine inlet temperature sensor simulator.

2.7.2 Test Procedure and Instrumentation

Instrumentation was provided to monitor the following fuel control parameters.

Parameters	Symbol
Power Lever Angle	PLA
Shutoff Lever Angle	SOLA
Control Speed	N_c
Compressor Discharge Pressure	P_{s4} or P_b
Compressor Inlet Temperature	T_{t2}
Metered Fuel Flow	Wf
Control Inlet Pressure (Pump Discharge Pressure)	P_D
Throttle Valve Differential Pressure	TV ΔP
Fuel Control Inlet Filter Differential Pressure	F/C $Filt_{in}$ ΔP
Fuel Control Wash Flow Filter Differential Pressure	F/C Wash ΔP
Wash Flow Inlet Pressure	$P_{wash\ in.}$
Supply Tank Pressure	P_{Tank}
Pump Inlet Pressure	$P_{in.}$
Pump Interstage Pressure	P_{int}
100 Mesh Inlet Screen Differential Pressure	$\Delta P_{100\ Mesh}$
Inlet Fuel Temperature	T_{in}
Supply Tank Fuel Temperature	T_{Tank}
Control Fuel Discharge Temperature	T_{Disch}
Fuel Temperature After Cooler	T_{Ret}

The test procedure for the fuel control tests consisted of the following (All tests were conducted at room temperature):

1. The control was pre-test calibrated with PMC 9041 to ensure proper fuel control operation.

2. Control Performance Test - Jet A.

   a. Starting and Acceleration Schedule at control speeds of 1000, 2500, 2800, 3200 and 3800 rpm and constant P_b of 207 KPa (30 psia), T_{t2} = 288K (60°F) and Max PLA.

   b. Acceleration Schedule Temperature Bias at 3200 Nc, 276 KPa (40 psia) P_b, Max PLA and 288K (60°F) T_{t2} compared to 233K (-40°F) T_{t2} and 2900 Nc.

   c. Maximum ratio line (Wf vs. Pb) at 3800 Nc, Max PLA, 288K (60°F) for P_b of 207 KPa (30 psia) and 690 KPA (100 psia).

   d. Idle speed governor at 2431 Nc, 242 KPa (35 psia) Pb, Idle PLA and 288K (60°F) T_{t2}.

      Max speed governor at 4228 Nc, 345 KPa (50 psia) Pb, Max PLA and 288K (60°F) T_{t2}.

      Overspeed governor (to determine speed shift) at 4360 Nc, 345 KPa (60 psia) Pb, Max PLA and 288K (60°F) T_{t2}.

   e. Idle speed governor temperature bias at 2431 Nc, idle PLA, 242 KPa (35 psia) Pb and 288K (60°F) T_{t2} compared to 233K (-40°F) T_{t2}.

      Max speed governor temperature bias at 4228 Nc, Max PLA, 345 KPa (50 psia) Pb and 288K (60°F) T_{t2} compared to 233K (-40°F) T_{t2}.

3. Control Performance Test - 16-pass antimisting kerosene-repeat steps 2a through 2e with 16-pass antimisting kerosene. In addition, measurements of antimisting kerosene filter ratio before and after the test were conducted.

4. Fuel control Extended Duration Test - The control and pump were subjected to an 8 hour closed loop cyclic test using 16-pass antimisting kerosene. The test consisted of running sixteen 30 minute cycles as follows:

   - o 8 minutes at idle PLA, 2431 rpm Nc, 242 KPa (35 psia) Pb and 288K (60^{o}F) T_{t2}.
   - o 2 minutes at Max PLA, 3800 rpm Nc, 966 KPa (140 psia) Pb and 288K (60^{o}F) T_{t2}.
   - o 20 minutes at Max PLA, 4228 rpm Nc, 1794 KPa (260 psia) Pb and 288K (60^{o}F) T_{t2}.

Every second cycle beginning with the first cycle and at the end of the cyclic test, minimum ratio data was recorded at 1035 KPa (150 psia) Pb and 3800 rpm Nc and idle power lever angle. Antimisting kerosene filter ratio measurements were made at the supply tank prior to the cycle test, and after 3.5 and 8 hours of testing.

The measurements at the last cycle were compared to those of the first cycle to determine if any change in the fuel control performance occurred during the duration test.

2.8 TASK 9 - FUEL PUMP PERFORMANCE TESTS

Fuel pump tests were conducted to evaluate the performance of a JT8D engine fuel pump on antimisting kerosene in X-253 stand. The fuel pump is described in Section 2.1.2.1.

2.8.1 Facility Description

The fuel pump was tested on a flow bench similar to the setup shown in Figure 30. The differences are that the control in Figure 30 is replaced with a bypass valve and the pressurization and dump valve, etc., is replaced with a

backpressure valve. During open loop operation, fuel was supplied from a supply tank under moderate nitrogen pressure and discharged into a collection tank. During closed loop operation, discharge fuel was returned to the supply tank. Figure 32 shows the fuel pump mounted on X-253 flow bench.

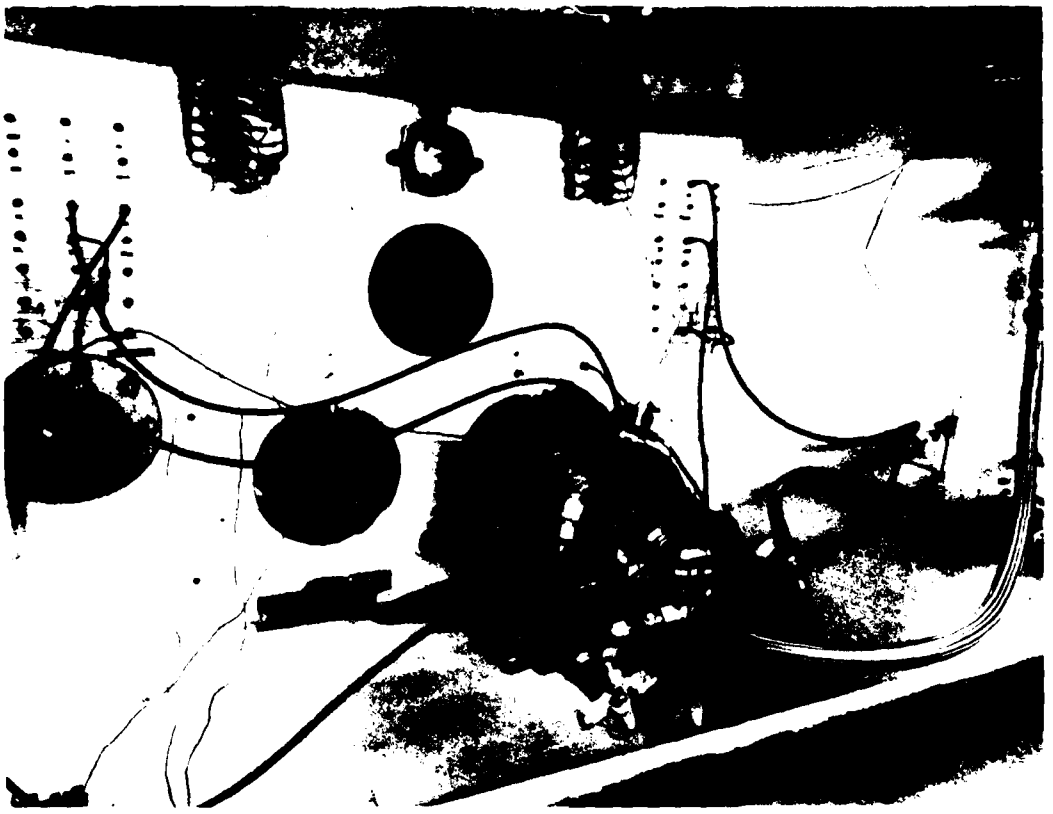

Figure 32 JT8D Engine Fuel Pump Mounted In X-253 Stand

2.9.2 Test Procedure and Instrumentation

Instrumentation was provided to monitor the following parameters.

Parameter	Symbol
Pump Speed	Np
Fuel Flow	Wf
Pump Inlet Pressure	P_{in}
Supply Tank Pressure	P_{tank}
Pump Centrifugal Stage Discharge Pressure	P_{cd}
Pump Interstage Pressure	P_{int}
Pump Discharge Pressure	P_{d}
Pump Inlet Filter Differential Pressure	ΔP_{filter}
100 Mesh Inlet Screen Differential Pressure	$\Delta P_{100\ mesh}$
Pump Inlet Fuel Temperature	T_{i}
Pump Discharge Fuel Temperature	T_{d}
Supply Tank Fuel Temperature	T_{tank}

The test procedure for the fuel pump tests was the following: (All tests were conducted at room temperature.)

1. Pump Durability Tests

   a. The fuel pump was subjected to a pre-test teardown inspection.

   b. The pump was assembled and calibrated using PMC 9041.

   c. Testing was conducted to determine antimisting kerosene degradation characteristics at various simulated engine operating conditions as described in Task 3.

   d. The pump was subjected to an interim calibration and teardown inspection after accumulating 25.5 hours of antimisting kerosene operation. The pump was reassembled and calibrated using PMC 9041 and Jet A.

e. The pump was subjected to further antimisting kerosene tests including an 8 hour fuel pump/control extended duration test as described in Task 3 and closed loop degradation from 3-pass antimisting kerosene to 16-pass antimisting kerosene as described in Task 3.

f. A post-test pump calibration was performed using Jet A fuel. The pump was then subjected to a post-test teardown inspection.

2. Pump Comparative Performance on Jet A and Antimisting Kerosene

a. The pump was subjected to a baseline gear stage calibration (without bypass loop) using Jet A fuel. The calibration was conducted with and without a pump inlet filter installed. Data taken without the inlet filter installed was used for comparison with antimisting kerosene operation, which required filter removal because of antimisting kerosene gelling characteristics as discussed in Section 3.3.2.5. Data taken with the filter installed was used as interim data to be compared with a post-test calibration on Jet A. Table XVI provides pump speeds and pressures at which the gear stage was tested. Stand supply tank pressurizing limitations did not allow pump speeds beyond 3900 rpm; therefore, the normal maximum rated pump speed of 4200 rpm could not be attained.

b. The fuel pump was calibrated with undegraded antimisting kerosene using the same procedure as for the Jet A baseline calibration except that high pressure drop across the 100 mesh test rig inlet screen, resulting from antimisting kerosene gelling characersitics, prevented pump operation above 2500 rpm. Therefore, the calibration was conducted at pump speeds up to 2500 rpm with additional test points at 1000, 1500 and 2000 rpm. Table XVII provides pump speeds and pressure at which the gear stage was tested. Fuel samples for filter ratio determination were taken at the supply tank prior to calibration and at the collection tank after the calibration.

c. The fuel pump was calibrated with 3-pass antimisting kerosene at conditions tabulated on Tables XVI and XVII using the Jet A baseline calibration procedure. Fuel samples for filter ratio determination were taken at the supply tank prior to calibration and at the collection tank after calibration.

TABLE XVI

GEAR STAGE TEST PARAMETERS WITH JET A

Pump Speed (rpm)	Pump Discharge Pressure KPa (psig)	Gear Stage Pressure Rise KPa (psig)
550	--	690 (100)
550	--	1035 (150)
550	--	1380 (200)
2500	3450 (500)	
3000	3450 (500)	
3500	3450 (500)	
3900	3450 (500)	
3900	6210 (900)	
3500	2760 (400)	
3500	5520 (800)	

TABLE XVII

GEAR STAGE TEST PARAMETERS
WITH UNDEGRADED ANTIMISTING KEROSENE

Pump Speed (rpm)	Pump Discharge Pressure KPa (psig)	Gear Stage Pressure Rise KPa (psig)
550	--	690 (100)
550	--	1035 (150)
550	--	1380 (200)
2500	2070 (300)	
2500	3450 (500)	
2500	5520 (800)	
1000	2070 (300)	
1500	2070 (300)	
2000	2070 (300)	
1000	3450 (500)	
1500	3450 (500)	
2000	3450 (500)	

3.0 RESULTS AND DISCUSSION

The results of the experiments described in Section 2.0 for each of the tasks are presented in this section.

3.1 TASK 3- FUEL HANDLING AND QUALITY CONTROL

Under Task 3, filter ratio measurements, antimisting kerosene chemical and physical property measurements, and a comparison between the JT8D engine fuel pump and Royal Aircraft Establishment degrader were conducted. Transitional velocity measurements, while closely tied to filter ratio measurements, were conducted under Task 5 and are reported in Section 3.3.1.

3.1.1 Viscosity Related Measurements

3.1.1.1 Comparison of Laboratory Methods for Viscosity Measurements

It was necessary to evaluate some degradation parameter of antimisting kerosene so that test results could be correlated with degradation level, independent of the degradation method chosen. Thus, a particular amount of antimisting kerosene processing needed to to achieve a given result (i.e., pass through a 40 μ filter without clogging) could be unambiguously identified and communicated. In this task, the four viscosity related measurements listed in Table XVIII were tested to meet this objective.

An initial comparison of the techniques for measuring viscosity was made by degrading small quantities of antimisting kerosene fuel with the laboratory blender for varying times from 1 minute to 120 minutes. Viscosity measurements with the glass bead bed proved impractical due to plugging of the bed under the suggested test conditions. The responsiveness of the remaining three techniques to change in fuel properties is illustrated in Figure 33 where filter

ratio, viscosity ratio and flow rate ratio* are plotted for the flow-through screen mesh, the ASTM viscometer, and the orifice cup, respectively, versus time of agitation in the blender. Data from two different lots of antimisting kerosene are shown and indicate good repeatability. The flow-through screen test and the orifice cup measurements are seen to be more definitive than the standard ASTM viscometer in establishing the degree of degradation of the antimisting kerosene. The responsiveness of the orifice cup falls off rapidly after approximately two minutes, whereas the flow-through screen test shows changes in filter ratio for times up to 120 minutes. The results are summarized in Table XVIII.

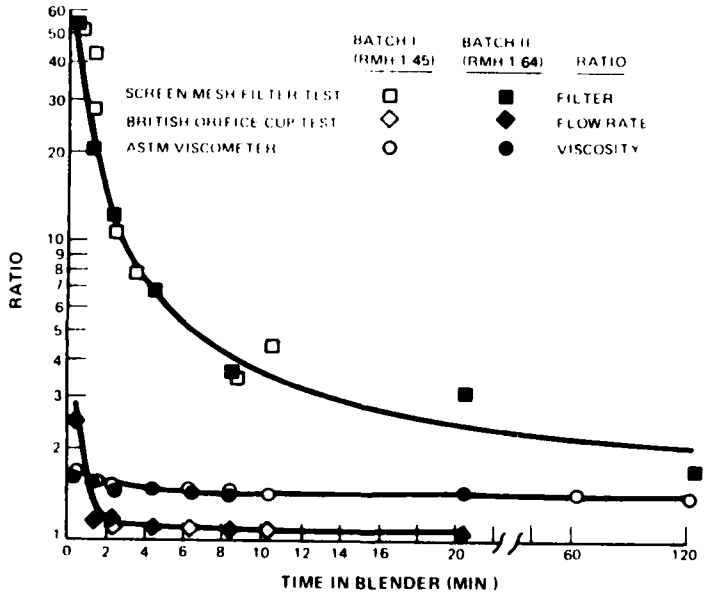

Figure 33 Correlation of Three Viscosity Measuring Device

*Filter Ratio (FR)- The time required for a fixed volume of antimisting kerosene to flow through a filter, divided by the time required for an equal volume of Jet A to flow through the same filter.

Viscosity Ratio (VR) - antimisting kerosene measured viscosity divided by Jet A measured viscosity using the standard ASTM viscometer.

Flow Rate Ratio - antimisting kerosene measured flow rate divided by measured Jet A flow rate using orifice flow cup.

TABLE XVIII

ANTIMISTING KEROSENE VISCOSITY MEASUREMENT TECHNIQUES

Method	Measurement	Result
Glass Bead	--	Unsuccessful
Screen Mesh Filter	Filter Ratio	Adequate Up to ~60 min. in Blender
British Orifice Cup	Flow Rate Ratio	Beyond 2 min., too insensitive
ASTM Viscometer	Viscosity Ratio	Too insensitive

Passing the antimisting kerosene through a JT8D engine fuel pump system was the degradation method used throughout most of this program. The sensitivity of filter ratio to number of passes can be seen in Figure 34. The measurement is adequate to about two or three passes. From 3 to 16-passes using filter ratio measurement as a means of discriminating degradation levels proved to be unacceptable due to lack of resolution. Most of the tests in this program were run with a degradation level of 3-pass or less and are, hence, reported in terms of both number of passes and filter ratio. In the filter, fuel control and fuel pump tests (Tasks 5, 8 and 9 respectively), it was believed necessary to degrade the fuel to 16-passes. For these tasks, a critical or transition velocity was developed to characterize the antimisting kerosene. The transition velocity is reported in Section 3.3.1 and was found to be adequately sensitive up to at least 16-passes.

3.1.1.2 Effect of Temperature Variations on Filter Ratio Test

The effect of temperature variations on the filter ratio test was evaluated by measuring the time for the fuel to flow between two reference marks at varying temperatures. Undegraded, 1-pass, and 3-pass antimisting kerosene and Jet A were tested. The results are shown in Figure 35. Temperature affected the antimisting kerosene flow times to a greater degree than for the parent fuel. The slope of the time vs. temperature curve for the undegraded fuel showed a large shift at a temperature of approximately 298K.

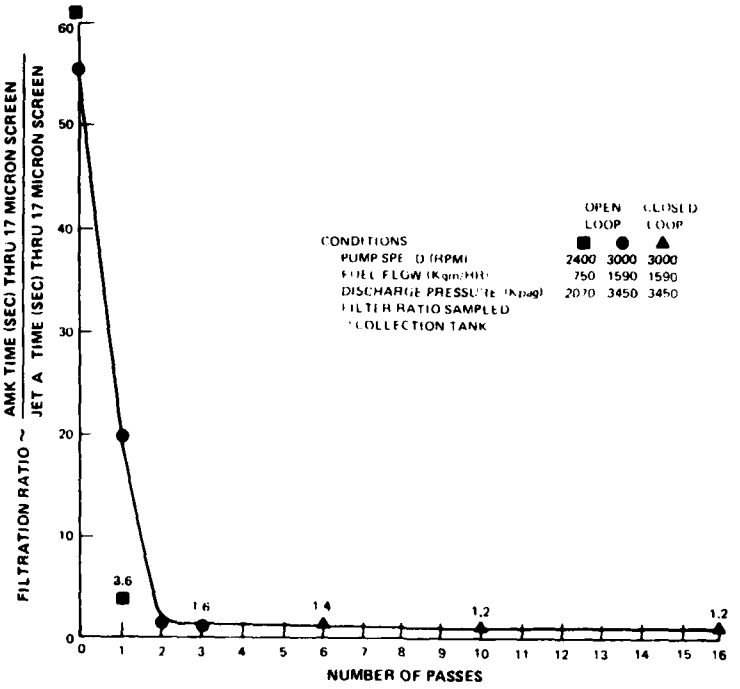

Figure 34 JT8D Fuel Pump System Filtration Ratio

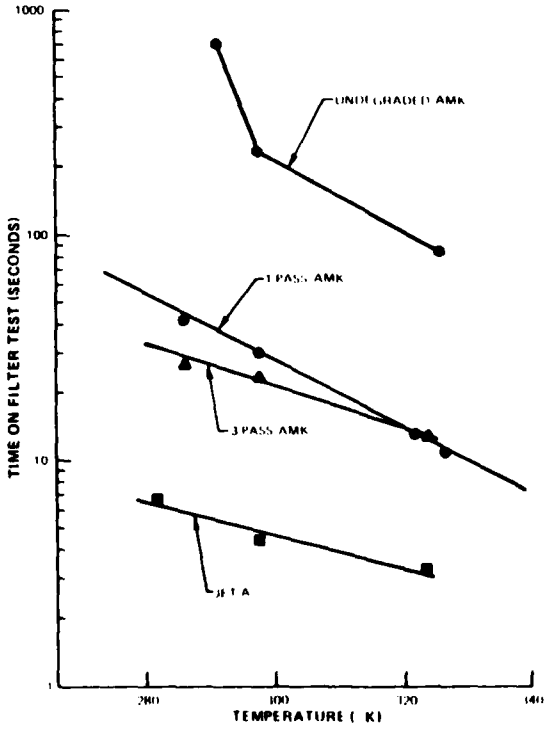

Figure 35 Screen Viscosity Temperature Chart

Table XIX shows the filter ratio as calculated from Figure 35. As temperature increased, the filter ratio showed a corresponding decrease. Also shown in Table XIX is viscosity ratio using a Cannon Fenske viscometer. It is interesting to note that the viscosity ratio went up as temperature increased. Over the temperature range of 238K to 372K the viscosity ratio of antimisting kerosene to parent jet fuel increased by a factor of 1.5.

TABLE XIX

EFFECT OF TEMPERATURE ON MEASURED FILTER AND VISCOSITY RATIO

Temperature (K)	Filter Ratio Undegraded	Filter Ratio 1-Pass	Filter Ratio 3-Pass
291	128	7.0	4.8
298	49	6.4	4.8
326	28	4.2	3.0

Temperature (K)	Viscosity Parent Fuel (cp)	Viscosity Antimisting Kerosene Fuel (cp)	Viscosity Ratio
238	8.72	10.71	1.21
273	2.75	4.16	1.51
298	1.58	2.65	1.68
311	1.27	2.17	1.71
372	0.59	1.17	1.96

5.1.1.1 Effect of Filter Type and Pore Size on Filter Ratio

would increase the sensitivity of the filter ratio measurement to degradation level.

A 10 μm metal screen and a 40 μm paper filter were used in the standard filter ratio test instead of the usual 17 μm metal screen. The results are shown in Table XX. Filter ratios were tabulated for undegraded fuel, 1-pass, 3-pass, 7-pass, and 16-pass antimisting kerosene. Filter ratio differences between 7 and 16-pass was at best 20 percent. Filter ratio from 16-pass to the highest possible level of degradation (antimisting kerosene properties identical to Jet A) was 30 percent at best. The difference in filter ratio between similar degradation levels (16-pass and 28-pass say) would probably be so small it would be virtually useless in discriminating between the two levels. Filter ratios recorded for the nominal 40 μm pump paper filter were much higher than either of the metal filters at levels of degradation less than 16-pass. The permeability of the paper filter to Jet A was approximately the same as the 17 μm metal screen as illustrated by the approximately equal flow through the two filters. The measured filter ratio of undegraded antimisting kerosene for the 10 micron screen (29) was significantly less than that measured with the 17 μm screen (43). The flow rate of Jet A through the 10 μm metal screen was approximately one-third the rate through either of the other two filters. Perhaps the lower flow rate allowed additional time for deformation of the antimisting kerosene additive aiding passage through the filter pores. The degree of tortuosity of the paper filter is considerably greater than either of the metal filters resulting in the greatest requirement for deformation. This factor may account for the greater filter ratios measured for the 40 μm paper filter.

3.1.2 Antimisting Kerosene Chemical and Physical Properties

3.1.2.1 General Observations

It was observed that the undegraded antimisting kerosene is not entirely a true solution of polymer in fuel. When a sufficient quantity of the fuel was examined in a glass vessel, the solution was found to be slightly turbid. The turbidity of an undegraded antimisting kerosene sample was measured by spectrophotometry at 400 nm in 10 cm cells using jet fuel as a reference. The light loss was 17%. The degree of turbidity was found to be somewhat variable from lot to lot of fuel. The polymer dispersion could not be separated by centrifugation in a laboratory centrifuge. Approximately 2 liters of undegraded antimisting kerosene was vacuum filtered through a 17 μm woven metal filter.

TABLE XX

EFFECT OF DIFFERENT FILTERS ON FILTER RATIO

	Filter Ratio/Flow[1]					
	17 μm Metal Screen		10 μm Metal Screen		40 μm Paper Filter	
Degradation Level	FR	Avg. Flow (cm^3/sec)	FR	Avg. Flow (cm^3/sec)	FR	Avg. Flow (cm^3/sec)
Undegraded	43	0.53	28.6	0.22	133	0.19
1-Pass	8.0	3.0	6.8	0.74	86	0.28
3-Pass	2.0	7.6	7.0	0.85	79	0.31
7-Pass	1.17	18	--	--	1.44	18
10-Pass	1.17	20	1.28	4.7	1.20	21

[1]Avg. Flow Rates of jet fuel containing no antimisting kerosene additive were 23.8 cm^3/sec, 5.85 cm^3/sec and 25 cm^3/sec for 17 μm metal screen, 10 μm metal screen and 40 μm paper filter, respectively.

Photographs of both the upstream and downstream sides of the filter is shown in Figure 36. The AMK is characterized by the presence of a small amount of translucent fibers and the occasional presence of globular clear material, perhaps the antimisting kerosene polymer, with a diameter up to 0.05 cm. The downstream side of the filter screen shows the gel that typically forms after passage of undegraded antimisting kerosene through filters.

3.1.2.2 Measured Properties

Properties typically measured to determine jet fuel quality were measured for four batches of antimisting kerosene and the parent fuel from which the antimisting kerosene was blended. In addition, an abbreviated characterization was made of a fifth batch of antimisting kerosene and parent fuel. The results of these measurements are given in Table XXI. Properties of the parent fuels in all cases appeared typical of Jet A fuel used for most commercial jet aviation. In the antimisting kerosene, there was no measurable change in freeze point. There is some suggestion of a very slight reduction in net heat of combustion; however, further testing would be required to show this conclusively. The

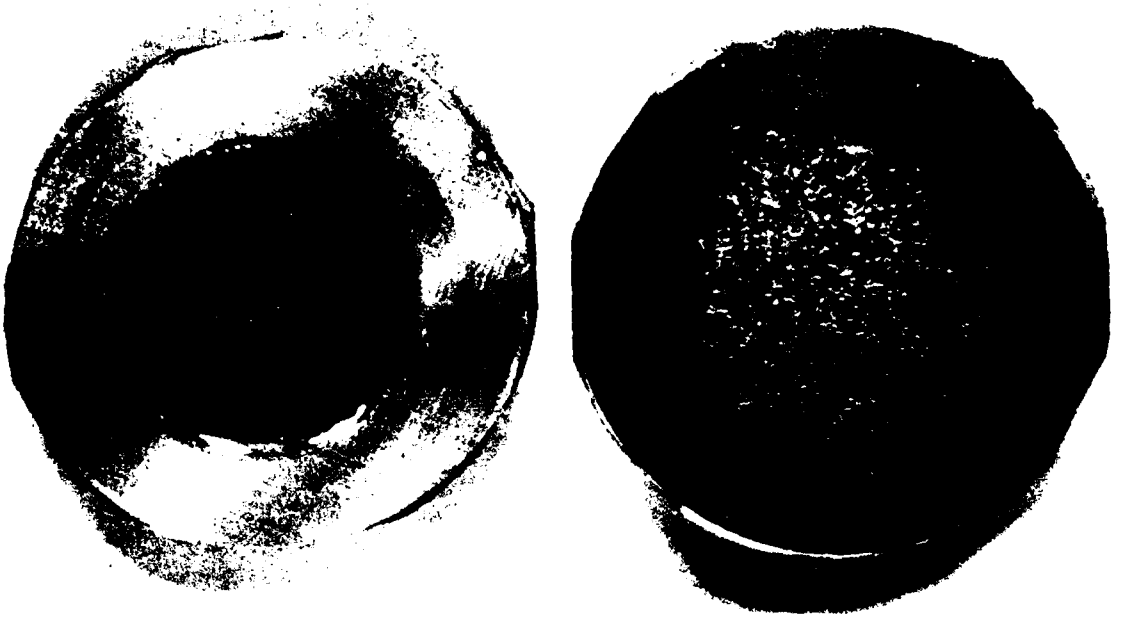

1.8 X
Downstream Side

1.8 X
Upstream Side

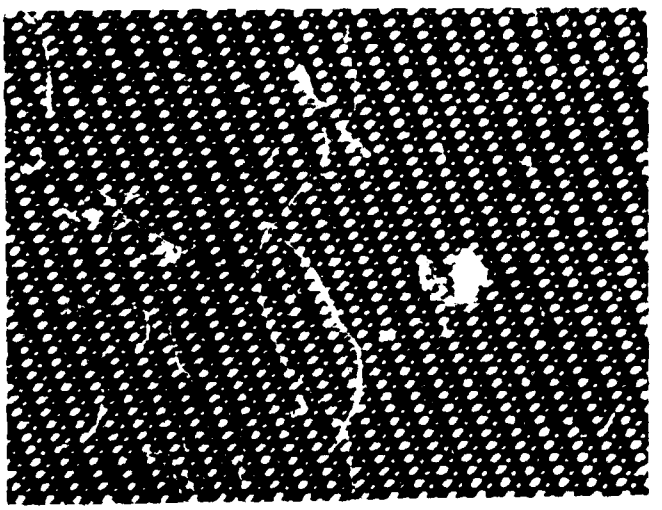

25X
Upstream Side Large Particle Diameter 500 μm

Figure 36 *Photographs of 17 μm Filter Screen After Filtering 2.3 Liter of Fuel Containing Anti-Mist Additive*

TABLE XXI

ANTIMISTING KEROSENE FUEL CHARACTERIZATION

	RMH 1-45		RMH 1-64		RMH 1-65		RMH 1-86		RMH 1-90	
	Neat Fuel	AMK	Neat Fuel	AMK	Neat Fuel	AMK	Neat Fuel	AMK	Neat Fuel	AMK
[illegible], Wt. %	13.59	13.61	13.93	13.87	13.82	13.80	14.18	13.91	13.91	
[illegible] Carbon Ratio	1.90:1	1.89:1	1.92:1	1.92:1	1.92:1	1.92:1	1.96:1	1.92:1	1.92:1	
Aromatics Content, Vol. %	22.6	21.3	19.8	20.5	20.0	19.9	18.9	21.1	20.9	
[illegible] Content, wt. %	0.04	0.04	0.02	0.02	0.02	0.02	0.01	0.02		
[illegible] Gravity, 60/60F	0.8146	0.8156	0.8086	0.8100	0.8100	0.8109	[illegible]	0.8090	0.8064	[illegible]
Flash Point, F	128	128	128	128	126	128	130	128		
Freezing Point, F	-56	-56	-49	-51	-50	-52	-56	-51		
Carbon Residue, 10 Vol. % Bottoms, Wt. %	0.09	--	0.05	--	0.10	--	0.06	--		
Heat of Combustion, net, Btu/lb	18,540	18,490	18,560	18,540	18,540	18,500	18,570	18,550	18,570	[illegible]
Smoke Point, mm	20	20	21	21	21	21	22	22		
Viscosity, 77F, cs	1.96	3.28	1.87	3.08	1.89	3.14	1.85	3.07	1.77*	1.91*
Additive Content, Wt. %	--	0.29	--	0.31	--	0.31	--	0.32		
Water Content, ppm	44	94	34	54	34	42	22	32		
Surface Tension, dynes/cm	29.7	30.1	29.3	29.5	29.6	29.7	29.5	28.8		
Thermal Stability, JFTOT, 260C										
ΔP, mm Hg	5	11	>25	0	>25	0	>25	3.5		
Deposit Code	1	1	1	1	1	1	1	1		
Distillation, F										
IBP	320	322	324	332	326	332	316	316		
10 Vol. %	369	368	365	367	367	366	361	363		
20	384	384	385	387	388	381	381	377		
30	396	397	396	395	396	392	393	391		
40	407	409	406	405	405	403	404	401		
50	418	419	416	416	416	414	413	411		
60	430	431	426	427	429	426	426	423		
70	443	443	438	440	441	439	437	436		
80	459	459	461	455	457	455	453	452		
90	480	480	473	476	476	471	476	472		
EP	530	517	531	522	522	521	529	509		
Recovery, Vol. %	98.9	98.8	99.0	99.0	99.0	99.0	99.0	99.0		
Residue	1.1	1.2	1.0	0.7	1.0	0.7	0.4	0.9		
Naphthalenes Content, Vol. %	[illegible]	2.1	1.9	1.6	1.9	1.6			1.69	
Nitrogen Content, ppm	11	27	10	28	8	26	4	21		
Mercaptan Sulfur, ppm	<10		<10	--	<10	--	<10	--		
Metallic Element Content, ppm										
Sodium	<0.02	0.3	<0.1	0.4	<0.1	0.4	<0.1	0.4		
Copper	<0.02	<0.02	<0.02	<0.02	<0.02	0.02	<0.02	0.02		
Calcium	<0.1	<0.1	<0.1	<0.1	<0.1	<0.1	<0.1	<0.1		
Lead	<0.1	<0.1	<0.1	<0.1	<0.1	<0.1	<0.1	<0.1		

*Measured at 260C

nitrogen content of the antimisting kerosene fuel increased slightly. The sodium content of the antimisting kerosene fuel were 0.3 to 0.4 ppm as contrasted to the parent Jet A which had no detectable sodium. Sodium can accelerate corrosion in the jet engine hot section. It is not known whether long term exposure to 0.4 ppm sodium in fuel would appreciably accelerate corrosion.

3.1.2.3 Filter Ratio of Undegraded Antimisting Kerosene

The antimisting kerosene was blended in lots of several hundred gallons by ICI, and then gravity filled into drums for shipment by truck to Pratt & Whitney Aircraft. Filter ratio measurements made on undegraded antimisting kerosene as-received samples are shown in Table XXII. Filter ratio was measured by both Pratt & Whitney Aircraft and ICI before shipment. Overall, the agreement was fairly good considering the nature of the measurement and differences in samples. There appeared to be some variation within shipments of different blend lots. When all eight drums of Blend Lot 1-115 were checked, there was little variation found; however, some variability was indicated by measurements made on Lot 1-92. Both Pratt & Whitney Aircraft and ICI measurements showed the filter ratio of Lots 112 to 115 to be significantly lower than previous shipments.

3.1.3 Fuel Shearing Comparison Between the JT8D Fuel Pump and Royal Aircraft Establishment Degrader

The objective of this test was to compare the antimisting kerosene degrading performance of the Royal Aircraft Establishment Degrader and the JT8D Engine Fuel Pump at various operating conditions.

The Royal Aircraft Establishment degrader was operated near its recommended condition of 15,000 rpm and 748 Kgm/hr (1650 pph). The degrader was also operated at JT8D pump engine idle speeds and flows. With a supply tank antimisting kerosene filter ratio of 52 to 64, the antimisting kerosene filter ratio at the degrader output varied from 27 to 40. Maximum power was 639 Kg meter/sec at the design condition. The maximum temperature rise was 19K ($35^{o}F$).

TABLE XXII

FILTER RATIO MEASUREMENTS ON UNDEGRADED ANTIMISTING KEROSENE SAMPLES

Shipment Date	Blend Lot	Filter Ratio Pratt & Whitney Aircraft	ICI
10-25-79	1-45	54	34
01-09-80	1-64	53	52
01-17-80	1-65	49	42
03-04-80	1-83	34	32
04-16-80	1-90	28	41
	1-91	42	44
	1-92 Drum 1	45	51
	2	37	
	1-93	33	60
	1-94	55	38
	1-95	59	62
07-02-80	1-112	16	27
	1-113	18	24
	1-114	21	26
	1-115 Drum 1	25	24
	1-115 2	21	
	1-115 3	21	
	1-115 4	23	
	1-115 5	21	
	1-115 6	21	
	1-115 7	19	
	1-115 8	22	

Additional Royal Aircraft Establishment degrader test results shown on Figure 37 indicate that the degrader pressure loss increases with flow rate and speed. The undegraded antimisting kerosene exhibited a higher pressure loss than the Jet A at identical conditions.

The JT8D engine pump was operated at or near simulated engine idle, cruise, and take-off power conditions. With a supply tank filter ratio of 64 to 68 the filter ratio at the pump discharge was 31 at the engine idle condition and 6.1 at the engine cruise and take-off condition. Maximum power was 1825 kg meter/sec at the take-off power condition. The maximum temperature rise was 8K ($14^{o}F$) at the cruise condition.

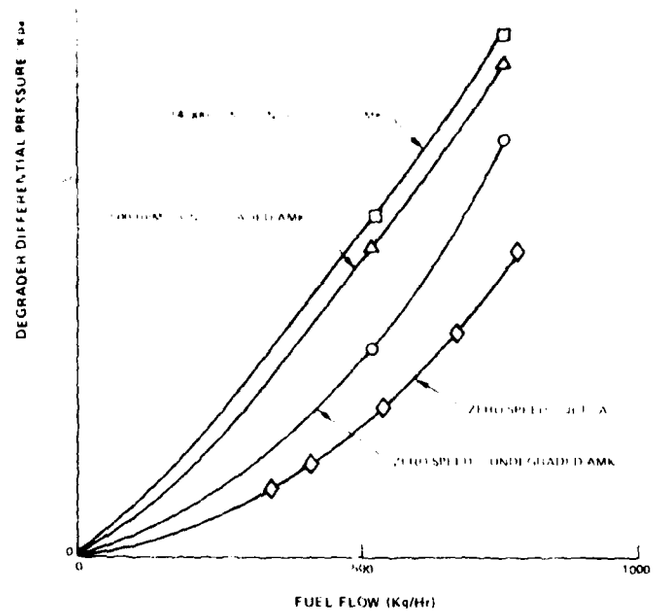

Figure 37 RAE Degrader Flow Characteristics

Table XXIII shows the degradation performance of the Royal Aircraft Establishment degrader and JT8D Fuel Pump. A comparison can be made between the two devices by observing the filter ratio difference or reduction across each test unit. The Royal Aircraft Establishment degrader at its design point should be compared to the JT8D fuel pump at idle since these points have equal flow rates. For this comparison the Royal Aircraft Establishment degrader had a lower filter ratio reduction, consumed more power, and had a higher temperature rise than the JT8D fuel pump. In addition, the Royal Aircraft Establishment degrader does no useful work in either pressurizing or pumping the fuel and would increase the work load on an aircraft engine pumping system by increasing the system pressure loss as indicated in Figure 37.

It is interesting to note that for JT8D fuel pump operation the difference in power consumption between passing undegraded antimisting kerosene and Jet A is negligible. This would imply that little of the total energy consumed by the pump goes towards degrading the antimisting kerosene.

Further data analysis of the antimisting kerosene degradation at various system locations indicated that the greatest combined degradation action was accomplished in the inlet line from the pressurization system as shown in Figure 38 and valves having differential pressure across them as noted in Table XXIII. A typical example extracted from the Table for the JT8D pump at 2400 rpm and 748 kgm/hr (1600 pph) through flow, the combined degradation due to the inlet line and differential pressure across the discharge valve was 25 (64-52+13) whereas the fuel pump filter ratio differential was only 21.

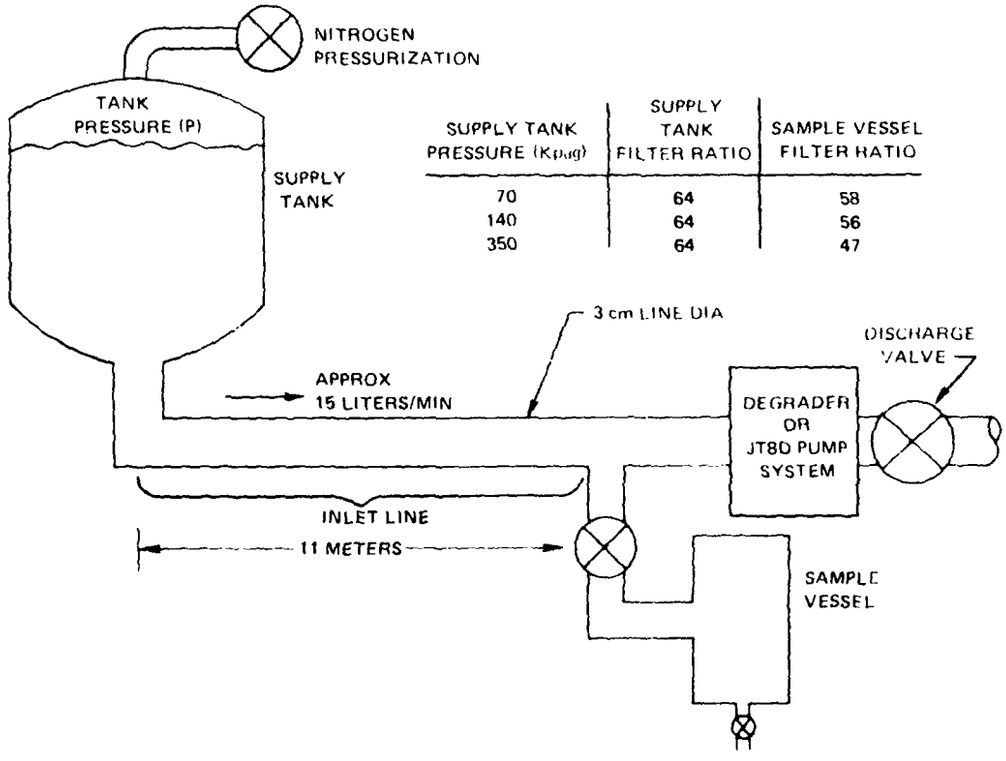

Figure 38 Apparent Pressure Sensitivity

TABLE XXIII

RAE DEGRADER - JT8D PUMP SYSTEM COMPARISON FOR ONE PASS

	Approx. Operating Condition	Speed (rpm)	Through Flow (kg/hr)	Approx. Recirculated Flow (kg/hr)	Pressure (kilopascals) Tank	Pressure (kilopascals) Discharge	Input Power (kg meter/sec)	Supply Tank Filter Ratio	Δ°	Filter Ratio Charge Across Unit (P_{in}-P_{out} = ΔP)	Collection Tank Filter Ratio	Filter Ratio Reduction Across Discharge Valve
RAE Degrader		2400	748	--	207	241	Negl.	50		35 - 27 = 8	24	3
		7400	522	--	207	265	Negl.	50		35 - 26 = 9	23	3
	Design Point	14100	748	--	207	339	839	51	10	50 - 40 = 10	31	-
JT8D Engine Pump System	Idle	2400	748	3334	207	2069	335	64	7	42 - 31 = 11	18	13
	Cruise	3000	1588	3610	207	3448	783	68	8	$P_{out} \sim 6.1$	19	-
	Takeoff	4300	4445	3164	276	4137	1955	69	9		No Data	-

3.1.4 Large Volume Processing of Antimisting Kerosene

It was necessary to develop a procedure that would degrade the antimisting kerosene in sufficient quantity to support other program tasks. The JT8D Fuel Pump and system was selected for the foregoing procedure since it provided the greatest single pass filter ratio reduction noted at the collection tank. Two additional system passes reduced the filter ratio to a level that fulfilled the contractual definition of "100 percent" degraded antimisting kerosene*. This level, for several batches of fuel, had a filter ratio range of 1.2 to 2.1. Approximately 1500 liters (400 gallons) of an initial 1900 liters (500 gallons) were degraded at one time. The loss during processing was due to the necessary drainage of residual unprocessed antimisting kerosene from the supply tank prior to filling it with additional processed antimisting kerosene. Figure 34 shows filter ratio attained versus system pass. The fuel pump antimisting kerosene degradation process system simulated a JT8D engine fuel system operating near engine idle condition. Approximately 748 Kgm/hr (1600 pph) was passed through the system while 3334 Kgm/hr (7350 pph) was recirculated back to the fuel pump gear stage inlet. During each system pass, some quantity of fuel was subjected to additional high pressure passes within the system.

Careful monitoring of inlet screen differential pressure during first pass processing was required. Occasionally, the degrading process was stopped when the screen differential pressure reached a prohibitive level. The process was restarted after the accumulated filter gell dissipated in the fuel. Subsequent system passes were accomplished with no screen clogging difficulty. The facility inlet screen characteristics and gelling phenomenon are discussed in section 3.3.2.5.

As noted previously, significant antimisting kerosene degradation occurred in the fuel feed inlet line. This degradation appeared to increase with increasing supply tank pressure as noted in the Table of Figure 38. This phenomenon was verified and used to inhibit the gelling rate on the inlet screen by increasing the system pressure level.

*100% degraded is defined as processed AMK whose viscosity decreases at a rate less than 5%/hr when processing a 1900 liter lot.

After subsequent Task 5 filter tests indicated that the defined 100 percent degraded antimisting kerosene (3-pass) would build up and clog the fuel control wash filter or the fuel pump paper filter, antimisting kerosene was further processed closed loop for a total of 16-passes.

3.2 TASK 4 - PHYSICAL CHARACTERISTICS EVALUATION

3.2.1 Thermal Stability of Antimisting Kerosene Fuel

The thermal stability property of jet fuel is of importance in avoiding coking problems in the fuel delivery systems of jet engines. Thermal stability was evaluated by measuring JFTOT breakpoint temperatures for undegraded, 3-pass, 16-pass, antimisting kerosene and the parent jet fuel from which the antimisting kerosene was blended. Data from these studies are shown in Table XXIV. A substantial increase in breakpoint is seen from parent fuel to antimisting kerosene at all levels of degradation. The failure mode for antimisting kerosene is deposit code, that is failing due to deposits forming on the heated tube while for Jet A the failure mode is pressure buildup on the metal filter. The increase in breakpoint temperatures for certain additives in Jet A fuel have been reported in the literature.

TABLE XXIV

THERMAL STABILITY MEASUREMENTS ON ANTIMISTING KEROSENE

Sample	Test Temperature (°C)	Δ P (mm Hg)	Deposit Code
Parent Fuel	260	184	1
	245	55	1
	230	4	1
Undegraded Antimisting Kerosene	290	1	4
	275	1	4
	260	?	1
3-Pass Antimisting Kerosene	275	1	4
	260	<0.5	1
16-Pass Antimisting Kerosene	290	<0.5	4
	275	<0.5	1

Sample	Breakpoint Range (°C)	Failure Mode
Parent Fuel	230-245	ΔP
Undegraded Antimisting Kerosene	260-275	Deposit Code
3-Pass Antimisting Kerosene	260-275	Deposit Code
16-Pass Antimisting Kerosene	275-290	Deposit Code

3.2.2 Effect of Water on Antimisting Kerosene Stability

When an attempt was made to determine the effect of the antimisting kerosene additive on water solubility, a major observation was that a white precipitate formed on contact of the antimisting kerosene fuel with free water. The precipitate did not go back into solution on standing and may be the polymer separating from the fuel. The separation may result from a direct reaction with the water, or, the water may be extracting a component of the additive mixture which stabilizes the polymer in the fuel. The white precipitate was concentrated at the water-fuel interface.

When the parent fuel was saturated with water, the water content of the fuel layer increased from 22 ppm to 62 ppm. The water content of the antimisting kerosene fuel layer after contact with free water increased by a smaller amount rising from 32 ppm to 38 ppm. However, these measurements are procedure dependent.

3.2.3 Corrosion of Copper

Reaction of copper with antimisting kerosene would be undesirable since some fuel system components are composed of alloys containing copper.

Measurements on the corrosion rate of copper in antimisting kerosene are tabulated in Table XXV. Copper dissolution was greatly enhanced in antimisting kerosene. Some copper dissolved in the parent fuel; however, the rate appeared to slowdown after 24-hour exposure. Copper concentrations increased in the antimisting kerosene fuel throughout the period of the study. Thermal stability problems of jet fuel have been attributed to traces of copper at concentrations as low as 0.02 ppm. Also, some increases in wear rates at long time exposure might be expected on hardware components containing brass or copper.

TABLE XXV

COPPER CORROSION STUDY

	ppm Cu	
Hours	Antimisting Kerosene	Parent Fuel
2	0.05	<0.02
24	0.64	0.05
48	1.5	0.05

3.2.4 Fuel - Oil Heat Transfer Coefficient

It is necessary to determine the effect antimisting kerosene has on the fuel heat transfer coefficient (h) in order to evaluate the fuel-oil cooler efficiency. An antimisting kerosene h much lower than a Jet A h would be unacceptable or at least require a moderate redesign effort.

The results for Jet A, 3 and 1-pass degraded antimisting kerosene and unsheared antimisting kerosene are shown in Figure 39. The h of the Jet A increased with fuel flow rate as expected. This is consistent with results previously obtained at Pratt & Whitney Aircraft. Above 3.4 Kg/hr the h of the undegraded antimisting kerosene was considerably different than the Jet A. Between about 4.5 and 10 Kg/hr the h of the undegraded antimisting kerosene leveled out. Beyond 10 Kg/hr it increased again. Qualitatively similar behavior between AVTUR and FM-4 additive was reported by Medani and Hayes (6). The h of the 1-pass antimisting kerosene increased with fuel flow rate less rapidly than either the 3-pass antimisting kerosene or the Jet A and at about 19 kg/hr crosses over and remained below the undegraded h. The 3-pass degraded antimisting kerosene was very similar to the reference Jet A. At low flow rates they were nearly identical, and at higher flow rates the 3-pass was about 10 percent lower than the Jet A.

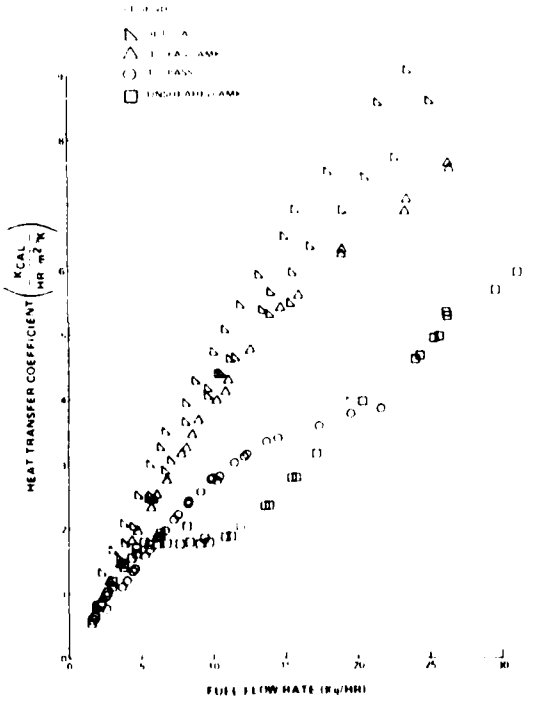

Figure 39 *Effect of Antimisting Kerosene On Heat Transfer In Fuel-Oil Cooling Tubes*

The 3-pass was acceptable, although marginally so at the higher fuel flow rates. The 1-pass and undegraded antimisting kerosene were not acceptable for use in the existing engine component.

The pressure drop versus fuel flow rate for the 1-pass and 3-pass antimisting kerosene was identical to the Jet A while the undegraded antimisting kerosene recorded a higher ΔP at a given fuel flow rate than did the Jet A.

3.2.5 Materials Compatibility - Elastomers

During engine operation the antimisting kerosene will continuously soak fuel system components possibly altering elastomer mechanical properties. This section documents those changes for three typical fuel system elastomers.

Results are presented as plots of elastomer immersion time in AMK versus volume change, tensite strength, elongation, and hardness in Figures 40 through 43 respectively. In all the tests little difference was observed between the 1-pass and 3-pass antimisting kerosene results. Hence it was decided to report the test data as an average of the results obtained for each of the two fuels. Three samples were run for each test point making the value of each point an average of 6 tests. Within experimental accuracy, little change occurred beyond 1 week for any of the measured properties.

The fluorosilicone exhibited a volume change (Figure 40) less than 15 percent and was insensitive to temperature. The other two elastomers have volume changes in excess of 50 percent with the fluorosilicone/fiberglass elastomer displaying appreciable temperature dependence.

Reduction in tensile strength for both the fluorosilicone and Butadiene (Figure 41) was significant. Tensile strength of the fluorosilicone was reduced by 1/3 while that of the Butadiene was reduced by 1/2.

Elongation of the fluorosilicone (Figure 42) was negligible while the Butadiene decreased by about 1/3.

Hardness (Figure 43) of the fluorosilicone was unchanged at 295K and was reduced by about 20% at 340K. The Butadiene and fluorosilicone/fiberglass hardness were reduced by about 10 percent and 30 percent respectively and both showed moderate temperature dependence.

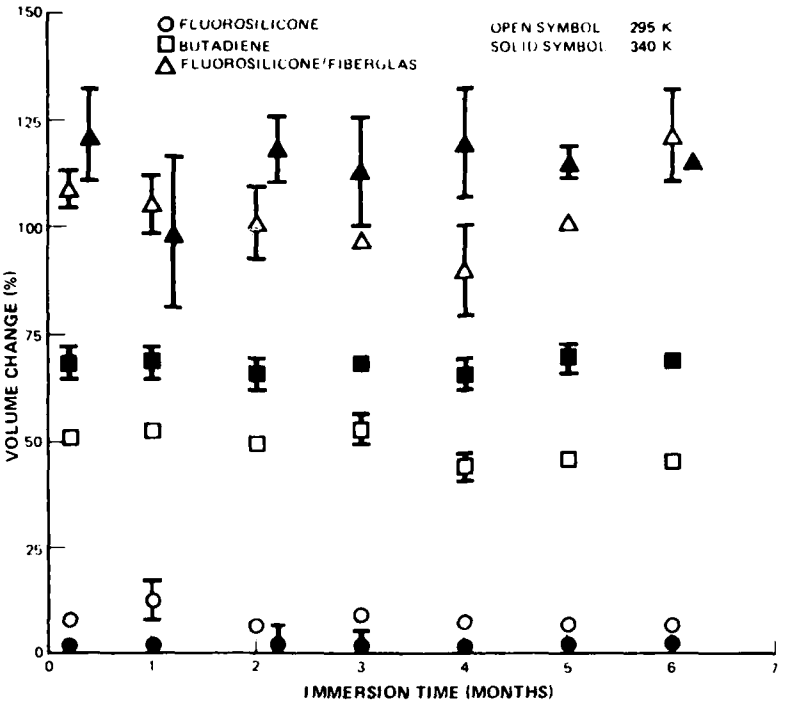

Figure 40 Effect of Volume Change On Elastomers Immersed In AMK

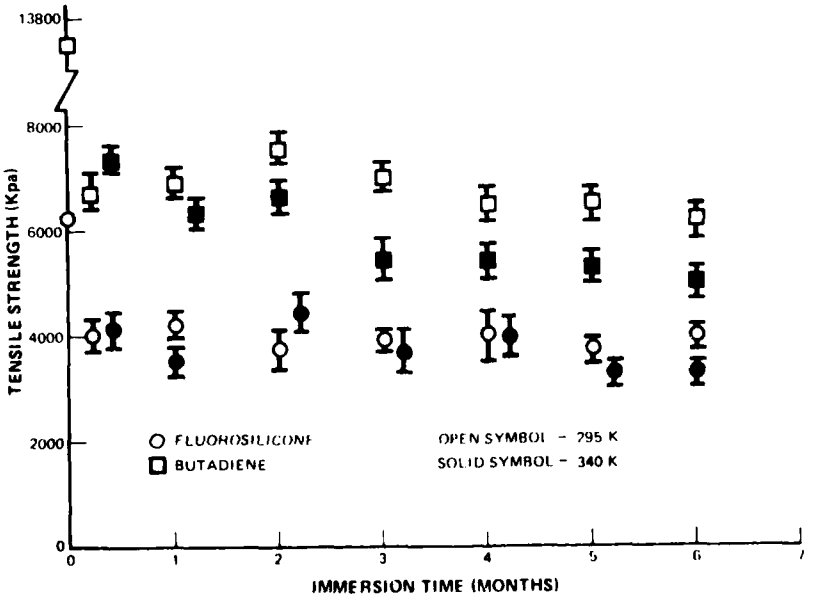

Figure 41 Effect of Tensile Strength On Elastomers Immersed In AMK

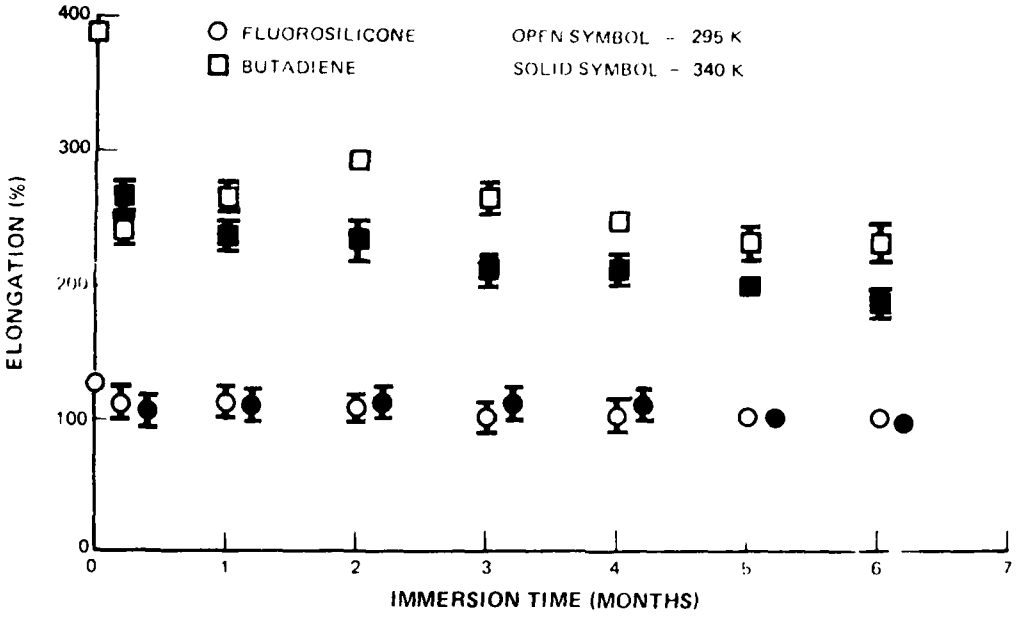

Figure 42 Effect of Elongation On Elastomrs Immersed In AMK

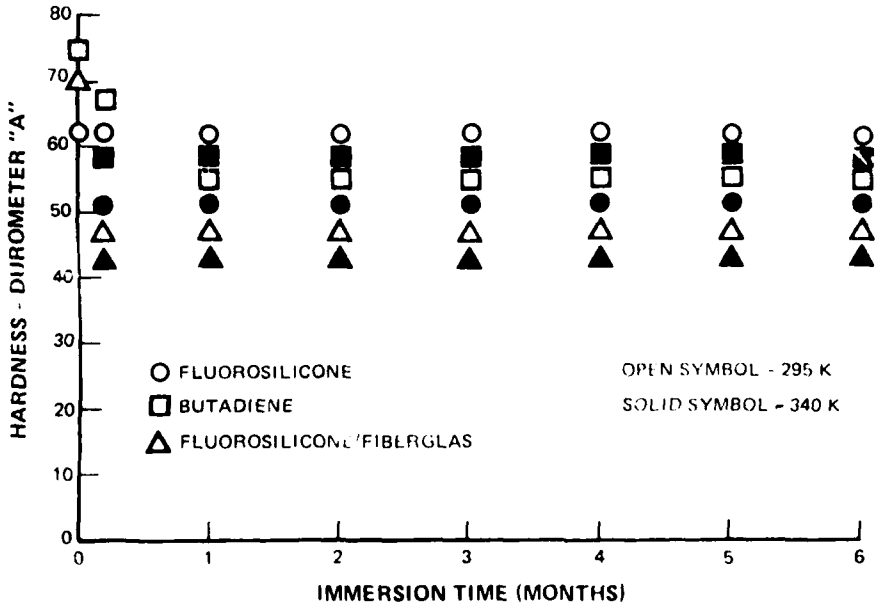

Figure 43 Effect of Hardness On Elastomers Immersed In AMK

Inspection of the elastomers at the conclusion of the 6 month testing showed no cracks or material crazing in any of the test specimens. Also, as mentioned earlier, the measured mechanical properties stabilized after one week of soaking. Based on these two facts it was concluded that all materials tested are compatible with antimisting kerosene.

3.2.6 Flow Meter Calibration

A calibration of turbine meters, venturiis, and the micro mass flowmeter was conducted. The micro mass flowmeter was found to be superior to the turbine and venturi meters in that its calibration did not vary with different levels of antimisting kerosene degradation levels.

Turbine meter and venturi measurement of flowrate is dependent on the fluid's viscosity and stress law. For antimisting kerosene the viscosity at least varies for different levels of antimisting kerosene degradation. Hence the calibration of the turbine meters and venturi is not constant necessitating a recalibration every time a different antimisting kerosene batch or degradation level is used.

Measurement of the mass flowrate with the micro mass meter was not dependent on any fuel transport properties so that the calibration was independent of antimisting kerosene degradation level. This was convenient since only one calibration was needed irrespective of the fuel used.

Throughout this program, where possible, the micro mass meter was used as the flow measuring standard.

3.3 TASK 5 - FUEL FILTER TESTS

3.3.1 Laboratory Filter Tests

In this section a successful method for measuring antimisting kerosene degradation, regardless of level, will be discussed. An evaluation of filter clogging with degraded antimisting kerosene was also undertaken.

AD-A104 673 PRATT AND WHITNEY AIRCRAFT GROUP EAST HARTFORD CT COM--ETC F/G 21/4
AN ASSESSMENT OF THE USE OF ANTIMISTING FUEL IN TURBOFAN ENGINE--ETC(U)
JUN 81 A FIORENTINO, R DE SARO, T FRANZ NAS3-22045
UNCLASSIFIED PWA-5697-29 FAA-CT-81-58 NL

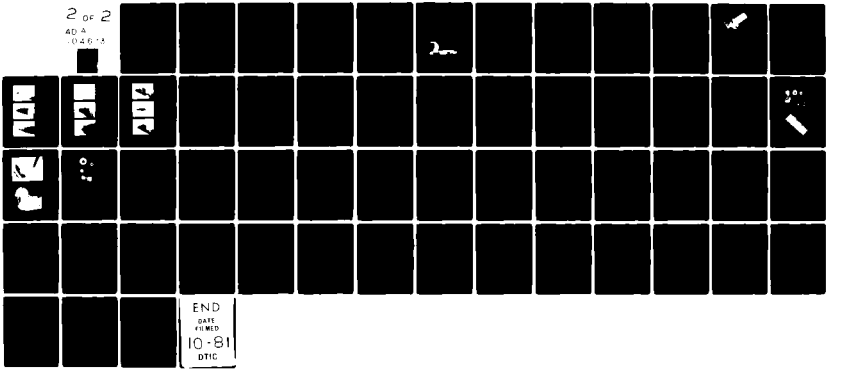

If antimisting kerosene flow through a filter is plotted as a function of increasing ΔP across the filter, one finds a dramatic increase in the flow resistance occurring at a well defined flow rate. This flow rate is termed the critical flow rate or transition flow rate. It has been found that the critical flow rate is a strong function of the number of passes through a JT8D fuel pump. Hence, critical flow rate can serve as a fuel degradation level measurement.

Laboratory tests with the following filters have been undertaken to pursue the critical flow concept.

1. 8 μm Nuclepore paper filter
2. Section of a 40 μm paper filter (used in JT8D fuel systems)
3. 10 μm metal screen
4. 17 μm woven metal screen

3.3.1.1 8 μm Nuclepore Paper Filter

Flow through Nuclepore filter papers in a standard Millipore filtration apparatus was chosen for study because of the ready availability of equipment and the well defined characteristics of the Nuclepore filters with respect to pore size, geometry and pore density. Figure 44 shows the flow characteristics through a 8 μm Nuclepore paper filter for Jet A. Data from three experiments are shown. The superficial flow (flow based on total cross section filter area) linearly increased with ΔP. At 10 to 12 cm/sec per cm there was an abrupt change in the slope in which flow rose at a slower rate with increasing pressure. Figure 44 also shows the flow characteristics for 1-pass, 3-pass, 7-pass, 16-pass and undegraded antimisting kerosene. The curves are qualitatively similar to the curve for Jet A; however, the superficial transition zone occurred at much lower flow rates and was strongly related to the degree of degradation of the antimisting kerosene. In addition a transitional flow velocity was calculated based on the actual filter flow area. Table XXVI compares the superficial flowrate, transitional velocity and filter ratio. The superficial transition flow rate and velocity changes quite significantly from 7-pass antimisting kerosene to 16-pass antimisting kerosene, while the filter ratio results show very little difference.

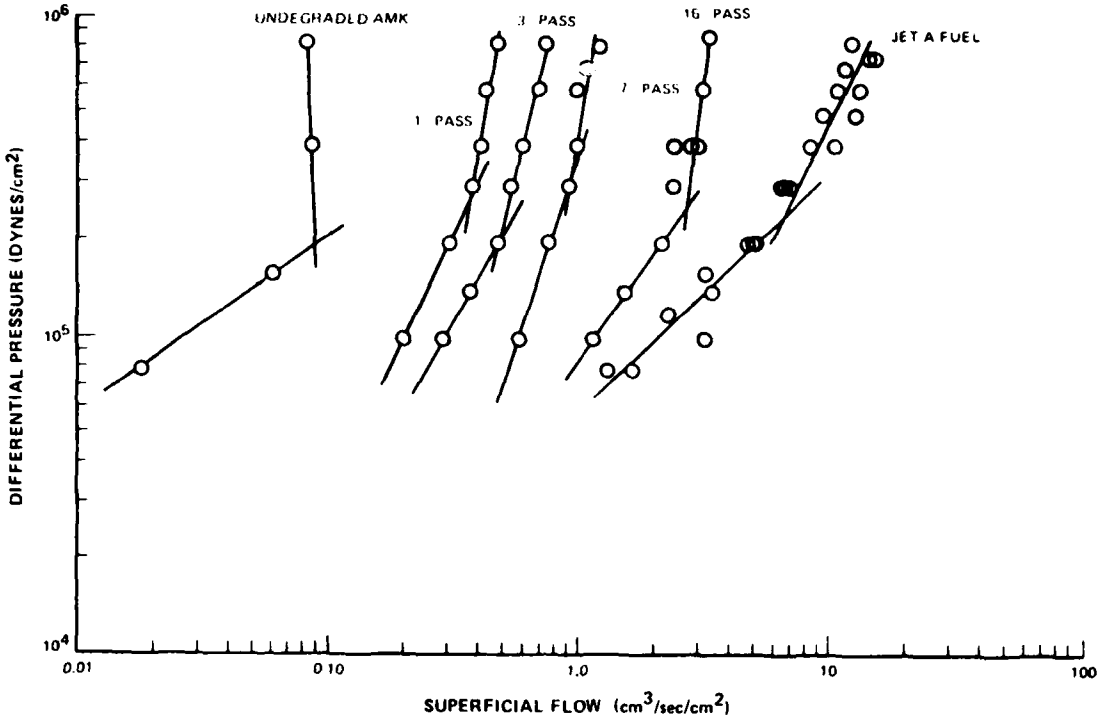

Figure 44. Flow Properties Through 8 μm Nuclepore Paper Filter

TABLE XXVI

FLOW PROPERTIES OF JET FUEL AND ANTIMISTING KEROSENE THROUGH 8 μm NUCLEPORE FILTER

Fuel Sample	Superficial Transition Flow Rate ($cm^3/sec/cm^2$)	Transition Flow[1] Velocity (cm/sec)	Filter Ratio (Standard 17 μm Screen)
Undegraded AMK	0.09	1.8	40
1-Pass AMK	0.4	8	8
3-Pass AMK	0.5	10	3
7-Pass AMK	1.6	32	1.2
16-Pass AMK	2.8	56	1.17
Jet A	10-12	200-240	1.00

[1]Based on actual flow area.

3.3.1.2 40 μm Engine Fuel Pump Paper Filter

Tests were conducted with filter sections cut from a 40 μm paper engine fuel pump filter. The flow rate of the undegraded antimisting kerosene through the filter was low necessitating a reduction in fuel volume used in the flow measurement from 300 (used in all other tests) to 25 cc. Results with the 40 μm paper filter are shown in Figure 45. Transition flow rates based on the superficial filter area (total filter cross sectional area)* were 0.7 and 20 cm/sec for 3-pass and 16-pass respectively. No transition was found for Jet A up to flows of 76 $cm^3/sec\ cm^2$.

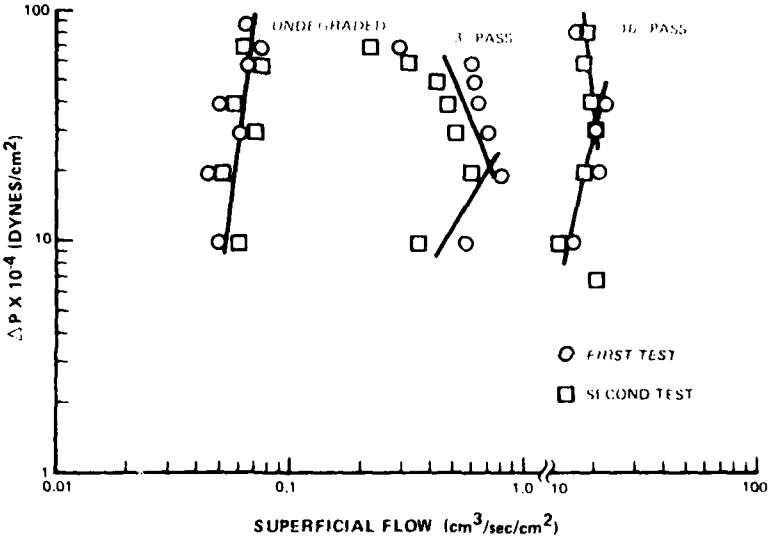

Figure 45 AMK Flow Through 40 μm Paper Filter

An indication of filter clogging was obtained by running the test at a fixed ΔP and recording the flow rate at two different times. This is shown in Figure 45 as "first test" and "second test". The rate of clogging appeared to decrease as the level of degradation increased. The clogging tendency of 16-pass antimisting kerosene was much lower than for the 3-pass. For any tested level of degradation, the rate of clogging was not dependent on the flow rate. Clogging rates were the same above and below the transition flow area. This small scale filter test predicted that during the full scale tests, 3-pass antimisting kerosene would clog faster than 16-pass.

*Actual flow area is unknown.

3.3.1.3 10 μm Woven Metal Filler

Flow curves for antimisting kerosene through 10 μm woven metal filter are given in Figure 46 at levels of degradation corresponding to 1-pass, 3-pass, 7-pass and 16-pass. Superficial transition flow rates are distinct for the 3, 7 and 16-pass but not for the 1-pass. The lack of an apparent transition for 1-pass antimisting kerosene and the steep slope of the flow curve indicate that the transition may occur at flow rates below the lowest measured for this filter.

3.3.1.4 17 μm Woven Metal Screen

Flow data for 1-pass and 16-pass antimisting kerosene, and Jet A through a 17 μm woven metal screen is shown in Figure 47. The very high flow rate through the 17 μm screen necessitated the use of an aperture to reduce the filter area to 0.5 cm^2. The screen showed a well-defined transition for 16-pass antimisting kerosene at a superficial flow rate of 20 $cm^3/sec/cm^2$. The transition for Jet A with no additive occurred at 55 $cm^3/sec/cm^2$.

3.3.1.5 Effect of Reduced Temperature on Flow Properites Through 10 μm Woven Metal Screen

The effect of lowered temperature on flow properties of 3-pass through 10 μm woven metal filter is shown in Figure 48. The shape of the curves (at lowered temperatures) cannot be readily explained. The antimisting kerosene demonstrated an enhanced tendency for clogging at lower temperatures. This may introduce nonreproducibility and procedure dependence into the measurements. The very viscous gel formed on the downstream side of the filter in the -26°C experiment is shown in Figure 49.

3.3.1.6 Summary of Transition Flow Rates

The transition flow velocities, based on the actual filter flow area, are summarized in Table XXVII. Transition velocities through the 40 μm paper filter are not tabulated because the actual flow area is not known. Given the wide range of actual flow rates among the three filters, the agreement in flow velocities is good. In addition, transition velocity is a strong function of the number of JT8D fuel pump passes and can be used as a degradation level indicator.

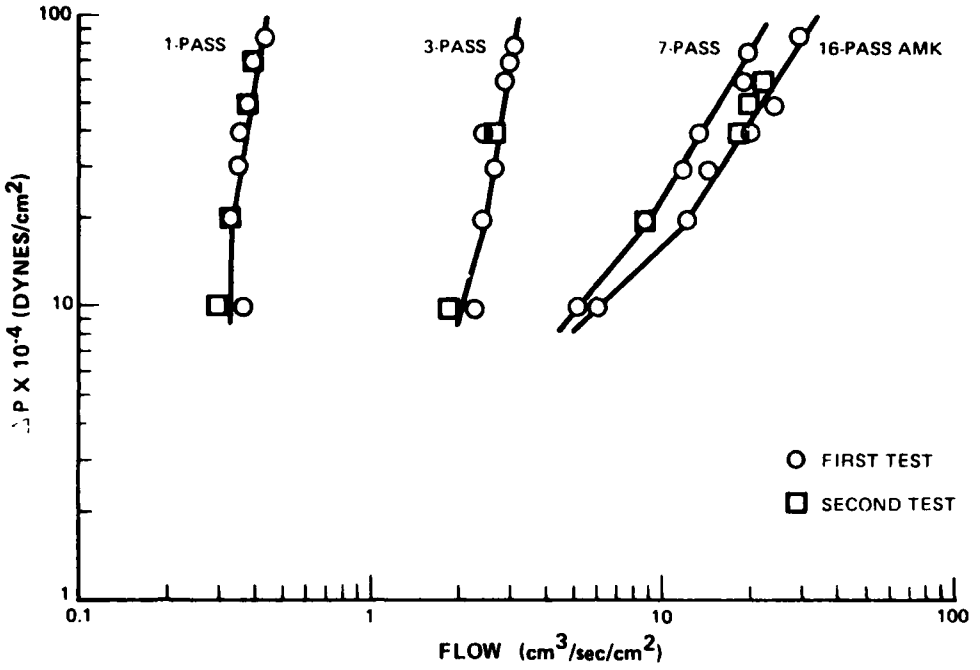

Figure 46 AMK Flow Through 10 μm Metal Screen

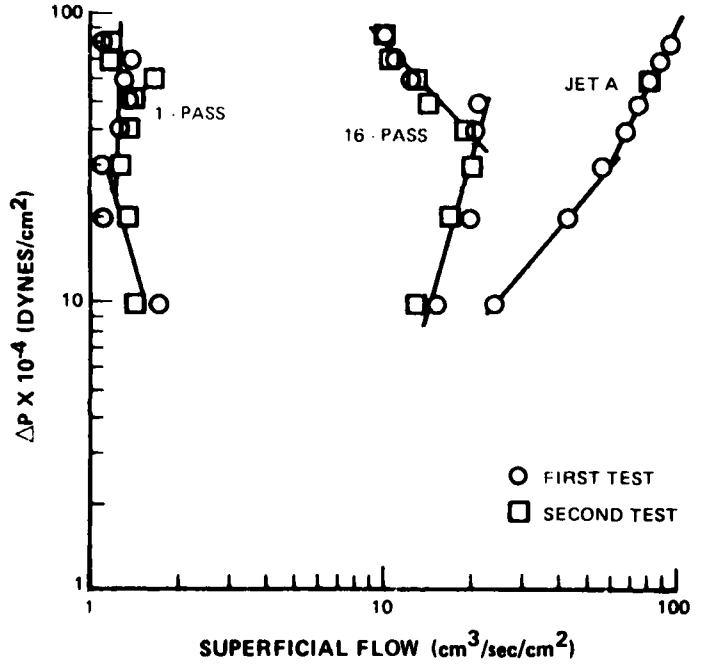

Figure 47 AMK Flow Through 17 μm Metal Screen

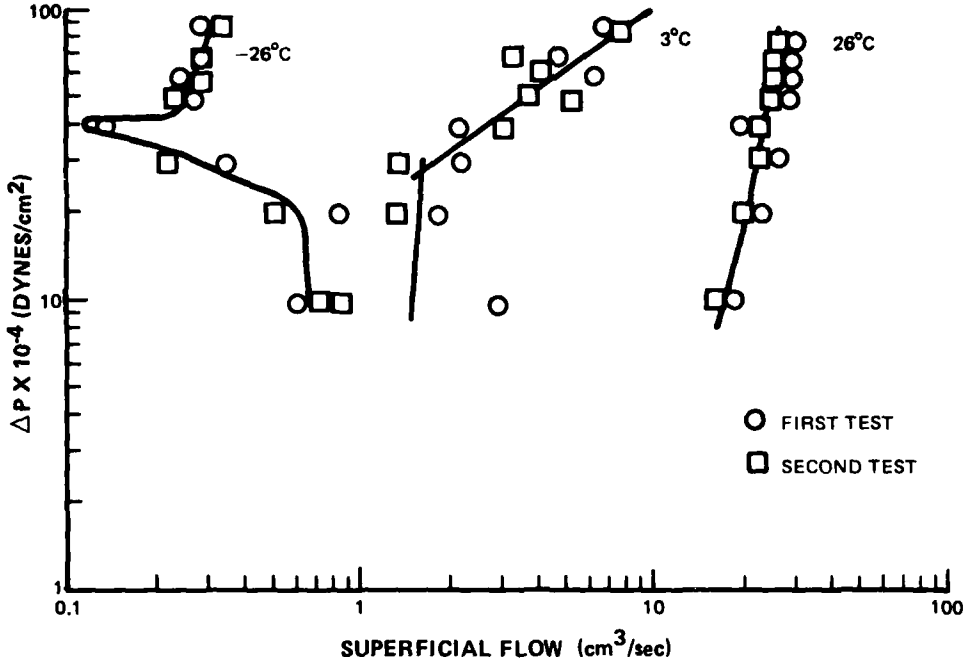

Figure 48 *Effect of Reduced Temperature On Flow Properties of 3-Pass, (F_R = 1.28) AMK Through 10 μm Metal Screen*

Figure 49 *Gel Formed On Downstream Side of 10 μm Metal Filter After Flow at -26°C*

TABLE XXVII

TRANSITION FLOW VELOCITY OF ANTIMISTING KEROSENE THROUGH FILTERS

Sample	Transition Flow Velocity (cm/sec) 8 μm Nuclepore	10 μm Screen	17 μm Screen
Undegraded AMK	1.6		
1-Pass AMK	8		
3-Pass AMK	10	10	
7-Pass AMK	32	38	
16-Pass AMK	56	47	53
Jet A	200-240		147

3.3.2 Full Scale Fuel Filter Tests

To ensure adequate engine operation it was necessary to determine the full scale fuel system filter behavior while flowing various levels of degraded antimisting kerosene. In this task, testing and evaluation of the flow rate versus differential pressure and clogging tendency of the various JT8D fuel system filters as a function of antimisting degradation level were achieved. Laboratory tests (Section 3.3.1.2) indicated that the undegraded and 3-pass antimisting kerosene would not pass through the fuel pump paper filter. The following tests indicated that 3-pass antimisting kerosene having a filter ratio in the range of 1.2 to 2.1, was near the threshold of gelling on the fuel pump paper filter and the fuel control servo system wash filter. The fuel control inlet filter and the servo system secondary filter at this antimisting kerosene degradation level were unaffected. In general, 16-pass antimisting kerosene was necessary for adequate operation of all the filters.

3.3.2.1 JT8D Engine Fuel Pump Filter Performance Tests

Figure 50 is a plot of the fuel pump filter flow rate as a function of filter pressure drop for different fuel samples. 3-pass antimisting kerosene is plotted at time zero and at a time 30 seconds later. The later time shows

increased flow resistance over the early time indicating filter clogging. In an attempt to bracket the degradation level necessary to avoid filter clogging 16-pass antimisting kerosene was run and is plotted along with Jet A. The data taken during the test were not time dependent indicating that no clogging was occurring. This is consistent with Section 3.3.1.2 predictions from laboratory experiments.

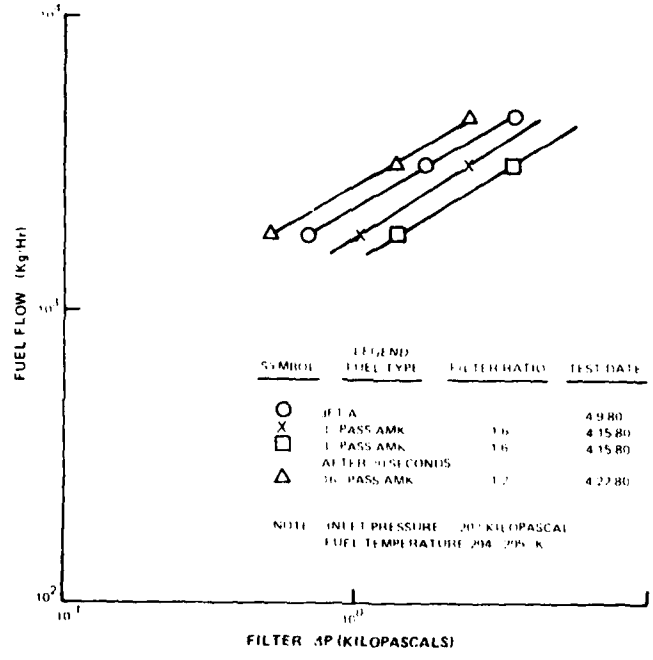

Figure 50 JT8D Main Fuel Pump Paper Filter Flow Characteristics

3.3.2.2 Fuel Control Filter Assembly Performance Tests

Figure 51 shows the wash flow filter characteristacs with 3-pass antimisting kerosene. Plotted is ΔP across the filter versus flow time for variations in flowrate. Under all tested conditions with 3-pass antimisting kerosene clogging occurred as is evidenced by the increasing ΔP with time. 16-pass, also tested but not plotted here showed no tendency to clog. The effect of flow velocity on filter clogging can be seen on Figure 51 by observing the zero through flow curve (318 kg/hr wash flow) with either the 1544 or 1634 kg/hr through flow rate. The 1544 or 1634 kg/hr through flow rate had a much higher filter flow velocity than did the zero through flow rate. At the higher flow velocity ΔP increased with time more rapidly than the lower velocity curves which indicated clogging occurred more rapidly as flow velocity increased through this filter.

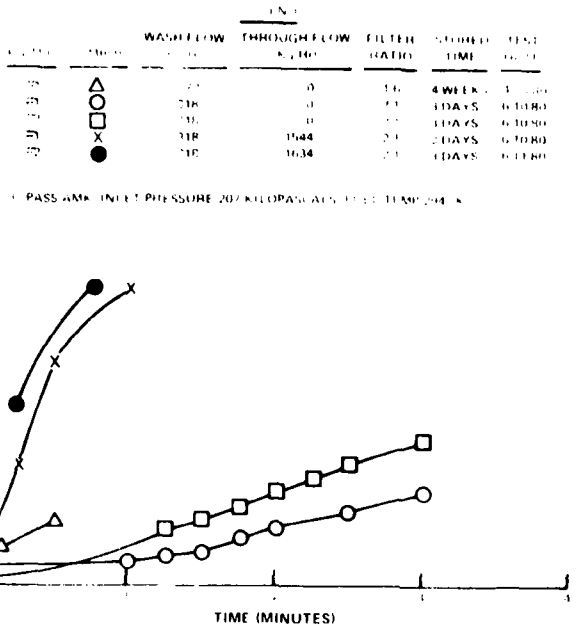

Figure 51 JT8D Fuel Control Wash Flow Filter Characteristics

The amount of time degraded antimisting kerosene was stored prior to being used appeared not to be a factor in filter clogging as determined by an exploratory test. 3-pass antimisting kerosene, stored for four weeks, was used in the wash filter test. This can be compared to 3-pass stored for three days. In both cases the filter ΔP increased at approximately the same rate with time and resulted in both filters clogging.

The fuel control inlet coarse screen showed no clogging tendencies with either 3-pass or 16-pass antimisting kerosene.

3.3.2.3 Servo Systems Secondary Filter Performance Tests

The servo system secondary filter showed no clogging with 16-pass antimisting kerosene. It is a very coarse filter and clogging was not expected.

3.3.2.4 Filter Duration Tests

The fuel pump and fuel control filters were subjected to 16-pass antimisting kerosene for one hour at the conditions tabulated in Table XXVIII.

TABLE XXVIII

EXTENDED DURATION FILTER TEST CONDITIONS

Time (minutes)	Fuel Pump Paper and Fuel Control Inlet Coarse Filter Flow (kgm/hr)	Fuel Control Wash Filter Flow (kgm/hr)
30	1361	317
10	2721	for
20	1270	1 hour

No differential pressure buildup was observed on any of the filters. Also, the filter ratios sampled upstream and downstream of the filters were the same.

3.3.2.5 Rig Inlet Screen

The test rig inlet screen was the first program item that indicated the anti-misting kerosene gelling phenomenon. As shown in Figure 52 a significant gell quantity formed on the downstream side of the screen while flowing undegraded antimisting kerosene at 1361 kgm/hr (3000 pph). During gelling, the differential pressure increased linearly with time. No pressure buildup was noticed when degraded fuel was used. In fact, the gel on a previously clogged screen was eliminated when a degraded antimisting kerosene fuel was run through the screen.

Early degradation attempts at lower supply tank pressures required intermittent rig operation and a gell dissipation characteristic was noted. As shown in Figure 53 the screen differential pressure increased rapidly during initial operation and then dropped to a lower level while the pump was stopped.

3.3.2.6 Filter Test Summary

To ensure adequate operation of all fuel system filters, a degradation level between 3-pass and 16-pass must be used. In addition, gelling is velocity sensitive regardless of the degradation level. Filters with high fuel velocities will more readily exhibit gelling than those with lower fuel velocities.

Previously gelled screens can be cleared by flowing highly degraded antimisting kerosene or Jet A through them or by leaving the filter undisturbed and allowing the gel to dissipate.

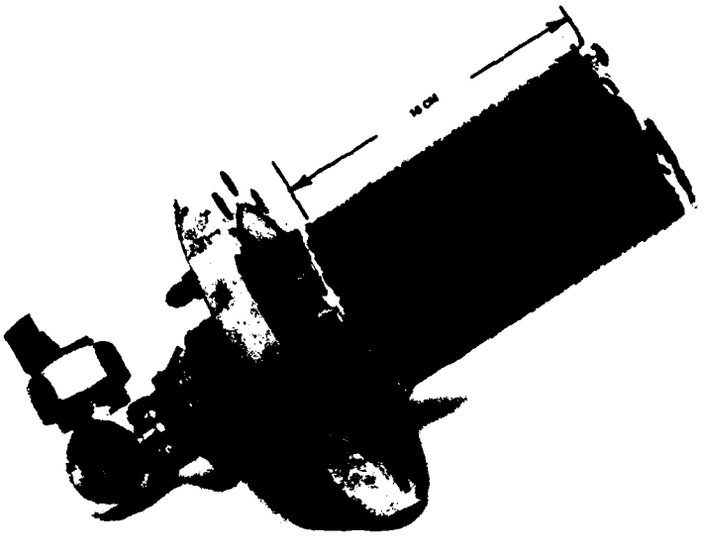

Figure 52 Degrader System Inlet Screen

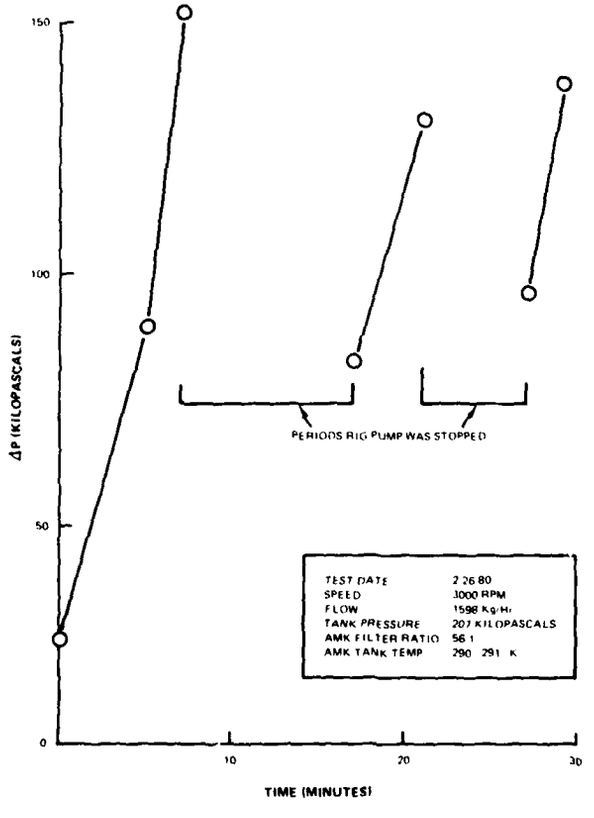

Figure 53 De-Gelling Phenomenon-100 Mesh Screen Differential

3.3.3 Task 5 - Summary

The laboratory and full scale filter tests are in agreement as to the degradation level required for successful short term flow tests (i.e., 16-pass). While they are in disagreement about the effect of flow velocity on clogging, the full scale tests were run at a higher flow range than the laboratory tests which might account for the difference. The transitional velocity appears to be the best method for measuring degradation level.

3.4 TASK 6 - INJECTOR SPRAY TESTS

The objective of this Task was to determine if any of the injectors were clearly superior to others in terms of the characteristics of the spray produced with the different fuels, and to determine the extent of degradation required to achieve an acceptable spray.

Results of the tests indicated that the use of antimisting fuels caused a noticeable degradation in the quality of the spray produced by all three of the injectors at all conditions tested. Photographs of the sprays produced with three different fuel nozzles are shown in Figures 54, 55, and 56. It is apparent from these photographs that the use of undegraded antimisting fuel resulted in a grossly incomplete atomization of the fuel with the spray being characterized by ligaments of fluid rather than droplets. Processing of the fuel enhanced the quality of the spray; however, the photographs clearly indicate that even the three-pass degraded fuel produced a spray inferior to that of Jet A. A listing of the droplet size information at each of the engine conditions for room temperature fuels is given in Table XXIX. Shown in the table are the value of the Rosin-Rammler characteristics droplet size (PE) and the Sauter mean diameter (SMD). It is believed that the characteristic size, PE, was a better indicator of the capability for a spray to be consumed when comparing nozzles of different types (pressure atomizers vs. air atomizers), however, the SMD has found more widespread use as a figure-of-merit for spray atomization. Regardless of the parameter inspected, however, the trend of increasing droplet size with decreasing extent of fuel preparation was apparent in the data.

Figure 54 Spray Pattern With JT8D B/M - Cruise

Figure 55 Spray Pattern With JT8D Low Emission Injector - Cruise

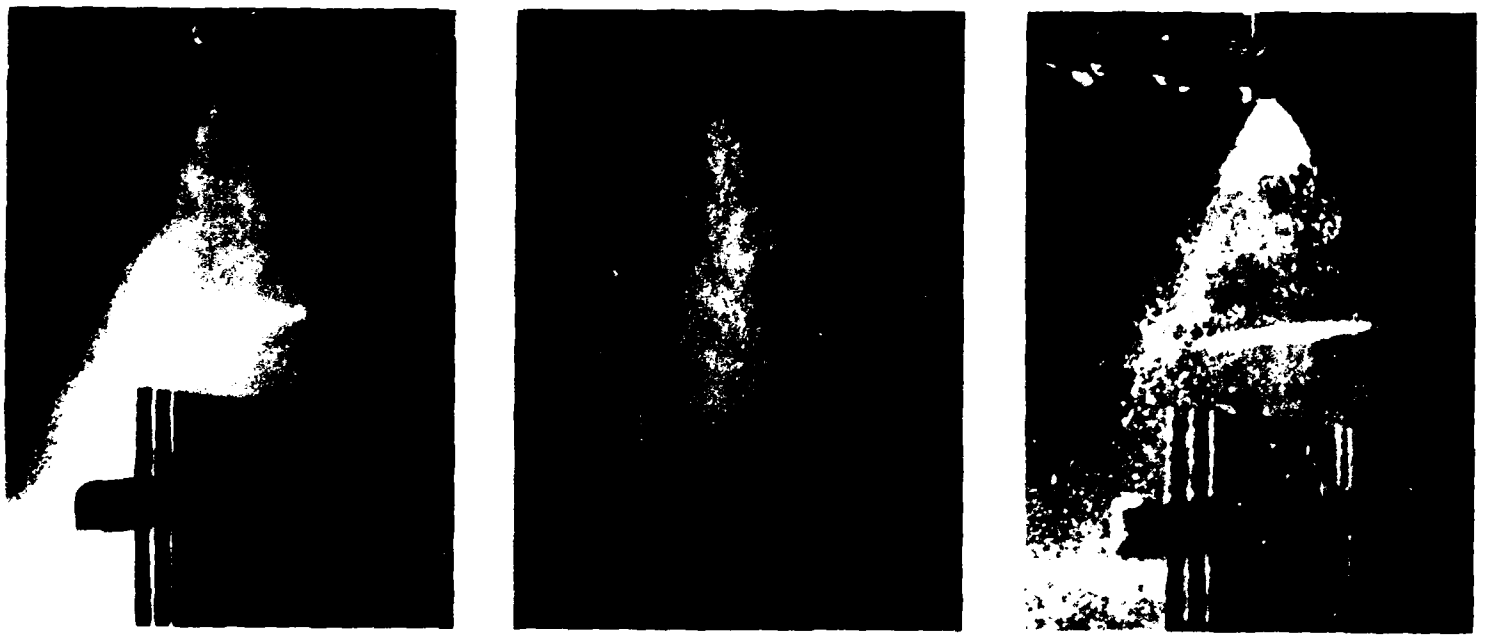

Figure 56 Spray Pattern With Air-Boost Injector - Cruise

TABLE XXIX

MEAN DROPLET SIZE PRODUCED WITH ROOM TEMPERATURE FUELS

Fuel	Condition	B/M PE microns	B/M SMD microns	Low Emission (LE) PE microns	Low Emission (LE) SMD microns	Air-Boost PE microns	Air-Boost SMD microns
Jet A	Ignition	85	46	97	60	40	20
	Idle	62	33	79	47	34	20
	Cruise	122	57	78	29	45	22
	SLTO	149	47.3	110	41	177	89
Three-Pass Degraded	Ignition	120	48	127	58	64	8
	Idle	110	50	85	31	66	8
	Cruise	171	72	142	45	133	24
	SLTO	151	70	191	61	159	50
One-Pass Degraded	Ignition	180	107	156	92	73	19
	Idle	143	76	111	59	84	15
	Cruise	176	88	139	52	151	38
	SLTO	140	65	152	71	168	71
Undegraded	Ignition	212	158	240	175	80	40
	Idle	137	119	279	210	89	37
	Cruise	251	134	243	144	167	62
	SLTO	150	100	239	164	176	130

Examination of the data indicated that the improvement in droplet size achieved by using three-pass degraded antimisting kerosene was small; it would be necessary to use more extensive processing to achieve spray quality approaching that of Jet A sprays.

Tests conducted with fuels at temperatures other than room temperature confirmed that the anticipated trends were experienced--droplet size decreased with increasing temperature. The atomization of the antimisting fuels at low temperature ($-29^{o}C$) revealed no special problems.

The droplet size data indicated, as expected, that the air boost injector was capable of producing an atomized spray even with the undegraded fuel, at the low flow conditions. The nozzle used in the tests had a smaller flow capacity than the JT8D injectors and did not perform well at SLTO conditions; a large

capacity nozzle probably would have produced satisfactory atomization at the high flow condition. Use of an air boost injector on an aircraft would, however, represent a major development effort because of the necessity of providing an onboard source of high pressure air. The fact that the conventional injectors produced atomized spray with the degraded fuel suggested that the radical design approach of employing air boost nozzles would be unnecessary.

The spray photographs indicate that the use of antimisting fuel caused a small reduction in the spray cone angle produced by the pressure-atomizing and air-blast atomizing nozzles; the cone angle produced by the air boost nozzle was not significantly affected. A tabulation of spray cone angles is presented in Table XXX. The double-entries in the table indicate the angles as measured at the face of the nozzle and as measured approximately 2.5 cm. downstream where the spray turning has been completed. As indicated in the table, when using undegraded fuel, no atomization of the fluid occurred at the lowest flow (emission) condition for two of the nozzles; the fluid simply issued from the nozzle as a single stream.

TABLE XXX

INJECTOR SPRAY CONE ANGLES

Fuel	Condition	B/M	Low Emission (LE)	Air-Boost
Jet A	Ignition	25/30	27.5/35	37.5/25
	Idle	35/40	35/35	37.5/25
	Cruise	25/27.5	30/37.5	40/30
	SLTO	40/35	25/27.5	42.5/35
Three-Pass Degraded	Ignition	20/20	32.5/35	32.5/27.5
	Idle	25/22.5	40/32.5	32.5/27.5
	Cruise	42.5/32.5	30/32.5	37.5/30
	SLTO	42.5/32.5	30/	40/35
One-Pass Degraded	Ignition	17.5/22.5	32.5/32.5	35/32.5
	Idle	20/12.5	40/30	40/25
	Cruise	27.5/27.5	27.5/27.5	40/27.5
	SLTO	32.5/30	32.5/37.5	
Undegraded	Ignition	0/0	0/0	37.5/27.6
	Idle	20/20	22.5/22.5	30/25
	Cruise	12.5/17.5	17.5/25	37.5/27.5
	SLTO	30/25	22.5/22.5	30/30

Further indication of the effect of fuel characteristics on spray distribution can be found by examining the patternator data. Typical fuel pattern profiles are shown in Figure 57; the curves show the flowrate of fuel in kilogram per hour entering the tip of the probe located at the indicated radial distance from the injector centerline. The curves shown in the figure indicate the fuel patterns obtained using the low emissions injector at the cruise flow conditions when flowing Jet A, undegraded antimisting fuels, and degraded antimisting fuels. The results indicated that for this injector use of antimisting fuel did not change the basic hollow-cone character of the fuel spray. Changes in the detailed features of the curves (shifts in the peak height or a change in the characteristics width of the peaks) were not of the magnitude to cause concern. Examination of the patternator data at the very low flow (ignition) condition indicated that the characteristics of the hollow cone spray produced by the bill-of-material pressure atomizing injector were preserved except in the case in which undegraded antimisting fuel was used. The patterns produced by the low emission injector undergoes significant shifts even for the three-pass degraded antimisting fuels. At the somewhat higher idle flow conditions, the low emissions injector showed less sensitivity to the extent of fuel processing although there was some indication that streaking had occurred with the use of the undegraded fuel. At the ignition and idle conditions, the low emission nozzle passed all fuel flow through the primary passage which is a pressure atomizer. These data suggested that the air passing through the secondary passages affected the spray cone produced by the pressure atomizer such that the spray spatial distribution was unstable. Patternator data acquired with this nozzle when the three-pass degraded fuel was passed through the secondary fuel passages rather than the primary at the ignition conditions indicated that a broad, flat fuel profile was generated, not the double peaked profile characteristic of a well-formed hollow cone spray. The patternator data for the air boost injector operating at ignition conditions indicated that a drastic shift in profile occurred when moving from Jet A fuel to undegraded fuel; a shift from a sharply peaked central spike profile to a broader flatter profile. At the highest flow (SLTO) conditions, the pressure-atomizing and the air-boost nozzle fuel profiles showed little sensitivity to the extent of fuel processing.

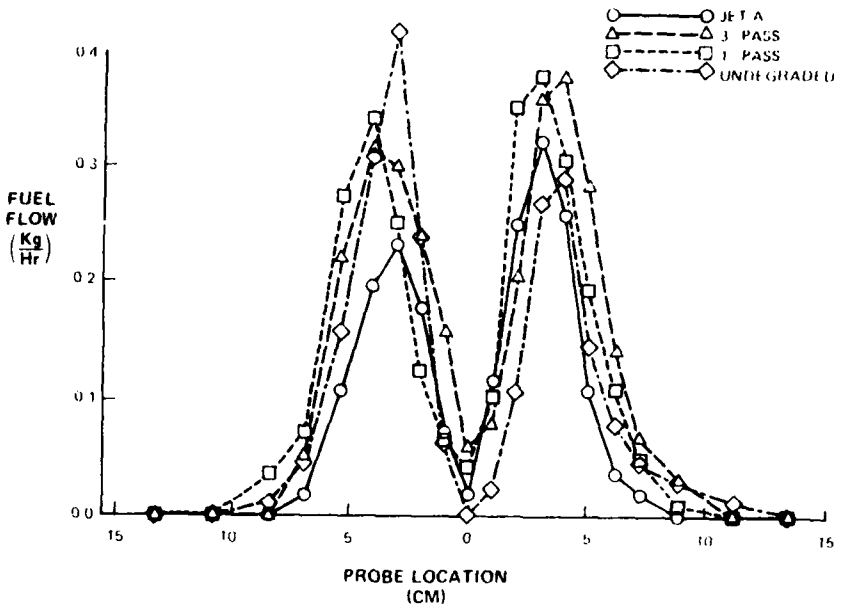

Figure 57 AMK Patternator Data L/E Injector at Cruise

The data for the low emission nozzle indicated that the hollow cone pattern produced showed some sensitivity to fuel type in that the peak values of flow rate captured by the probes were higher in the case when Jet A fuel was used and were lower when undegraded antimisting fuel was used. This implies that the spray sheath thickened as the fuel quality decreased. This in itself is not disadvantageous in terms of spray patterns, however, it does indicate that changes in burner airflow patterns might have to be made in order to preserve the desired turbine entrance temperature profiles.

Comparison with Combustor Data

The combustor rig data was obtained at several engine simulated conditions, i.e., idle, cruise and sea level takeoff. In general, there were no adverse emissions or combustion efficiency effects at the cruise or sea level takeoff conditions using the 3 or 1-pass antimisting kerosene fuels and the only effects were at the idle condition (see Section 3.5.1.1). This result was not surprising and was due to the high loading factors at cruise and sea level takeoff and the fact that the idle condition was probably the more marginal condition for the JT8D engine.

The combustor rig idle test results indicated that for bill-of-material and low emission injectors the use of Jet A fuel yielded lower emissions, higher combustion efficiency and lower blowoff limits than any tested level of degraded antimisting kerosene. This trend was consistent with the smaller PE and SMD values found for the two JT8D injectors using Jet A when compared to 3-pass and 1-pass degraded antimisting kerosene.

The engine tests also indicated a more significant degradation in the emission and combustion efficiency for the low emission injector when compared to the bill-of-material injector. The droplet data alone indicated the reverse, the performance of the bill-of-material injector degraded more rapidly than the low emission injector at the idle condition. This inconsistancy could possibly be explained by the idle patternator data for the two injectors. The low emission injector fuel distribution changed from a hollow cone Jet A spray with no fuel in the center to a semi-hollow spray cone using 3 and 1-pass antimisting kerosene and this change could disrupt the primary zone recirculation pattern.

In the idle engine studies using 3-pass antimisting kerosene, the emission levels for the low emissions nozzle were not affected by flowing all the fuel through the secondary, even though the ambient spray results indicated a larger PE and SMD. This discrepancy could possibly be explained by the idle patternator data. The spray width was larger, the spray cone more hollow and the fuel concentration lower when all the fuel passed through the secondary and these changes could have compensated for the larger PE and SMD.

In cases in which the type of fuel injector changed, i.e., a pressure atomizer or aerating nozzle or air-boost nozzle and/or the fuel type changed, i.e., Jet A or antimisting kerosene, it was often difficult to explain the combustor test results based solely on the measured SMD. Instead the droplet distribution data together with the patternator data must be studied. Even knowing all this information it was still quite difficult to determine the "best" configuration due to the limited amount of combustor and ambient flow visualization data collected to date.

SUMMARY

1. The use of antimisting additives in turbine fuels caused a drastic deterioration of fuel spray quality as measured by droplet size. Degradation of additive by shearing the fuel, resulted in improvement of the fuel spray characteristics, but mean droplet sizes produced with three-pass degraded fuel were larger than those produced with Jet A fuel.

2. Air boost nozzles produced better atomization than air-blast or pressure atomizing nozzles; however, the latter nozzles produced sprays which may be of satistatory quality when highly degraded fuel is used and these nozzles do not require the development of an auxiliary high pressure air system as would the air boost nozzle.

3. At high flow conditions the spatial spray distribution produced by the nozzles tested showed no major deficiencies although there was some tendency to produce smaller spray cone angles. At the lower flow condition, the pressure atomizing bill-of-material nozzle produced a stable hollow cone spray pattern whereas the low emission nozzle produced patterns which suggested an unstable or streaking and the air boost nozzle produced a center peaked profile. Only the air boost nozzle was able to produce a distributed spray when utilizing undegraded fuel. The reasonably well atomized spray and minor patternator variations obtained for the bill-of-material nozzle when using three-pass degraded fuel suggested that, if improved degradation methods were made available, existing fuel nozzles would be adequate for use with antimisting fuels.

4. Operation of nozzles using antimisting fuels with fuel temperatures ranging from $-29^{o}C$ to $46^{o}C$ produced no unanticipated effects.

5. The low emission injector was tested with the fuel split between the primary and secondary and with all the fuel through the secondary. In general, the SMD, PE and W were all lower when the low emission injector was used as it was designed, i.e., flow split between primary and secondary.

6. The degradation in the performance of the JT8D engine using the bill-of-material and low emission injectors at the idle condition using the antimisting kerosene fuels can be correlated with the increase in the SMD and PE. However, the droplet data alone cannot be used to explain the relative performance of the two JT8D injectors. The droplet data and the patternator data must be considered together.

7. Undegraded antimisting kerosene, for the bill-of-material and low emission injectors, should not be used for combustor studies because of the very poor spray produced.

3.5 TASK 7 AND OPTIONAL TASK A - COMBUSTOR PERFORMANCE TESTS

The emissions, high altitude relight, and sea level ignition of the bill-of-material and low emission combustors using Jet A and antimisting kerosene are presented in this section.

3.5.1 High Pressure Tests

High pressure rig tests were utilized to determine the effect various levels of degraded antimisting kerosene have on performance and emission parameters as compared to Jet A. In addition, differences between the bill-of-material and low emission combustors using antimisting kerosene were of interest. Measurements of emissions, liner cold side temperatures, lean blow out limits and observations of nozzle and combustor deposits were made.

3.5.1.1 Emissions

Emission results for the Jet A fuel were consistent with results obtained previously at Pratt & Whitney Aircraft for the same configurations. The antimisting kerosene emissions can therefore be conveniently compared to a well established Jet A emission baseline

Emission differences between Jet A and antimisting kerosene occurred at idle. No differences were observed at high power. Under all conditions, the smoke numbers and NO_x levels were not affected by the use of antimisting kerosene. For the low emissions burner, flowing all the fuel through the secondary also had no effect on the emission levels.

The effect of fuel on emissions and combustion efficiency (η_c) can be seen in Figures 58a, b, and c. Plotted are η_c, CO_{EI} and THC_{EI} at nominal idle versus type of fuel.*

In all cases Jet A fuel yielded lower emissions and higher η_c than any tested level of degraded antimisting kerosene. Going from Jet A to 3-pass to 1-pass the emissions became progressively worse for both combustor configurations. From Jet A to 3-pass the carbon monoxide went up by 20 percent for the bill-of-material and more than doubled for the low emission combustor. From 3-pass to 1-pass the increase was 5 percent for the bill-of-material and 30 percent for the low emission combustor. The total hydrocarbons, Figure 58c, showed similar trends, though the low emission combustor increase in total hydrocarbons from Jet A to 1-pass was much higher than for carbon monoxide. The higher the level of antimisting kerosene degradation, the lower the emissions. While 16-pass antimisting kerosene was not run in these tests it is expected that its emissions would be much closer to that of the Jet A.

The low emission combustor had lower emissions than the bill-of-material with Jet A. When antimisting kerosene was used, the situation was dramatically reversed. These emission results can be explained by the injector performance tests. See Section 3.4.

3.5.1.2 Lean Blow Out

Lean blow out is defined as the minimum fuel air ratio at idle that will support combustion. The lean blow out for both the bill-of-material and low emission combustors is shown in Figure 58d. The antimisting kerosene required higher fuel air ratio for lean blow out than the Jet A. The low emission combustors fuel air ratio was very similar to the bill-of-material up to 3-pass, but increased rapidly at 1-pass.

*Emissions at lean idle are, in some cases, considerably higher than at nominal idle.

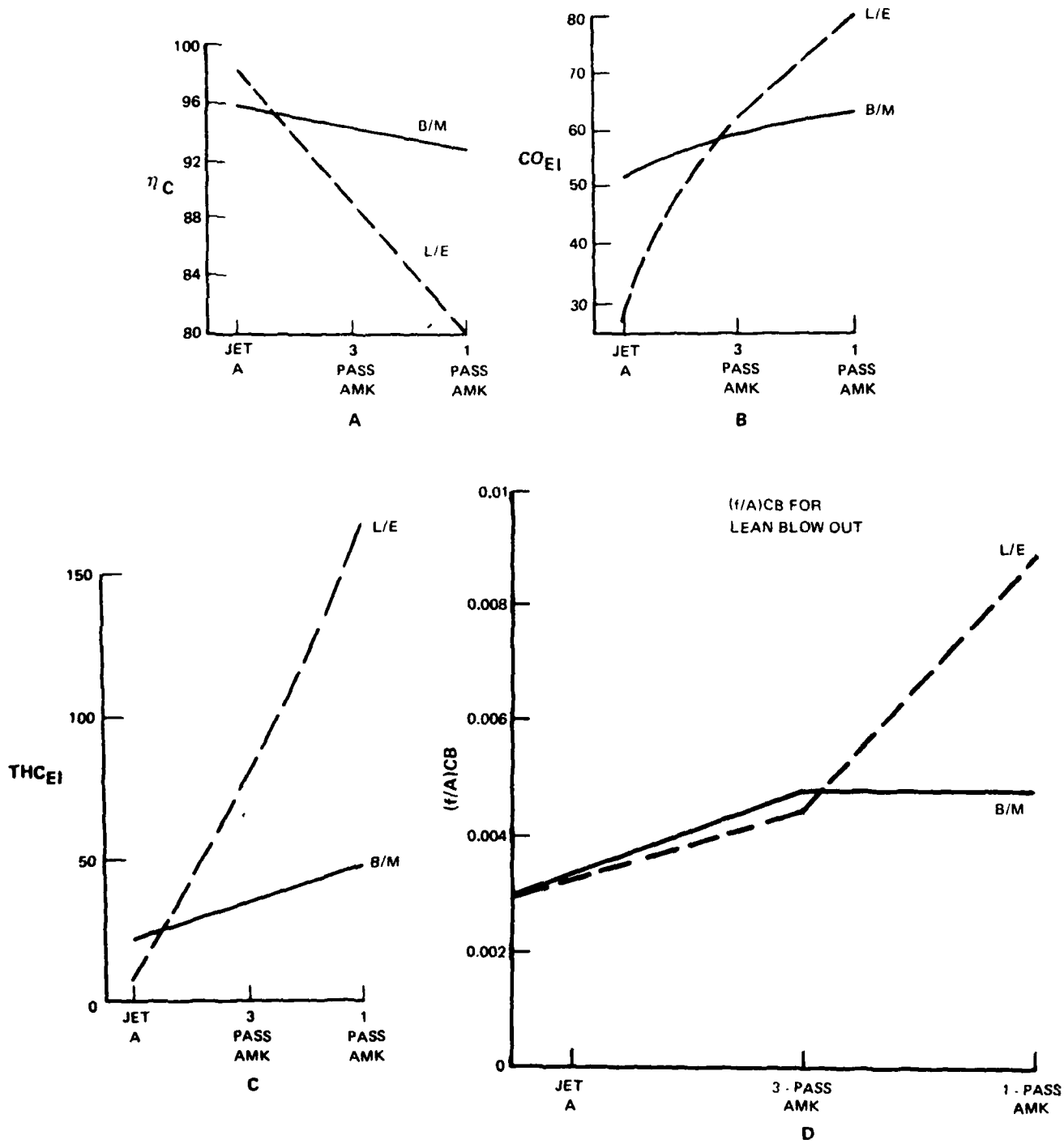

Figure 58 Low Power Emissions (Idle)

3.5.1.3 Combustor Cold Side Liner Temperatures

With antimisting kerosene as a fuel, the liner cold side temperatures were essentially the same (typically 5 to 10K lower) as Jet A. The small difference was possibly due to the AMK's lower heat of combustion (see Table XXI).

3.5.1.4 Post Test Observations

The bill-of-material and low emission combustor cans and fuel nozzles were photographed at the completion of running the test conditions (listed in Table XI) for each of the two degraded antimisting kerosene levels. Hence, 4 sets of photographs were taken:

1) Bill-of-material tested with Jet A and 3-pass antimisting kerosene
2) Bill-of-material tested with Jet A and 1-pass antimisting kerosene
3) Low emissions tested with Jet A and 3-pass antimisting kerosene
4) Low emissions tested with Jet A and 1-pass antimisting kerosene

The bill-of-material configuration with 3-pass antimisting kerosene had some gelling in the fuel nozzle and a small pool of gell in the combustor can. Figure 59 shows the disassembled nozzle and Figure 60 a close-up of a spring. The lower half is heavily gelled. In Figure 59, several other components are also gelled. Figure 61 shows the inside of the bill-of-material combustor can. A small pool of gell collected just downstream of the combustor hole.

The bill-of-material with 1-pass antimisting kerosene and the low emission with 3-pass antimisting kerosene showed no gelling or deposits of any kind at the completion of the tests.

The low emission configuration with 1-pass antimisting kerosene showed extensive carbon deposits in the combustor can and some carbon deposits in the fuel nozzle. Figure 62 is a photograph of the downstream end of the combustor can. The deposits can be seen on the louver lips. The deposits occurred on all the upstream lips not shown in the photograph. Figure 63 shows the disassembled nozzle. Deposits can be seen on some of the components.

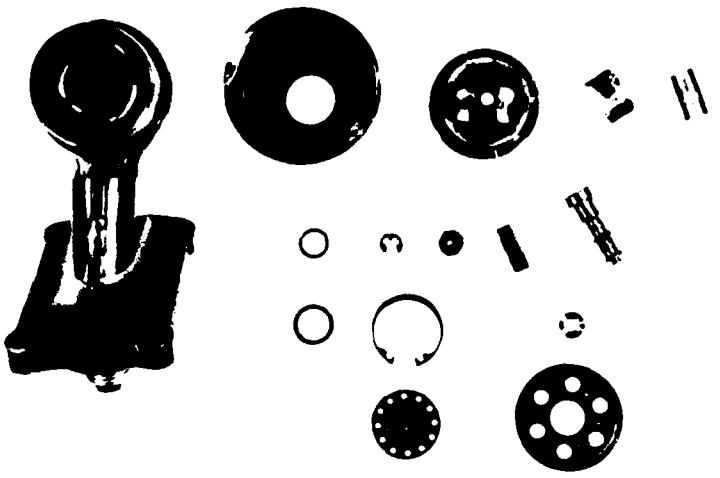

Figure 59 Post Test Disassembly of B/M Nozzle

Figure 60 Gel On Spring From B/M Nozzle

Figure 61 Post Test Photograph of B/M Combustor Can

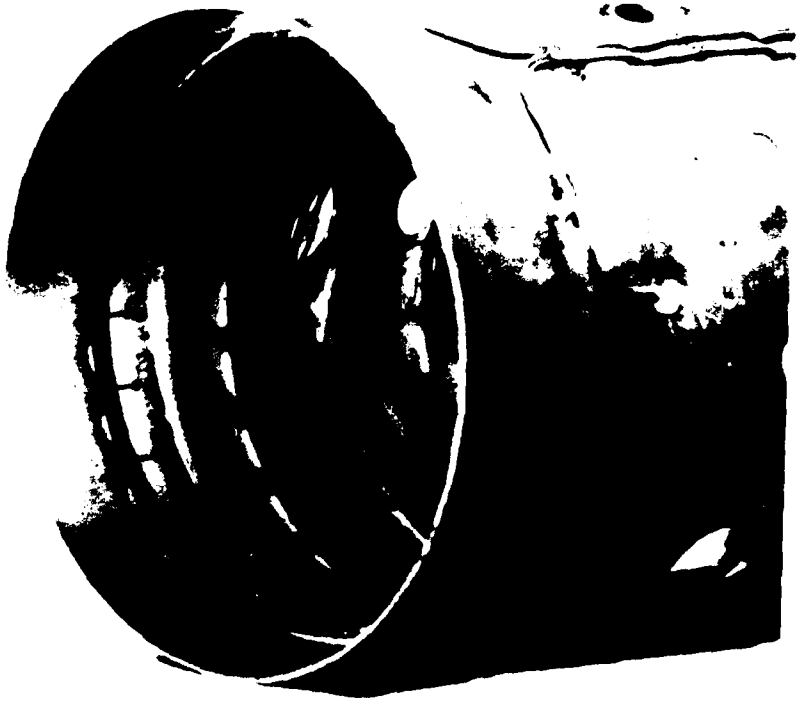

Figure 62 Post Test Photograph of L/E Combustor Can

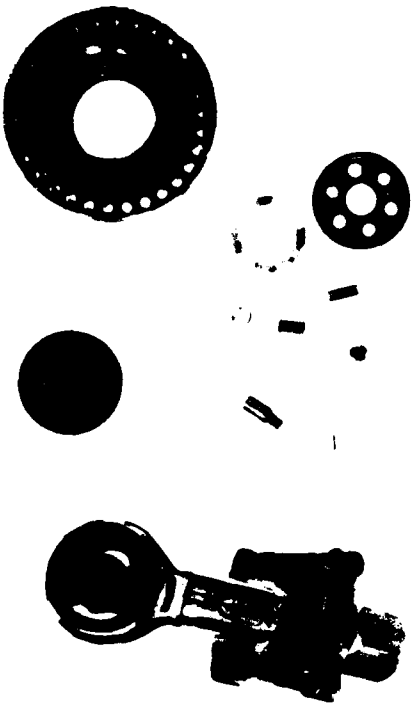

Figure 63 Post Test Disassembly of L/E Nozzle

3.5.1.5 Summary

The emission levels produced from both the 1-pass and 3-pass antimisting kerosene were unsatisfactory. A degradation level higher than 3-pass was necessary. Although 16-pass antimisting kerosene was produced during the latter stages of this program, it was not feasable to test it in the combustor rig due to scheduling constraints. Based on spray analysis results extrapolated from 3-pass it is postulated that 16-pass antimisting kerosene would generate emission levels close to that of Jet A.

3.5.2 High Altitude Relight Tests

The following section describes the altitude relight results for the bill-of-material and low emission combustors operating with Jet A and 3-pass antimisting kerosene.

Figures 64 through 67 show these results. Plotted is simulated altitude versus flight Mach number with station 4 (burner plus turbine bleeds) airflow as a parameter. The open symbols indicate a light (5 or more of the burner cans lit) and the closed symbols a no light (4 or less of the burner cans lit). The 3-pass antimisting kerosene consistently exhibited poorer relight characteristics than the Jet A. Figures 64 and 65 are for the bill-of-material combustor, Jet A and 3-pass antimisting kerosene respectively. For the Jet A, a light was achieved at 10,000m for 2.27 kg/sec airflow and at about 7,600m for the 3.18 kg/sec airflow. At an airflow of 4.08 kg/sec results were ambiguous since the two achieved lights were indispersed with no lights. No light was achieved at 5.22 kg/sec airflow. For the 3-pass antimisting kerosene, the only light achieved was for the 2.27 kg/sec airflow at an altitude of 6000m Figures 66 and 67 show the relight characteristics for the low emission combustor, Jet A and 3-pass respectively. For both fuels, the relight behavior was erratic At a constant airflow lights and no-lights were achieved as the simulated altitude changed. The 3-pass in the low emission combustor appeared better than it did in the bill-of-material, but still was not as good as the Jet A. At an airflow of 2.27 kg/sec for the low emission combustor the 3-pass and Jet A were about equal in their relight capability. For the other airflow, the Jet A was superior.

3.5.3 Sea Level Ignition

In this section the sea level ignition with antimisting kerosene is compared to Jet A for the bill-of-material and low emission combustors. Both 244K and 290K inlet temperatures were used.

In Figures 68 through 71 the fuel flow rate, with Jet A and 3-pass antimisting kerosene, versus number of burner can lights for a fixed airflow and fuel temperature is plotted. In general, the Jet A had better ignition characteristics than the 3-pass antimisting kerosene. Also, fuel at 290K was better than fuel at 244K for the bill-of-material combustor, while temperature had no effect on the 3-pass antimisting kerosene with the low emission combustor. In Figure 68 the bill-of-material combustor with a fuel temperature of 290K is shown. For Jet A, a 9 can light was achieved with a fuel flow rate down to 295

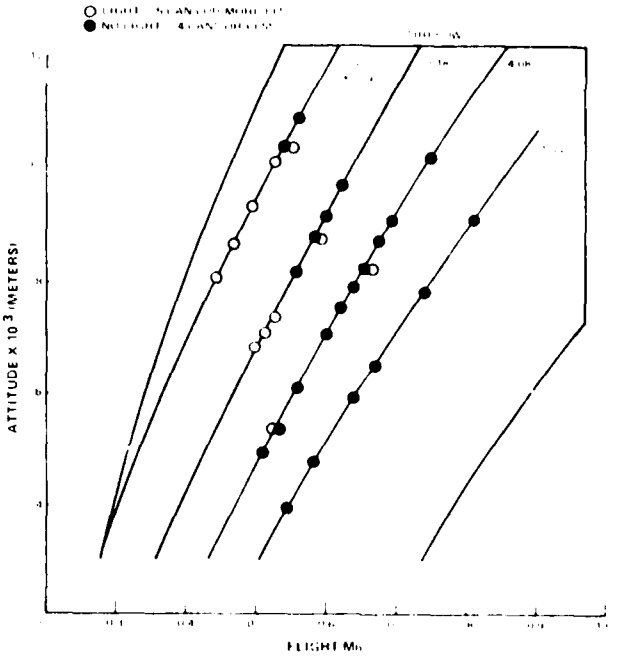

Figure 64 *JT8D-17 Airstart Envelope - Bill-of-Material Combustor, Jet A*

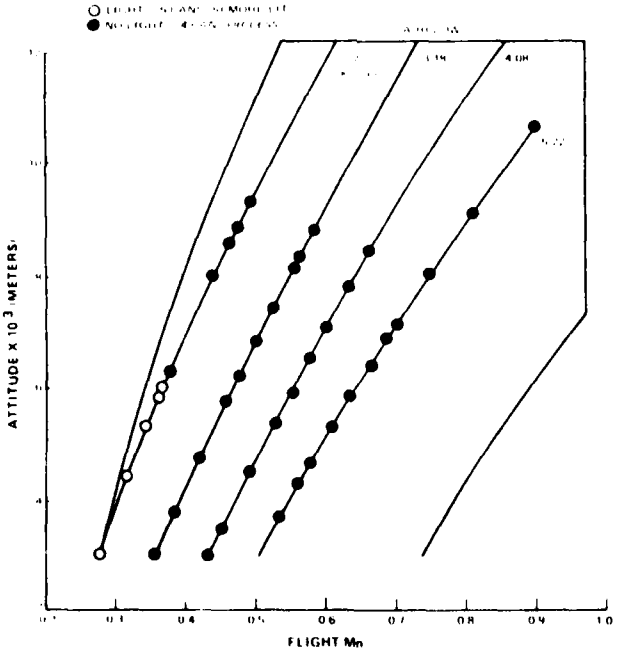

Figure 65 *JT8D-17 Airstart Envelope - Bill-of-Material Combustor, 3-Pass AMK*

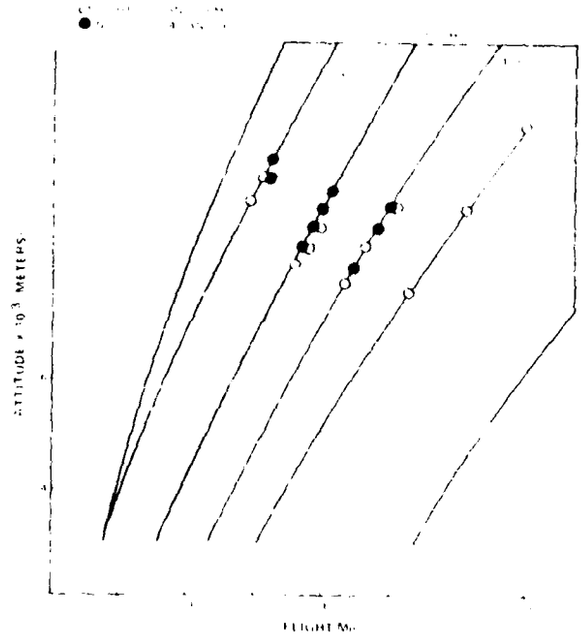

Figure 66 *JT8D-17 Airstart Envelope - Low Emissions Combustor, ·t A*

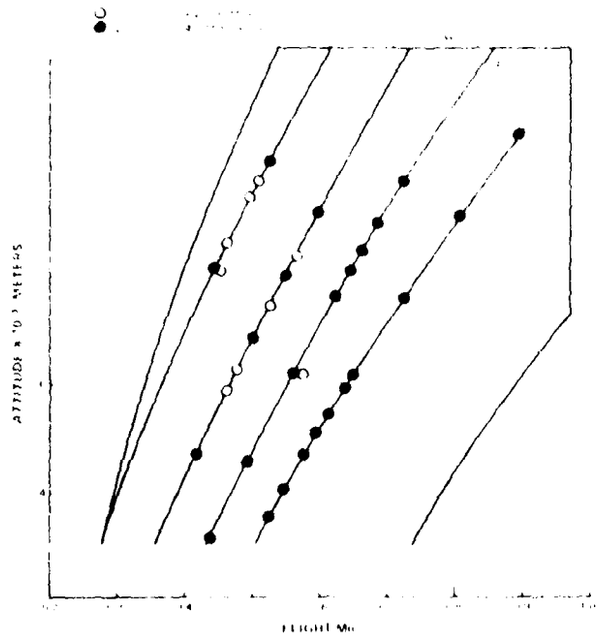

Figure 67 **Airstart Envelope - Low Emissions Combustor, 3-Pass AMK**

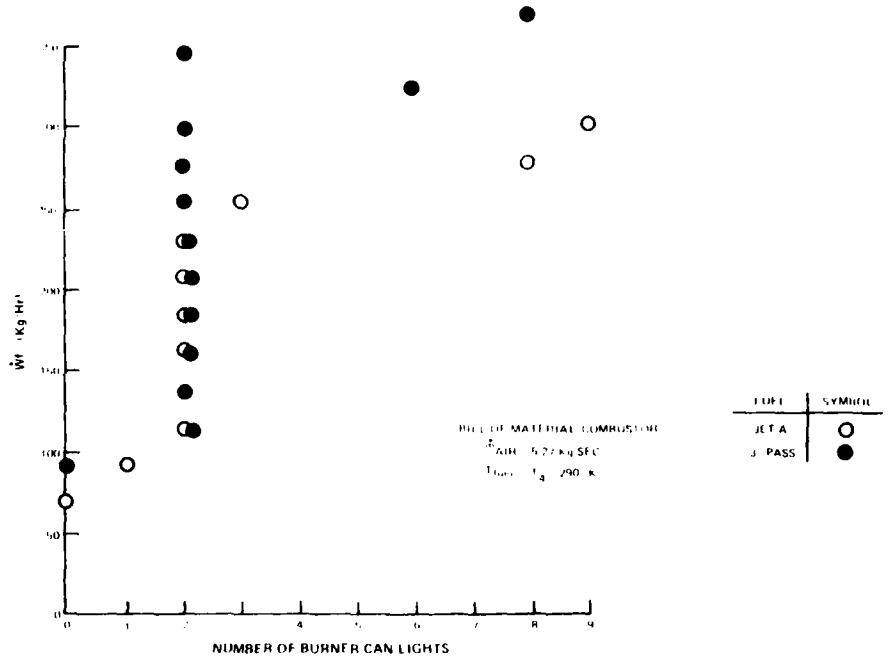

Figure 68 Sea Level Ignition

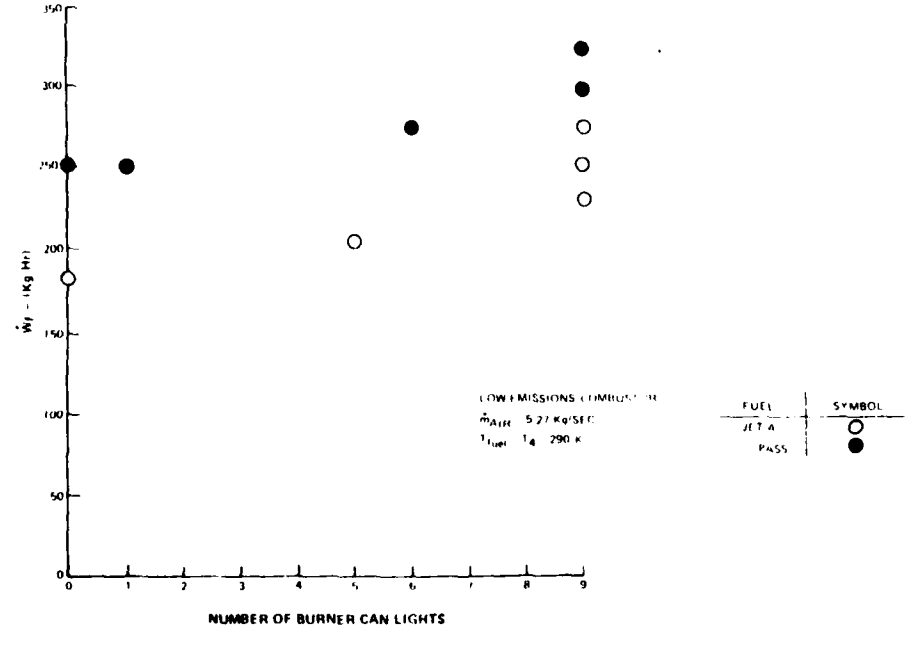

Figure 69 Sea Level Ignition

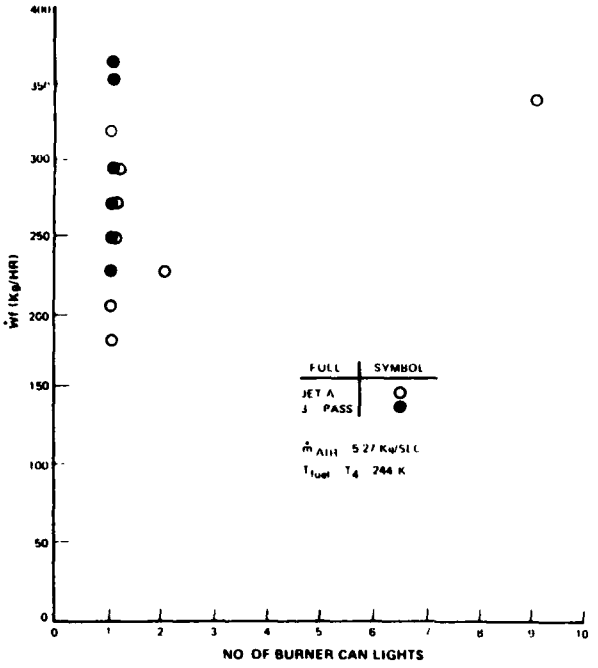

Figure 70 Sea Level Ignition - Bill-of-Material Combustor

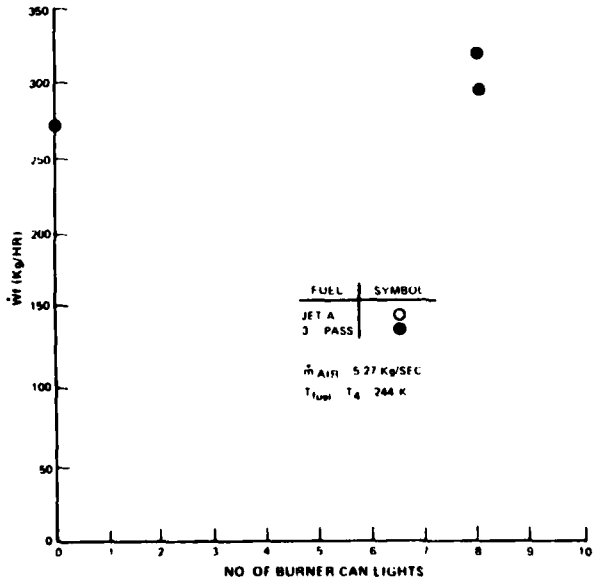

Figure 71 Sea Level Ignition - Low Emissions Combustor

kg/hr. The 3-pass never achieved a full 9 can light with the fuel flow rate as high as 365 kg/hr. In Figure 69 the low emission combustor with a fuel temperature of 290K is shown. For Jet A, a full 9 can light was achieved with a fuel flow rate down to 230 kg/hr while the 3-pass antimisting kerosene required 340 kg/hr for a full 9 can light. In Figure 70, the bill-of-material combustor with fuel at 244K, the Jet A required at least 340 kg/hr for a full 9 can light while the 3-pass antimisting kerosene could, at best, achieve a 1 can light at 365 kg/hr. In Figure 71, the low emission combustor with 244K 3-pass antimisting kerosene is shown. Jet A was not run. A full 9 can light was achieved with a fuel flow rate down to 295 kg/hr. Comparing this to Figure 69 for 3-pass, it is seen that no performance penalty was incurred for the low emission combustor at 244K.

3.5.4 Task 7 Summary

A summary of the Task 7 test results is given in Table XXXI. These results indicate the emission levels produced from 1 and 3-pass antimisting kerosene are unacceptable. Furthermore lean blow out, relight and starting characteristics are somewhat inferior.

TABLE XXXI

COMBUSTOR PERFORMANCE TEST QUALITATIVE
COMPARISON OF DEGRADED ANTIMISTING KEROSENE TO JET A

	Bill of Material		Low Emissions	
	1-Pass	3-Pass	1-Pass	3-Pass
NO_x	0	0	0	0
Smoke	0	0	0	0
CO	-	-	--	--
Total Unburned Hydrocarbon	-	-	--	--
Lean Blow Out	-	-	--	-
Relight	Not Run	-	Not Run	-
Sea Level Ignition	Not Run	-	Not Run	-

0 = Same
- = Worse
-- = Much Worse

3.6 TASK 8 - FUEL CONTROL SYSTEM TEST

In this section the performance of the fuel control with Jet A is compared to 16-pass antimisting kerosene. An extended duration test was also run with 16-pass.

3.6.1 Fuel Control Performance Tests

Fuel control performance with Jet A fuel as compared to its performance with 16-pass antimisting kerosene was within typical repeatability and accuracy limits. A comparison of performance is presented in Figures 72, 73 and 74. Maximum performance change in terms of ratio units (Wf/Pb) occurred during deceleration (minimum ratio) where ratio units decreased by 6 percent with 16-pass antimisting kerosene as compared to Jet A operation. Maximum temperature bias change in terms of ratio units was 5 percent. A shift in the control speed sensing system was not detected.

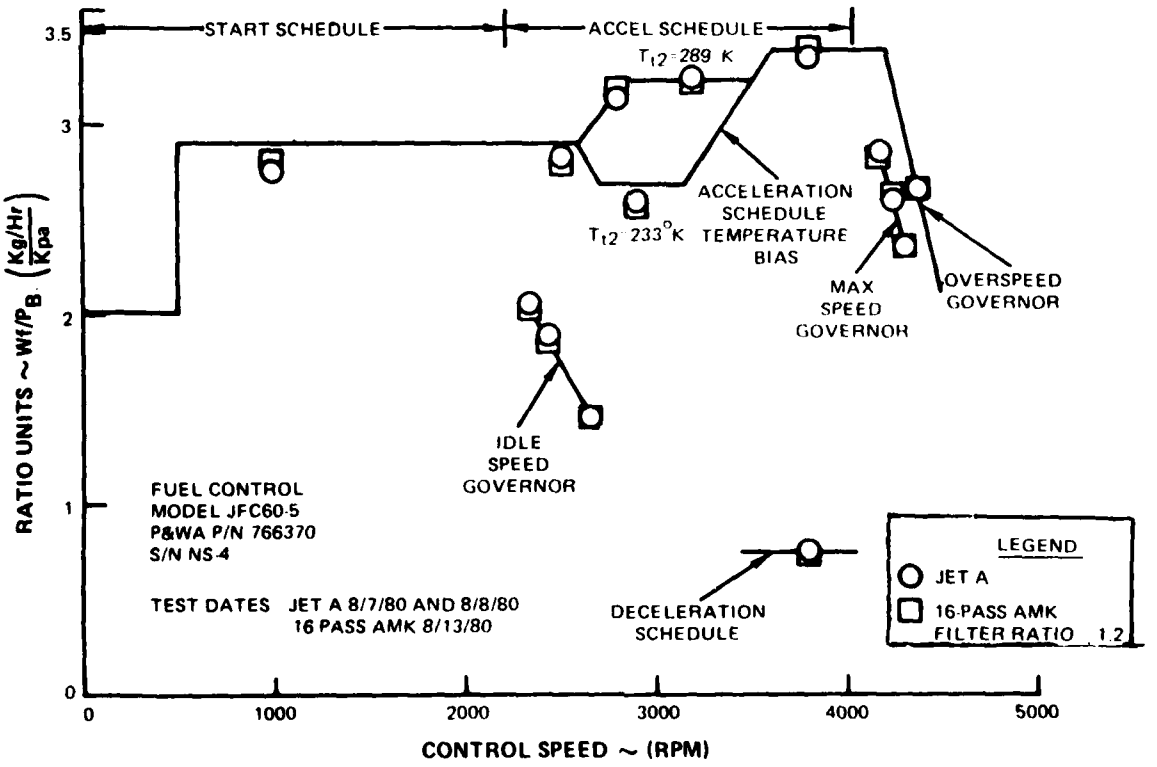

Figure 72 JT8D Fuel Control Comparative Performance

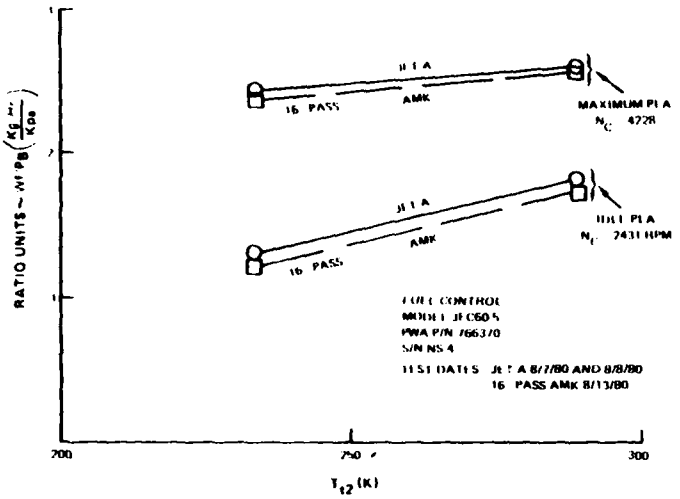

Figure 73 *JT8D Fuel Control Comparative Performance.Idle and Maximum Governor Temperature Bias*

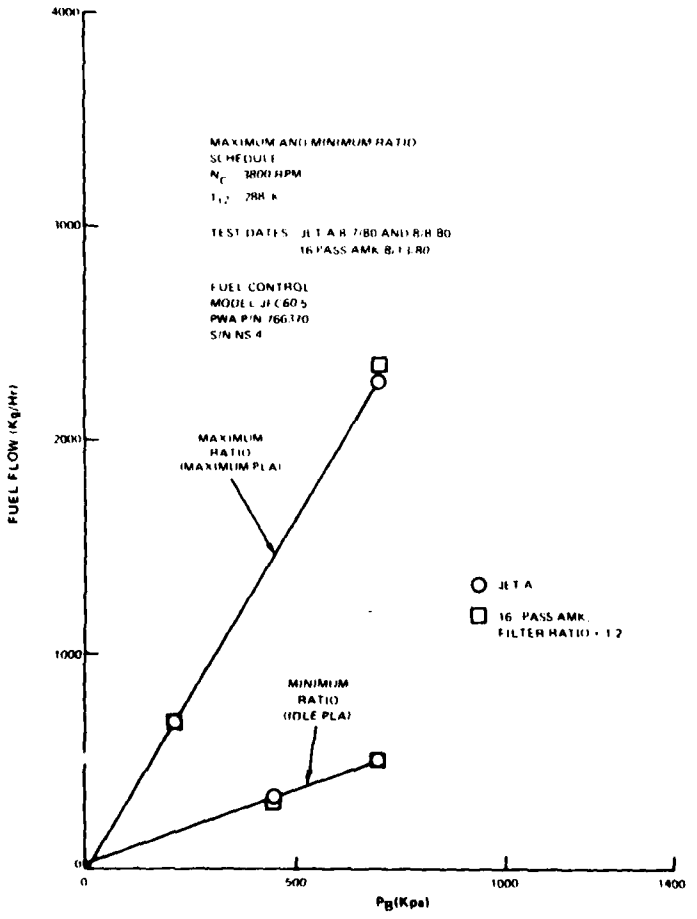

Figure 74 *JT8D Fuel Control Comparative Performance•Maximum and Minimum Ratio Schedules*

3.6.2 Fuel Control Extended Duration Tests

An 8 hour closed loop cyclic test with 16 pass antimisting kerosene produced no noticeable fuel control performance changes through the test. The last cycle which served as a post-test calibration showed very little shift in performance functions as compared to the first cycle. Pre and post test data is tabulated on Table XXXII.

[illegible] XXXII

[illegible]

Condition	Nc rpm	PLA	Pb KPa (psia)	[illegible]	[illegible]	[illegible]	[illegible]	[illegible]	[illegible]
Idle Governor	2431	[illegible]	242 (35)	[illegible]	[illegible]	[illegible]	[illegible]	[illegible]	[illegible]
Max Ratio	[illegible]	Max	966 (140)	[illegible]	[illegible]	[illegible]	[illegible]	[illegible]	[illegible]
Max Governor	4,228	Max	1794 (260)	[illegible]	[illegible]	[illegible]	[illegible]	[illegible]	[illegible]
Min Ratio	3800	[illegible]	103 (1503)	[illegible]	[illegible]	[illegible]	[illegible]	[illegible]	[illegible]

Antimisting kerosene filter ratios of supply tank samples from start to finish of cyclic test did not change significantly within the repeatability of the measuring technique. However, transition velocity changed significantly indicating antimisting kerosene degradation occurring in this test (See Table XXXIII).

TABLE XXXIII

DEGRADATION OF AMK DURING EXTENDED DURATION TEST

Fluid Sample Test Condition	Filter Ratio	Transition Velocity ($cc/sec/cm^2$)
Jet A	-	10-12
16-Pass Prior to Test	1.2	1.5
16-Pass + 3.5 Test Hours	1.3	-
16-Pass + 8 Test Hours	1.3	3.1-4.4

Pressure differential across the fuel control inlet filter, noticeably the wash flow portion, was essentially the same for 16-pass antimisting kerosene and Jet A during performance evaluation. The wash flow filter pressure differential did not increase throughout the 8 hour cycle test indicating absence of the gelling phenomenon.

3.6.3 Summary

The fuel control is capable of operating successfully with 16-pass antimisting kerosene for a period of at least 8 hours. No test data is available for longer test times. At the completion of the tests, the fuel control was judged to be in operational condition (within service accuracy limits) and suitable for continued use.

3.7 TASK 9 - FUEL PUMP PERFORMANCE TESTS

In this task, the effect of the antimisting kerosene on the JT8D fuel pump performance and durability was compared to Jet A.

3.7.1 Pump Durability

A comparison of pump calibration data as presented in Table XXXIV shows little change in pump calibration throughout the antimisting kerosene program. At the interim test point (25.5 hours), delivered flow improved by 2.0 percent at cranking speed and 0.7 percent at rated speed of 4200 rpm. After teardown and reassembly and an additional 86 hours of operation on antimisting kerosene, a 0.8 percent reduction in delivered fuel flow was noted at cranking speed while delivered flow at 3500 rpm was essentially unchanged.

Pre and post test teardown inspection was conducted on the fuel pump. The condition of specific parts after completion of the antimisting kerosene program was essentially unchanged. The following is a summary of the teardown inspection results.

TABLE XXXIV

FUEL PUMP GEAR STAGE CALIBRATION
PRE-, INTERIM- AND POST-TEST
S/N 1361 PUMP X-253 STAND

Condition	Calibration Fluid	25.5 HOURS ON AMK Fuel Flow (Liters/min (gpm)) Pre-Test	Interim Before Teardown		86 HOURS ON AMK Fuel Flow (Liters/min (gpm)) Interim After Pre-Assembly	Post-Test	
Cranking Np = 550 rpm P_D-PIN 1035KPa (150 psig)	Jet A				14.61 (3.86)	14.5 (3.83)	-0.7
Rated Np = 4200 rpm P_D = 3450 kPa (500 psig)	PMC 9041	139 (36.9)	140 (36.99)	+0.7			
NP = 3600 rpm P_D = 3450 kPa (500 psig)	Jet A				116 (30.67)	116 (30.64)	

TOTAL PUMP TIME = 111.5 HOURS ON ANTIMISTING KEROSENE

o Housings

The cover housing exhibited no apparent additional wear as a result of anti-misting kerosene testing.

The main gear housing was also found to be unchanged from its condition prior to antimisting kerosene testing. Any additional gear pocket milling in the pump bores was negligible. There was no evidence of cavitation on either the inlet or discharge ports.

o Main Stage Pumping Gears

The main stage gears were found to be in an unchanged condition. The gear journals were as smooth and polished as at the start of the program except for a few scratches which resulted from running the pump without the pump paper filter installed.

o Main Stage Bearings

The main stage bearings completed the test without any significant changes in appearance. Copper leaching was not evident. There was no evidence of distress or change to surfaces that rely on hydrodynamic film or boundary layer for lubrication.

o O-Ring Seals

All O-ring seals were in good condition and free of cracks.

o Other Pump Hardware

All other pump hardware was essentially unchanged.

In general the condition of the pump components permitted pump reassembly for further service use.

3.7.2 Pump Performance Comparison

A comparison of Jet A gear stage performance with 3-pass and undegraded antimisting kerosene, as presented on Figures 75, 76 and 77, shows a significant improvement with antimisting kerosene at cranking speed and some improvement with antimisting kerosene at higher speeds. It is believed that improved performance may have resulted from reduced internal leakage due to the antimisting kerosene clogging small passages.

Although the reduced leakage had no detrimental effect on this pump other pumps might be adversely affected due to a reduction in bearing cooling flow and hydrodynamic lubrication.

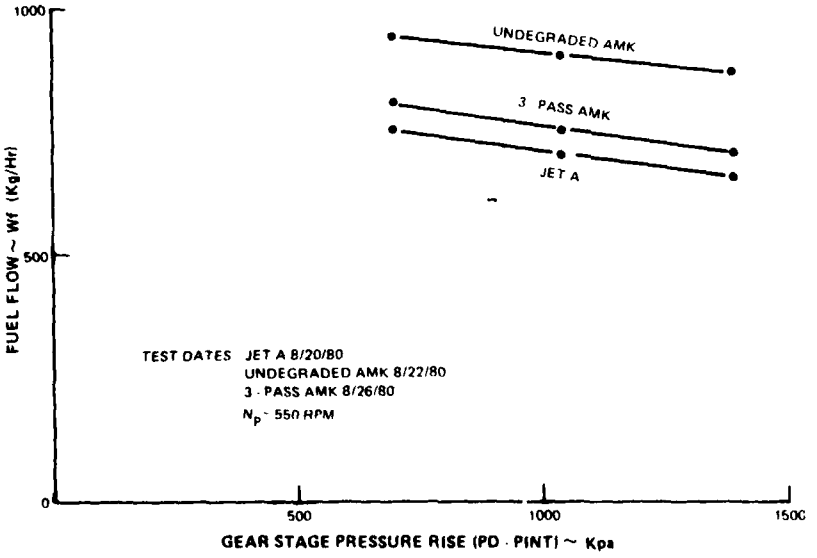

Figure 75 Fuel Pump Gear Stage Performance Without Pump Inlet Filter

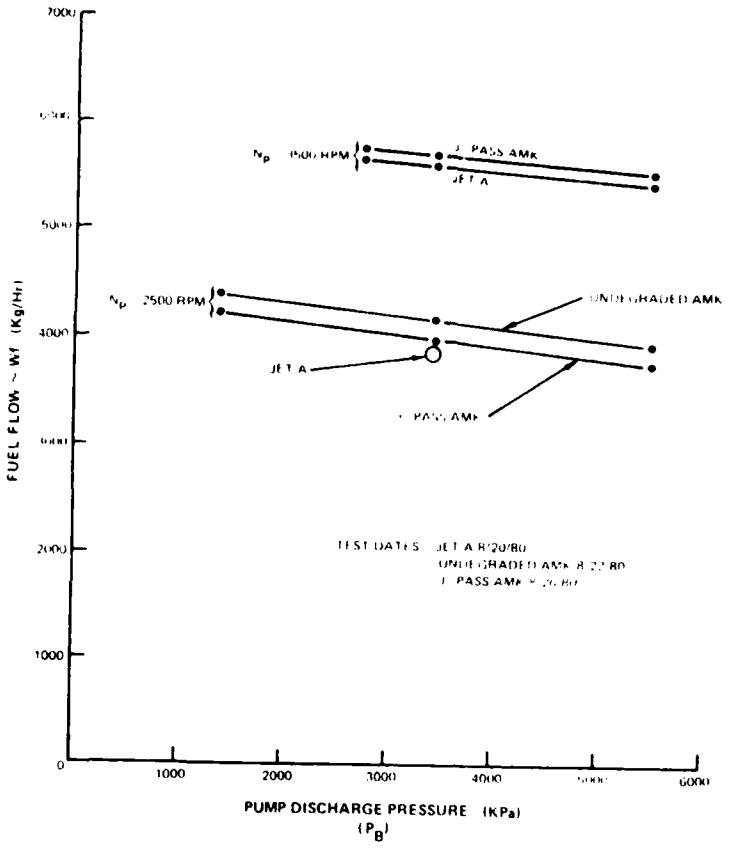

Figure 76 *Fuel Pump Gear Stage Performance S/N 1361 Fuel Pump Without Pump Inlet Filter*

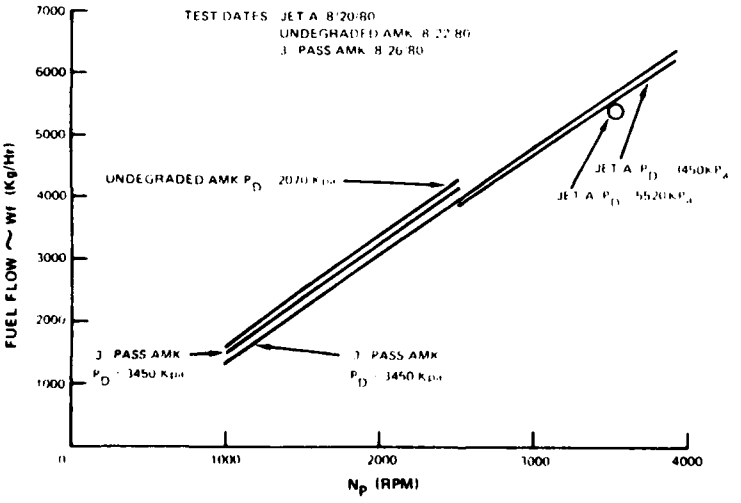

Figure 77 ***Fuel Pump Gear Stage Performance Without Pump Inlet Filter***

Delivered fuel flow versus gear stage pressure rise is plotted on Figure 75. At cranking speed delivered fuel flow compared to Jet A improved by approximately 50 Kg/hr (110 pph) with 3-pass antimisting kerosene and approximately 202 Kg/hr (450 pph) with undegraded antimisting kerosene.

Delivered fuel flow versus pump discharge pressure (P_D) is plotted on Figure 76. At 2500 rpm pump speed, delivered fuel flow compared to Jet A improved by approximately 100 Kg/hr (225 pph) with 3-pass antimisting kerosene and approximately 300 Kg/hr (665 pph) with undegraded antimisting kerosene.

Delivered fuel flow versus pump speed is plotted on Figure 77. At pump discharge pressure of 3450 KPa (500 psig), delivered fuel flow compared to Jet A improved by as much as 145 Kg/hr (320 pph) with 3-pass antimisting kerosene and 300 Kg/hr (665 pph) with undegraded antimisting kerosene.

In summary, the antimisting kerosene does not appear to affect the JT8D fuel pump performance. The fuel pump, on the other hand, does significantly degrade the antimisting kerosene. The degradation effects of the JT8D fuel pump assembly on the antimisting kerosene can be found in Section 3.1.3.

4.0 CONCLUSIONS AND RECOMMENDATIONS

4.1 CONCLUSIONS

Based on the results of this limited 13 month exploratory program nothing was uncovered which would preclude the use of presheares antimisting kerosene containing 0.3 percent FM-9 in a jet engine application. However, the testing and analytical studies conducted have not fully evaluated all the necessary requirements for safe engine implementation. The conclusions drawn from a series of laboratory and bench scale experiments, and full scale component tests are discussed below:

Fuel Flow Characterization

Improvements in measuring the flow characteristics of antimisting kerosene were developed (i.e., filter ratio, superficial and critical flow velocity) which adequately quantified the degradation level of antimisting kerosene. Additionally these laboratory tests indicated the need for a filter ratio of less than 2 (using 17 m filter) for compatibility with JT8D fuel system components.

Gelling or clogging of fuel system components was found to be fuel flow velocity sensitive. However, a good correlation between filter ratio or critical flow velocity and JT8D fuel system clogging tendencies could not be made.

Antimisting Kerosene Properties

The addition of 0.3 percent FM-9 by weight in Jet A did not significantly alter the properties of the Jet A parent fuel except for a slight reduction in net heat of combustion and an increase in sodium content. It is not known whether long term exposure to the level of sodium detected will adversely affect jet engine hot section durability.

Physical Characteristics Evaluation

Laboratory thermal stability tests made with both unsheared and sheared levels of antimisting kerosene indicated a significant improvement in thermal stability compared to the parent Jet A.

Water solubility tests exposed the formation of a precipitate which did not return to solution on standing and is a concern in filter clogging.

Heat transfer measurements indicated the need to shear the antimisting kerosene to a filter ratio lower than 2 to ensure acceptable operation in the fuel-oil heat exchanger.

Based on a six month static soak test elastomer seal materials normally employed in a jet engine fuel system (i.e., fluorosilicone, butadiene) were found to be compatible with ambient and hot antimisting kerosene.

Combustor System Evaluation

Combustor rig tests conducted with antimisting kerosene limited to a shearing level equivalent to a filter ratio of approximately 2 revealed deficiencies in exhaust emissions and altitude relight with both the current and advanced low emissions JT8D combustor configurations. It is projected that the further shearing of the antimisting kerosene will result in significant improvements in combustion characteristics.

Fuel System Performance

The ambient short term performance of the JT8D fuel pump and fuel control was acceptable. The fuel control was capable of operating satisfactorily with antimisting kerosene sheared to a filter ratio of approximately 1.2 for periods of at least eight hours while the fuel pump showed no signs of deterioration after accumulating 112 hours on several levels of sheared antimisting kerosene.

Based on an assessment of the aforementioned conclusions and other test results generated by this program, two additional general conclusions can be made.

- o The only major engine modification projected to be required at this time for the successful use of antimisting kerosene is the need for a practical shearing device upstream of the engine to provide the necessary level of shearing.

- o The application of the results obtained from the JT8D components tested in this program can most likely be applied to similar components from other modern aircraft jet engines.

4.2 RECOMMENDATIONS

The literature surveys, laboratory and full scale component tests, and analytical projections conducted under this program revealed areas of inadequacy of existing data, insufficient information to understand fundamental mechanisms, and the need for additional technology improvement before serious consideration can be given to widespread engine use in the near future. Recommendations for future research activities and technology development are discussed in the following section.

- o A multi-pass pumping arrangement that was employed in this program to shear the polymer in antimisting kerosene fuel is satisfactory for experimental fuel property investigations but it cannot be seriously considered for ultimate use in aircraft. Methods of shearing or reverting antimisting kerosene to a satisfactory operational level must be evaluated so that a practical cost and energy effective, flightworthy apparatus can be developed.

- o Further chemical and physical characterization of the fuel is required as a function of shearing level, pressure, temperature, velocity, and filter medium so that accurate predictions can be made of the compatibility of

the necessary shearing level of antimisting kerosene with any engine fuel delivery system. In addition an evaluation of the compatibility of antimisting kerosene with approved Jet A additives such as anti-corrosion, lubricity and anti-icing should be made.

- Limited low temperature testing in the recently completed program indicated a fall-off in antimisting kerosene flow performance capability. For this reason a low temperature performance evaluation of fuel system components is strongly recommended. This would include a de-icing test to determine the effect of melting ice crystals on the stability of antimisting kerosene and the performance of the de-icing system.

- Fuel system component endurance tests are required to assess both the gelling tendencies as well as the possible deterioration of wear surfaces with time. A long term endurance test of at least several hundred hours is recommended in a closed loop that includes components such as filters, pumps, controls, valves, heat exchangers, etc.

- Corrosion and/or durability of engine hot sections can only be assessed by extensive rig and engine testing designed to exercise the engine component at real operating conditions. This type of extensive evaluations is only warranted following successful completion of some of the more basic technology recommended in the proceeding sections.

- Short duration engine tests should first be conducted to document the impact of the antimisting kerosene fuel on the performance, operational and emissions characteristics of the engine. During this phase of engine testing combustor liner and exhaust temperature distribution will be measured to identify possible shifts caused by differences in fuel atomization, spray pattern or combustion rate of the antimisting kerosene fuel. In addition, during the test time outlined above for temperature acquisition, starting and emission characteristics should be assessed.

The results of the preceding engine phase will provide inferences and data for analytically estimating the effect of the antimisting kerosene fuel on the durability of the hot section, i.e., the combustor and turbine. In fact, these prerequisite tests may infer that further degrading of the fuel is required or that the long duration engine test is not warranted at this time.

- Hot section durability can be affected by differences in liner heat load and temperatures, fuel injector fouling, and particulate or corrosive emissions from the combustor. Only through long duration cyclic endurance testing can these influences be substantiated. Therefore it is recommended that cyclic tests be formulated that will accelerate the anticipated distress modes. The engine endurance cycle should be selected to provide a combination of low cycle fatigue cycles, resonance cycles, extended hot time and engine starts that can be compared to established experience with Jet A fuel.

  Pre- and post-test calibrations and inspections of the hot section and fuel section components would provide the basis for substantiating the life limiting distress modes and estimating the impact of the use of the particular antimisting kerosene fuel on overall component life.

The results from the above described engine test program will establish the feasibility of the use of the FM-9 additive in existing in-service engines.

REFERENCES

1. McAdams, W. H., Heat Transmission, McGraw-Hill, 1954.

2. Roberts, R., Peduzzi, A., Vitti, G. E., "Experimental Clean Combustor Program, Phase I", Final Report, NASA CR-134736, October 1975.

3. "Aircraft Gas Turbine Engine Exhaust Smoke Measurement", SAE Aerospace Recommended Practice 1179, May 1970.

4. "Procedure for the Continuous Sampling and Measurement of Gaseous Emissions from Aircraft Turbine Engines", SAE Aerospace Recommended Practice 1256, October 1971.

5. Niedzwiecki, R. W. and Jones, R. E., "Parametric Test Results of a Swirl Can Combustor", NASA TMX-68247, June 1973.

6. Medani, M. S. and Hayes, K. G., "Heat Transfer to Aviation Fuels", Journal of Eng. Sci., V. 4, No. 1, 1978.

BIBLIOGRAPHY

1. Miller, R. E.: Safety Fuel Research in the United Kingdom, Materials Department, RAE GU146TD, 1974.

2. Weatherford, Jr. and B. R. Wright: Status of Research on Antimist Aircraft Turbine Engine Fuels in the United States, AGARD/NATO, 45 Meeting, April 1975.

3. Cretcher, R. E. and G. W. Gandee: Evaluation of Western Research Col, FR-3 Fuel Additive, U. S. Air Force Aero Propulsion Laboratory, Technical Memorandum AFAPL-TM-68-1, 1968.

4. Gandee, G. W. and R. G. Clodfelter: Evaluation of the Effectiveness of Antimist Fuel Additives in Prevention of Aircraft Fuel Tank Village Fires and Explosions, Air Force Aero Propulsion Laboratory, Wright-Patterson Air Force Base, Report No. AFAPL-TR-73-111, Jan. 1974.

5. Shaw, L. M.: Safety Evaluation of Antimist Fuels, Dynamic Science Division, Ultrasystems, Inc., Dyn Sci Report No. 9130-73-112, November 1973.

6. Urban, C. M, Bowden, J. N. and J. T. Gray: Emulsified Fuels Characteristics and Requirements, USAAVLABS Technical Report No. 69-24, prepared by USAFLRL, Southwest Research Institute, March 1969 (AD 688167).

7. Weatherford, W. D., Jr. and F. W. Shaekel: Emulsified Fuels and Aircraft Safety, 37th Meeting of AGARD/NATO Propulsion and Energetics Panel, The Hauge, Netherlands, May 1971 (AGARD-CP-84-71).

8. Weatherford, W. D., Jr. and M. E. LePera: U. S. Army Fuel Developments, Industry-Military Jet Fuel Quality Symposium, San Antonio, TX, January 1973.

9. Wright, B. R., L. L. Stavinoha and W. D. Weatherford, Jr.: A Technique for Evaluating Mist Flammability, USACCL Technical Report, prepared by USAFLRL, Southwest Research Institute, December 1973 (AD 776965).

10. Modified Jet A Fuel Reduces Post-Crash Aviation Used and Space Technology. July 9, 1979.

11. Eklund, T. I. and J. C. Cox: Flame Propagation through Sprays of Anti-misting Fuels, NAFEC Technical Letter Report NA-78-66-LR, November 1978.

12. Zinn, S. V., T. I. Eklund and W. E. Neese: Photographic Investigation of Modified Fuel Breakup and Ignition, Report FAA-RD-76-109 FAA 1976.

13. Pardue, R. E. Aircraft Fuel System Simulator Tests with Antimisting Kerosene (Jet A Fuel with FM-9 Additive), Lockheed-Georgia Co., Report No. FAA-RD-79-52, May 1979.

14. Miguel, A. S.: Antimisting Fuel Kinematics Related to Aircraft Crash Landings, J. Aircraft Vol. 15, No. 3, March 1978.

16. Polymeropoulous, C. E. and Das, S.: "The Effect of Droplet Size on the Burning Velocity of Kerosene - Air Spray, Combustion and Flame, Vol. 25, 1975.

17. J. Herrin, "Combustion Characteristics of Fuels with Antimist Additives", Naval Air Propulsion Center, JTCG/AS-77-T-001, September 1979.

18. Symposium on Aircraft Research and Technology for Future Fuels, NASA-Lewis Research Center, April 16, 1980.

DISTRIBUTION LIST*
NAS3-22045
An Assessment of the Use of Antimisting Fuel in Turbofan Engines

	Name	Address
	Dr. R. E. Milles Mr. E. A. Timby Dr. P. Wilford Mr. B. Jamieson	Royal Aircraft Establishment Farnborough Hants GU14-6TD England
(2)	J. McAbee K. Clapp	ICI America, Inc. Wilmington, DE 19897
	Oliver St. John	C.A.A. House 45-59 Kings Way London WC2B 6TE England
(2) (2) (2)	Bill Westfield Eugene Klueg Gary Frings	FAA Technical Center ACT 320 Atlantic City Airport, NJ 09405
(2)	Dick Kirsch Tom Horeff	FAA 800 Independence Avenue Washington, DC 20519
	John Enders	Pres. Flight Safety Foundation, Inc. 5510 Columbia Pike Arlington, VA 22204
(2)	A. T. Peacock	Douglas Aircraft Company Code 36-41 3855 Lakewood Blvd. Long Beach, CA 90846
(2)	S. Walter Sweet	Dir. Bureau of Technology N.T.S.B. Washington, DC 20594
(3)	Dr. V. Sarohia, Code 67-201	Jet Propulsion Lab 4800 Oak Grove Drive Pasadena, CA 91103
(2)	Dr. R. Mannheimer	Southwest Research Institute San Antonio, TX 78284

*One (1) each except as noted.

DISTRIBUTION LIST (Cont'd)

	Name	Address
	Dr. M. Golub Dr. J. Parker R. Altman	NASA Ames Research Center Moffett Field, CA 94035
(10)	Mr. A. R. Tobiason, RJT-2	NASA Headquarters Washington, DC 20546
	Thor Ekland Bob Salmon	FAA Technology Center Atlantic City Airport, NJ 08405
	Raymond Colladay RTP-6	NASA Headquarters Washington, DC 20546
	Steven Wander, RTP-6	NASA Headquarters Washington, DC 20546
	Jack Grobman, MS 86-6 R. Niedzwiecki, MS 86-6 J. Haggard, MS 86-6	NASA Lewis Research Center 21000 Brookpark Road Cleveland, OH 44135
(2)	Benito P. Botteri	Air Force Propulsion Lab Wright Patterson AFB, OH 45433
	C. C. Kimmel	Parker Hannifin Corp. 18321 Jamboree Blvd. P. O. Box C-19510 Irvine, CA 92713
	D. C. Nordstrom	Boeing Airplane Company P. O. Box 3707, MS 73-01 Seattle, WA 98124
	Edward F. Versaw	Lockheed California Company P. O. Box 551 Burbank, CA 91520
	Irving Fagin	FAA AFS-105 800 Independence Avenue S.W. Washington, DC 20591
(40)	T. Fiorentino	Pratt & Whitney Aircraft Group Commercial Products Division 400 Main Street East Hartford, CT 06108

DISTRIBUTION LIST (Cont'd)

	Name	Address
(10)	NASA Representative	NASA Scientific and Technical Information Facility P. O. Box 8757 Balt./Wash. International Airport Maryland, 21240 (with completed DRA (3 copies))
	Harold Schmidt, MS 100-1 (3 + remaining copies)	NASA Lewis Research Center 21000 Brookpark Road Cleveland, OH 44135
(2)	Lewis Library	NASA Lewis Research Center 21000 Brookpark Road Cleveland, OH 44135
	E. C. Wood, Executive Director	Federal Aviation Administration Office of Aviation Safety Dept. of Transportation 800 Independence Avenue S.W. Washington, DC 20591
	J. A. Bert	American Petroleum Institute 2101 L Street N.W. Washington, DC 20037
	J. Chavkin	Federal Aviation Administration Chief, Aircraft Engineering Division Office of Airworthiness 800 Independence Avenue S.W. Washington, DC 20591
	J. M. DelBalzo	Federal Aviation Administration Technical Center Director, National Aviation Facilities Experimental Center Atlantic City, NJ 08405
	W. M. Fanning	National Business Aircraft Association Manager, Technical Services 11th Floor, One Farragut Sq. S. Washington, DC 20006
	M. Goland	Southwest Research Institute San Antonio, TX 78284
	Ray Walder	International Air Transport Association Director, Engineering and Environment 1000 Sherbrooke West; 26th Fl. Montreal, Quebec H3A2R4

DISTRIBUTION LIST (Cont'd)

Name	Address
S. J. Green	General Aviation Manufacturers Assoc. Vice President - General Counsel Suite 517 1025 Connecticut Ave., N.W. Washington, DC 20036
B. V. Hewes	Air Line Pilots Association Chairman, ALPA Rescue & Fire Committee 1625 Massachusetts Ave., N.W. Washington, DC 20036
C. F. Hitchcock	Aviation Consumer Action Project Attorney 1346 Connecticut Ave., N.W. Box 19029 Washington, DC 20036
K. E. Hodge	National Aeronautics and Space Administration Transport Aircraft Office 4th St. & Maryland Ave., S.W. Washington, DC 20546
C. Huggett	National Bureau of Standards Deputy Director Center for Fire Research Washington, DC 20234
E. L. Hutcheson	Helicopter Association of America Safety Consultant 1110 Vermont Ave., N.W. Washington, DC 20005
C. W. McGuire	Department of Transportation Office of Environment & Safety 400 7th St. S.W. Washington, DC 20590
L. R. Perkins	E. I. DuPont de Nemours 1007 Market St. Wilmington, DE 19898
E. Podolak	Federal Aviation Administration Technical Center Program Scientist, Office of Aviation Medicine Atlantic City, NJ 08405

DISTRIBUTION LIST (Cont'd)

Name	Address
J. P. Reese	Aerospace Industries Association Director, Airworthiness Programs 1725 DeSales St., N.W. Washington, DC 20036
S. H. Robertson	Arizona State University Director, Safety Center Tempe, AZ 85281
J. Searle	Association of Flight Attendants Coordinator, Fire & Rescue Committee 1625 Massachusetts Ave., N.W. Washington, DC 20036
E. L. Thomas	Air Transport Associatio· Vice President - Engineering 1709 New York Ave., N.W. Washington, DC 20006
Phil Jones	Explosafe America, Inc. Suite 180 2081 Business Center Dr. Irvine, CA 92715
Miss I. A. Burgess	Explosafe America, Inc. 2500 Virginia Ave., N.W. Washington, DC 20037
W. G. Dudek	Exxon Research & Engineering Co. P. O. Box 111 Linden, NJ 07036
R. Fisher	Lockheed-California Co. Safety Engineer 2555 N. Hollywood Way Box 551 Burbank, CA 91520
R.G.E. Furlonger (Observer Only)	British Embassy Civil Air Attache - Safety 3100 Massachusetts Ave. Washington, DC 20008
J. D. Galloway	Uniroyal, Inc. Chief Engineer, Fuel Cells 1230 Ave. of the Americas New York, NY 10020

DISTRIBUTION LIST (Cont'd)

Name	Address
G. J. Grabowski	Fenwal, Inc. Vice President - Protective Systems Division 400 Main Street Ashland, MA 01721
L. Hebenstreit	Walter Kidde & Company New Products Research Specialist 400 Main Street Ashland, MA 01721
J. T. Leonard	Naval Research Laboratory Head, Special Project Section 4555 Overlook Ave. S.W. Washington, DC 20032
T. Madgwick	British Aerospace, Inc. Suite 207 2101 L Street N.W. Washington, DC 20037
S. A. Manatt	AiResearch Manufacturing Co. of California Senior Program Specialist 2525 W. 190 St. Torrance, CA 90509
M. M. McCormick	National Transportation Safety Board Senior Air Safety Investigator Bureau of Technology 800 Independence Ave. S.W. Washington, DC 20594
E. Nichols	Piper Aircraft Corp. Chief Powerplant Engineer 3000 Medulla Rd. Lakeland, FL 33803
H. Nordermeer	KLM Royal Dutch Airlines Engineering & Manufacturing Division Schiphol Airport Amsterdam, Holland
N. R. Parmet	Trans World Airlines, Inc. Vice President - Engineering & Quality Assurance 605 Third Avenue New York, NY 10016

DISTRIBUTION LIST (Cont'd)

Name	Address
T. W. Reichenberger	Gates Learjet Corp. Chief of Powerplants Box 7707 Wichita, KS 67277
K. Rosen	United Technologies Corporation Sikorsky Aircraft Division No. Main Street Stratford, CT 06602
H. Skavdahl	Boeing Commercial Airplane Company Chief, Propulsion Research & Preliminary Design Box 3707 Renton, WA 98124
H. D. Smith	Goodyear Aerospace Corp. Manager, Engineered Fabrics Development 1210 Massillon Rd. Akron, OH 44315
T. Street	Gates Learjet Corp. Box 7707 Wichita, Kansas 67277
D. F. Thielke	Flight Engineers International Assoc. 905 16th Street N.W. Washington, DC 20006
R. Volz	Scott Paper Company Manager, Commercial Development Scott Plaza Philadelphia, PA 19113
E. P. Webb	Firestone Coated Fabrics Company P. O. Box 887, Waldo Highway Magholia, AK 71753
A. Weisner	Piper Aircraft Company Powerplant Engineer 3000 Medulla Rd. Lakeland, FL 33803
J. H. Wivell	British Airways 245 Park Ave. New York, NY 10017

U.S. GOVERNMENT PRINTING OFFICE 1981 0 707 230